Л. М. Митник

"Космос-1500" и радиолокационное зондирование океана

Основные даты
Часть II. Вторые сорок лет
"Космос-1500" и радиолокационное зондирование океана

Дек 1977 – по настоящее время, ТОИ –с.н.с., зав. лаб., зав. отд., г.н.с.

28 сентября 1983 – запуск спутника "Космос-1500"

1982 -1992 участник рейсов на НИС Академик Виноградов,
Академик Несмеянов, Академик Лаврентьев, Проф. Богоров.
1993-1994, 1995-1996, 1998 приглашенный профессор в ун-тах Тайваня
1995 защита диссертации, д.ф.-м.н: Исследование параметров и явлений в системе океан-атмосфера СВЧ-радиометрическим и радиолокационным методами, ИКИ РАН.

1999-2000, 2001-2002 - Приглашенный профессор в ун-тах Германии и Японии
2010, присвоено ученое звание профессора.

10 октября 2018 - 80 лет

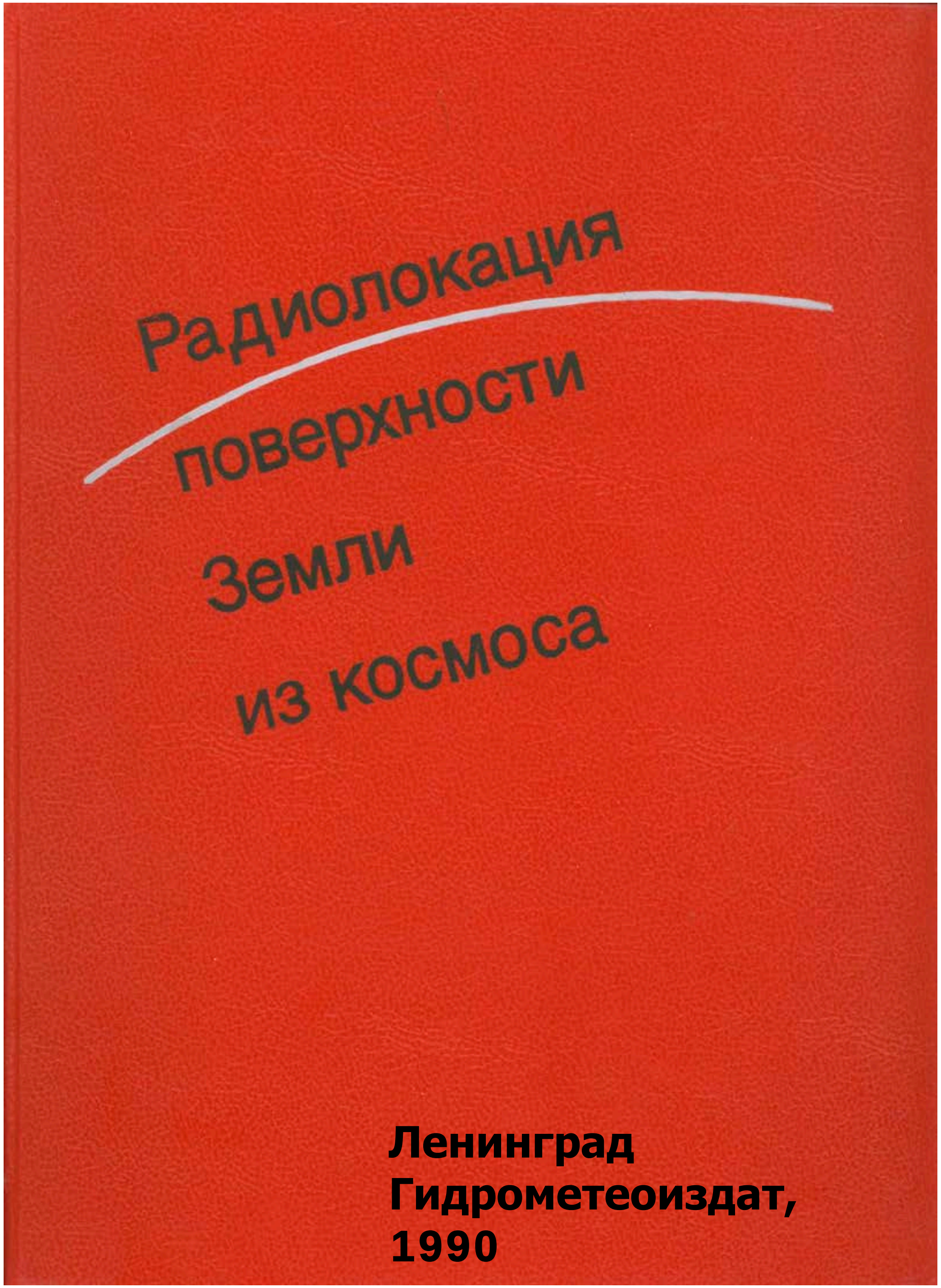

Ленинград
Гидрометеоиздат,
1990

1. **Экспериментальный океанографический спутник «Космос-1500»**
2. **Физические основы РЛ-съемок с орбиты ИСЗ.**
3. **Радиолокационная система бокового обзора ИСЗ «Космос-1500»**
4. **Предварительная обработка данных РЛС БО**
5. **Характеристики морской поверхности**
6. **Характеристики морского льда**
7. **Характеристики материкового льда**

Под редакцией
канд.физ-мат.наук Л. М. Митника,
канд.физ-мат.наук С.В. Викторова

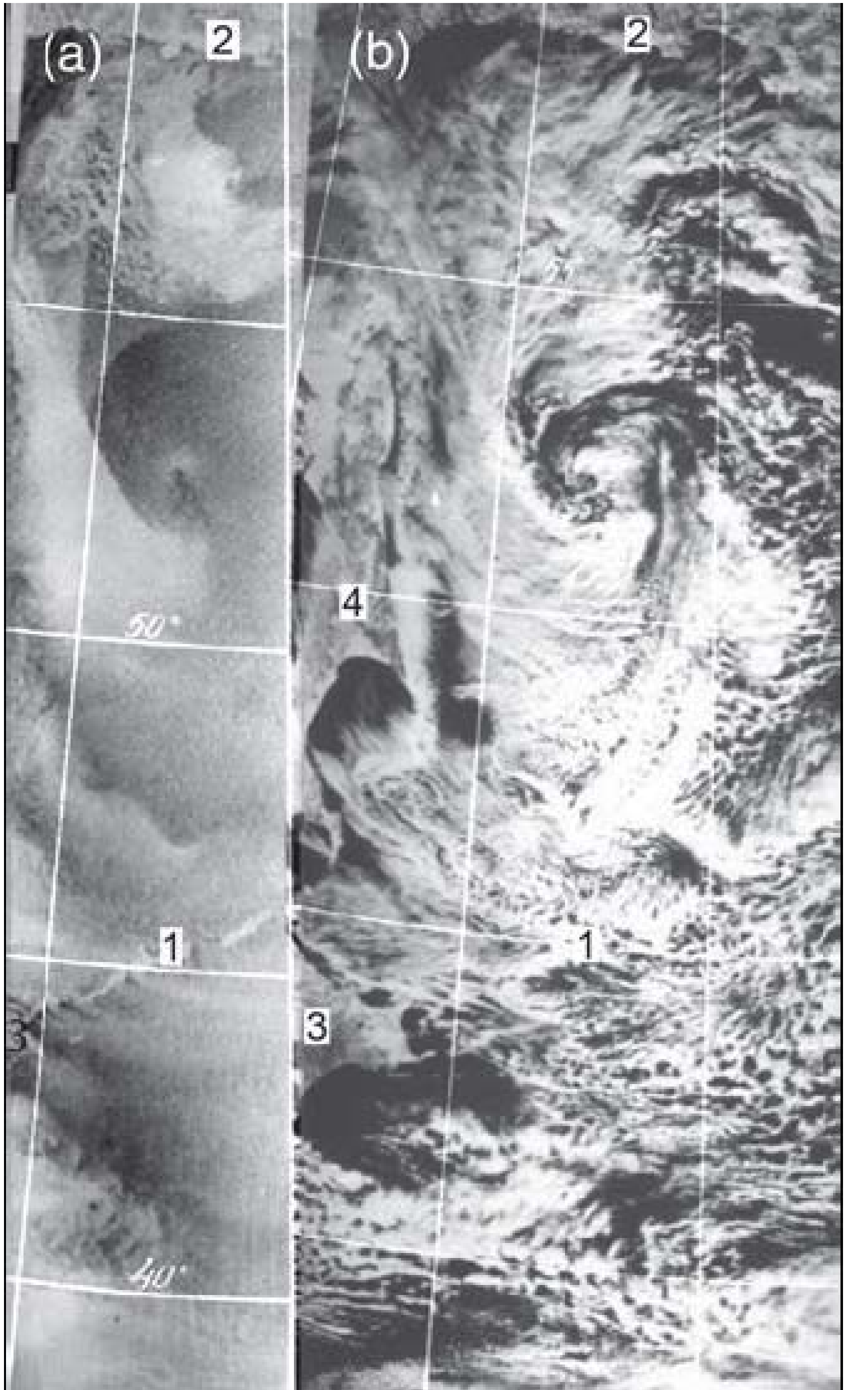

КОСМОС-1500

Seen on the left (a) is a *Real Aperture Radar (RAR)* and on the right (b) a visible image of an occluded cyclone over the Okhotsk Sea taken by ***Kosmos-1500*** on 29 December 1984. Iturup Island (1), northern coast of the Okhotsk Sea (2), Hokkaido (3), and Sakhalin (4) are identified. Brightness of the ***RAR*** image is influenced by wind speed and direction (relative to the radar direction), with brightness increasing with increasing wind speed. Comparison of two images shows a high correlation of wind field in (a) with cloudiness in (b). Radar images such as this have demonstrated their potential for monitoring the sea surface under all-weather conditions.

Courtesy of Leonid Mitnik.

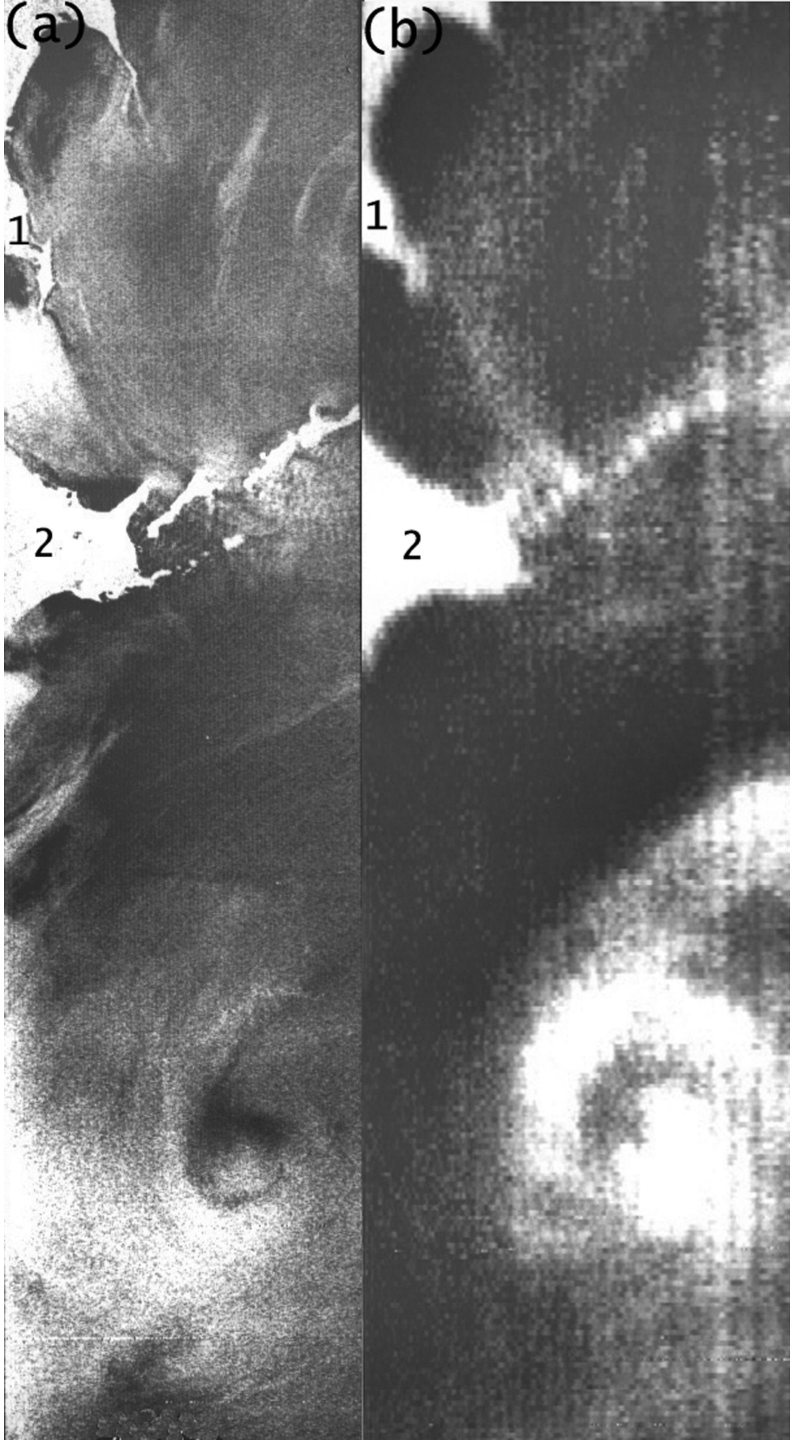

Tropical Storm Agnes

TC Agnes as seen by the RAR (a) and the 0.8-cm microwave radiometer (b) carried aboard *Okean-1*. These images were taken on 31 July 1988 in the western North Pacific in the vicinity of Sakhalin (1) and Hokkaido (2) Islands. Changes in brightness temperature in (b) are due to precipitation, cloud liquid water, and wind action. *Courtesy of L. Mitnik.* *Results from Kosmos-1500, -1602 and -1776 have been presented* *Mitnik and Victorov (1990).* **The unique capability of this series, the *simultaneous acquisition of overlapping images by three different sensors at three different wavelengths*, enabled an improved interpretation of measurements and a reduction in errors of retrieved parameters. (Such a capability would be employed on later satellites such as TRMM and ADEOS-II.)**

Sea ice on "Ocean-7" images

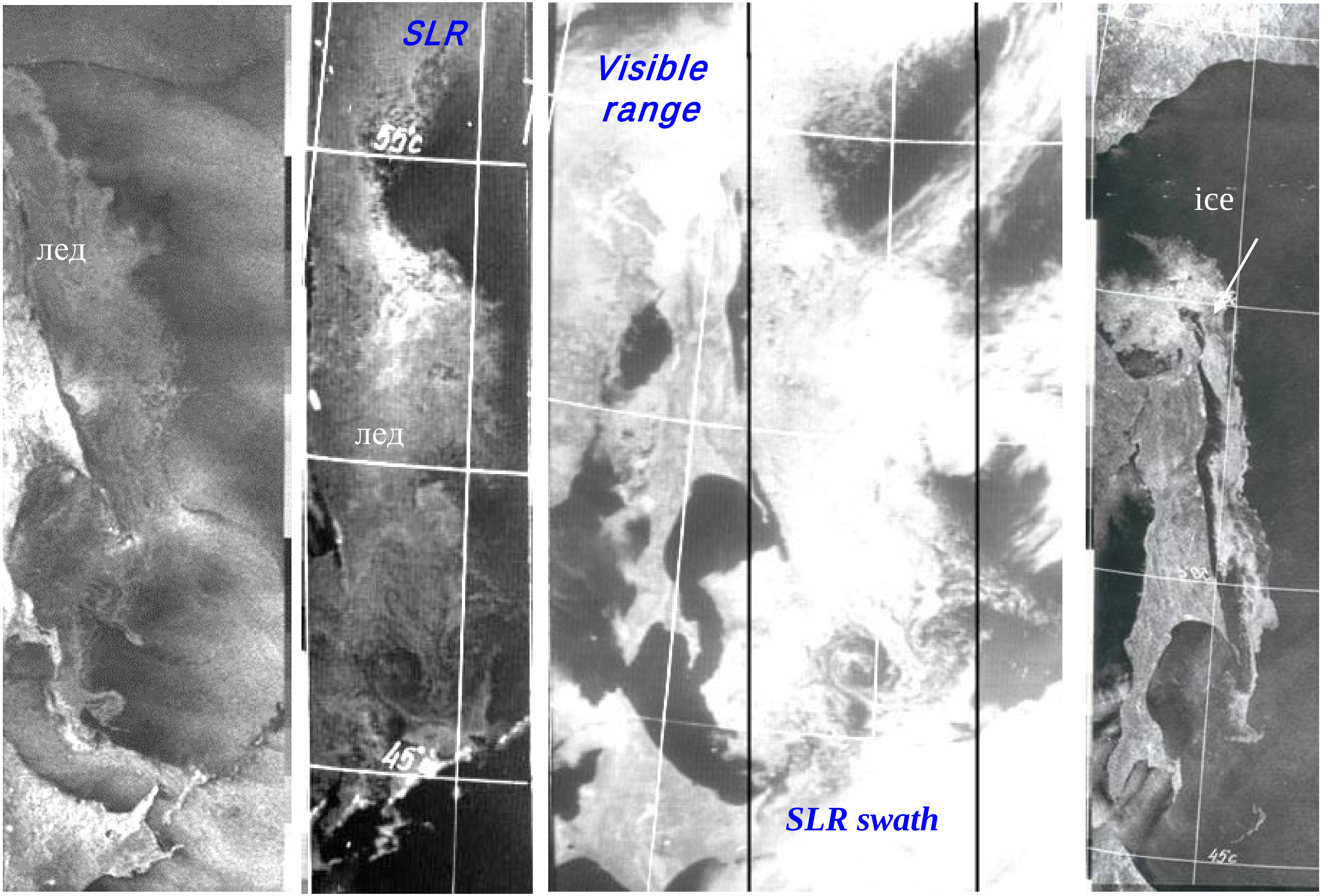

24 Jan 1996 — *28 March 1997* — *4 May1996*

Typhoon Herb

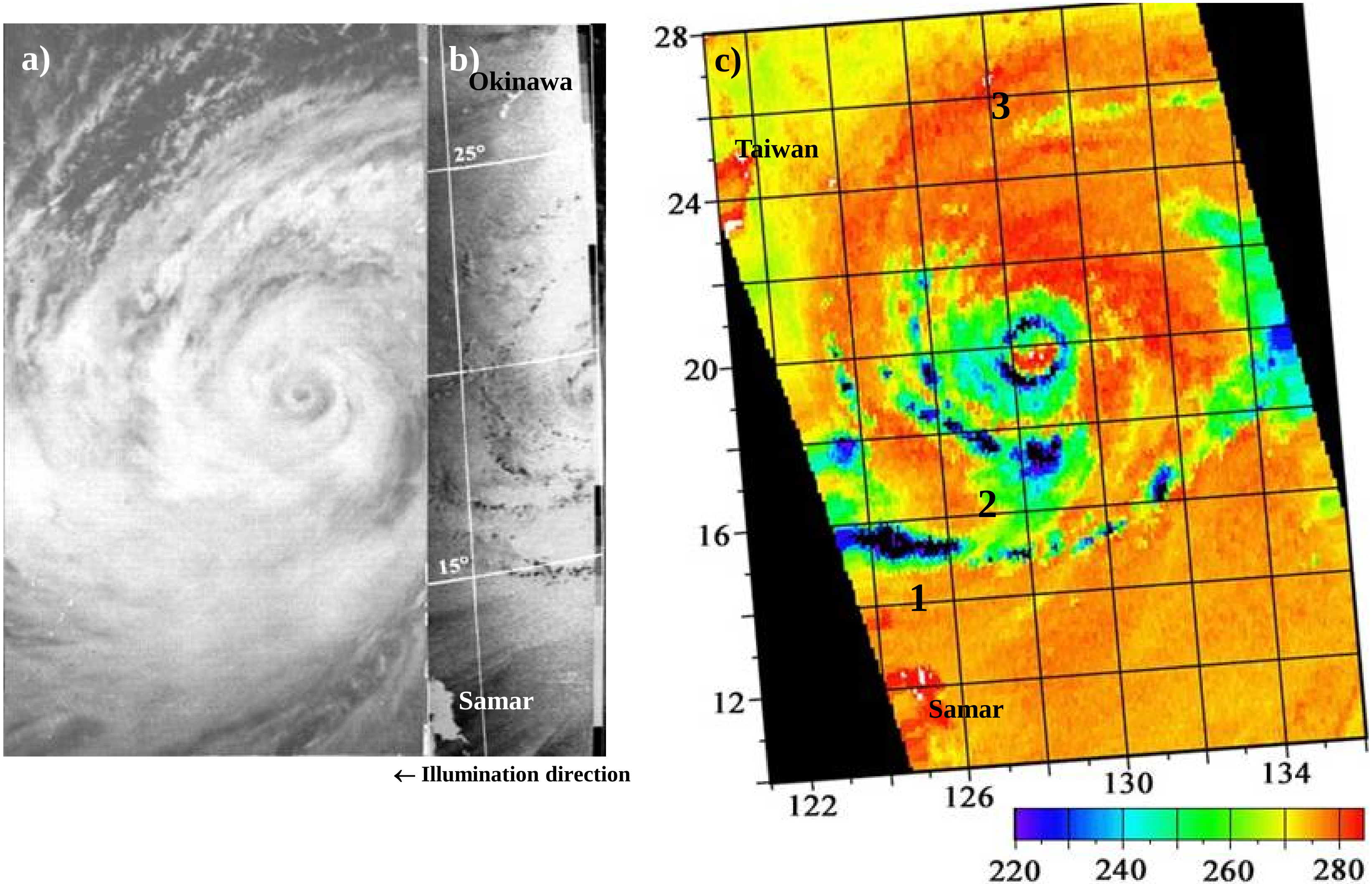

Typhoon Herb as measured on 29 July 1996: (a) visible and (b) radar images from Okean-7 satellite and (c) brightness temperature at frequency 85 GHz from DMSP

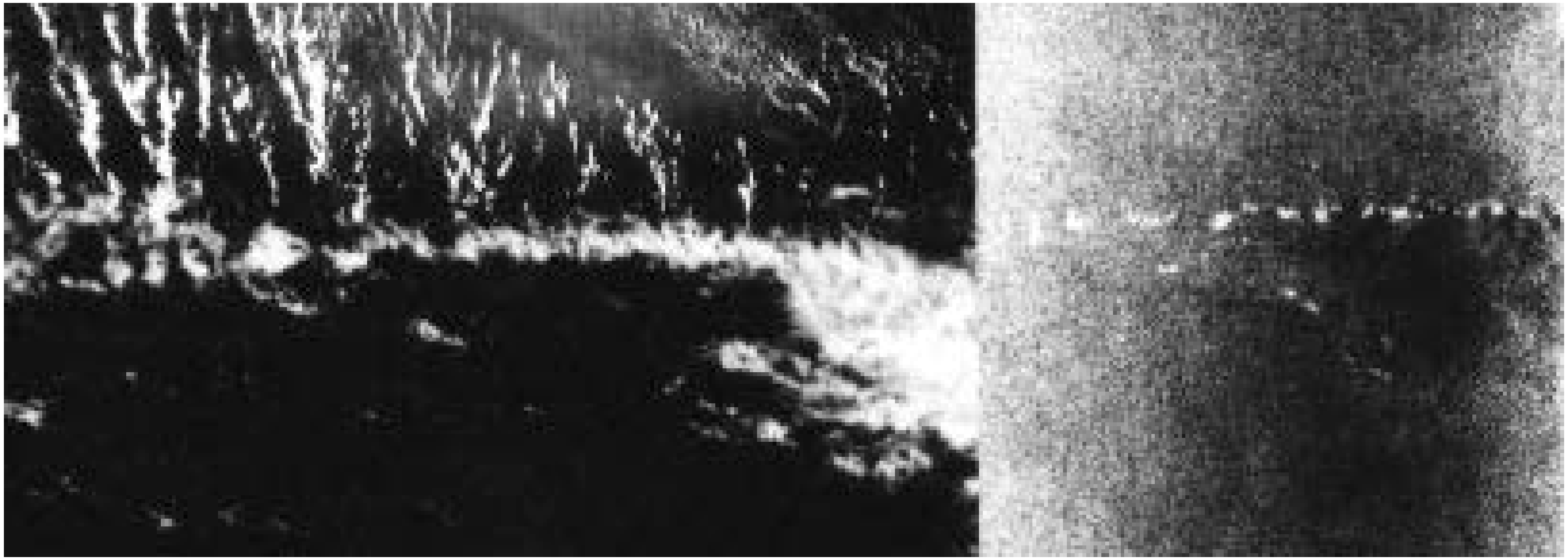

Kosmos-1500 (a) visible and (b) RAR images of rain cells extended along latitude south of equator at 1037 UTC 9 March, 1985. A width of a RAR swath is 460 km. Dash lines note the boundaries of RAR swath on visible image.

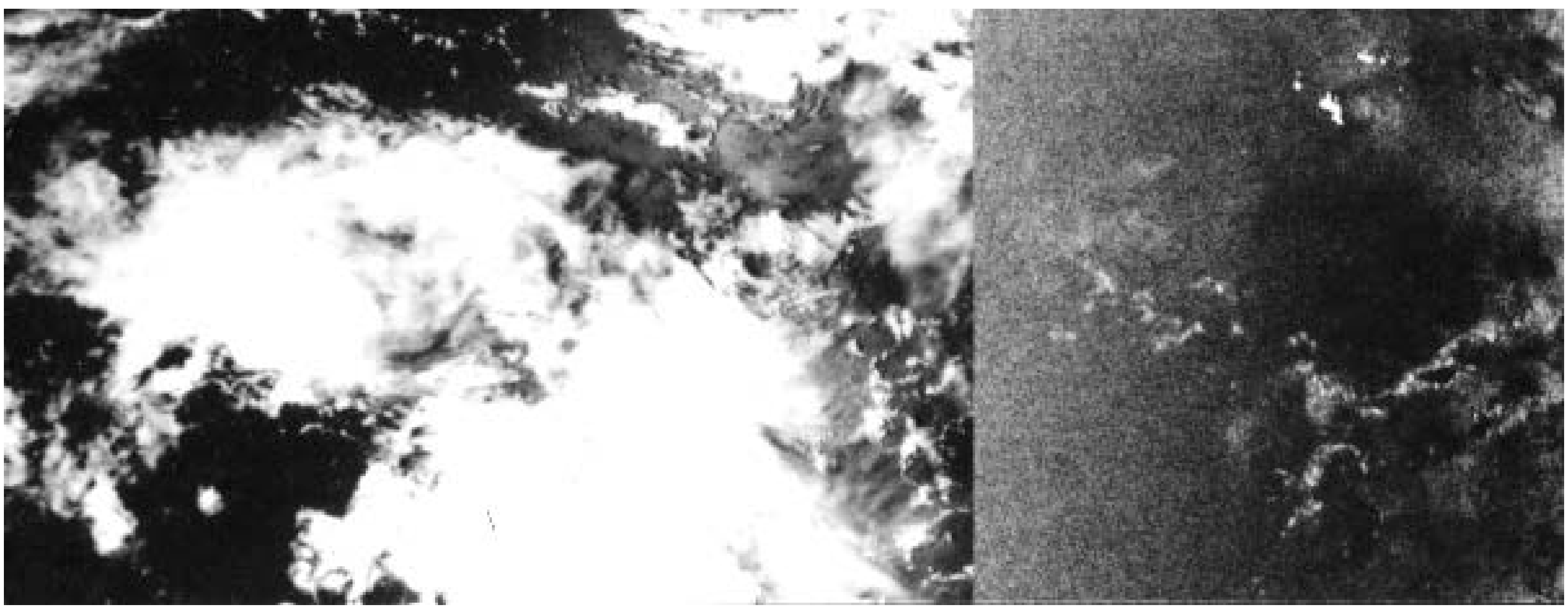

Kosmos-1500 (a) visible and (b) RAR images of rain cells and band in a tropical cloud cluster at 1057 UTC 15 March, 1985. Dash lines note the boundaries of RAR swath.

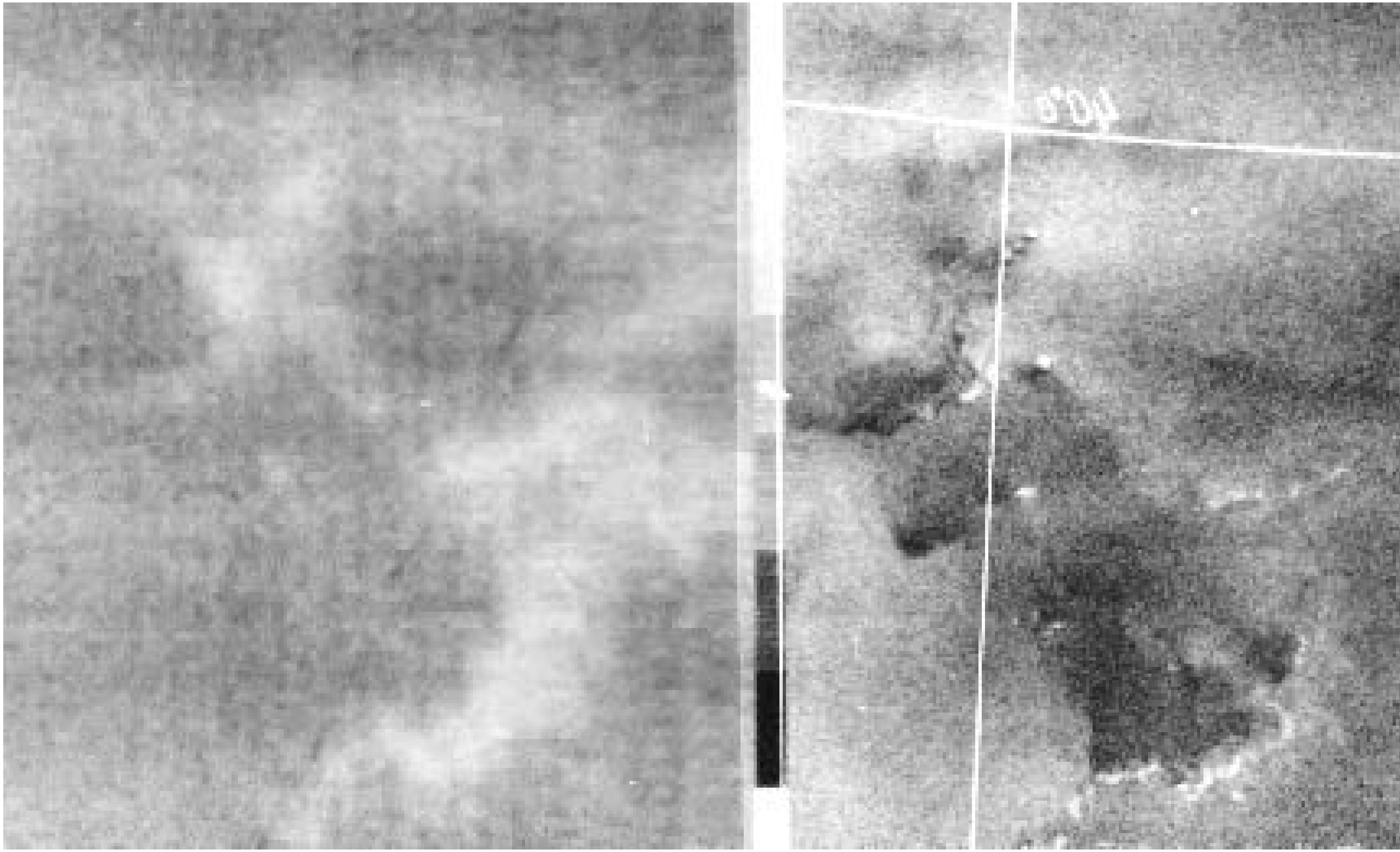

Okean-7 microwave (a) and radar (b) images of heavy cloudiness over the Pacific Ocean at 1204 UTC 12 Dec, 1996. Swath width of microwave image is 550 km.

Kuroshio-Oyashio and synoptic eddies

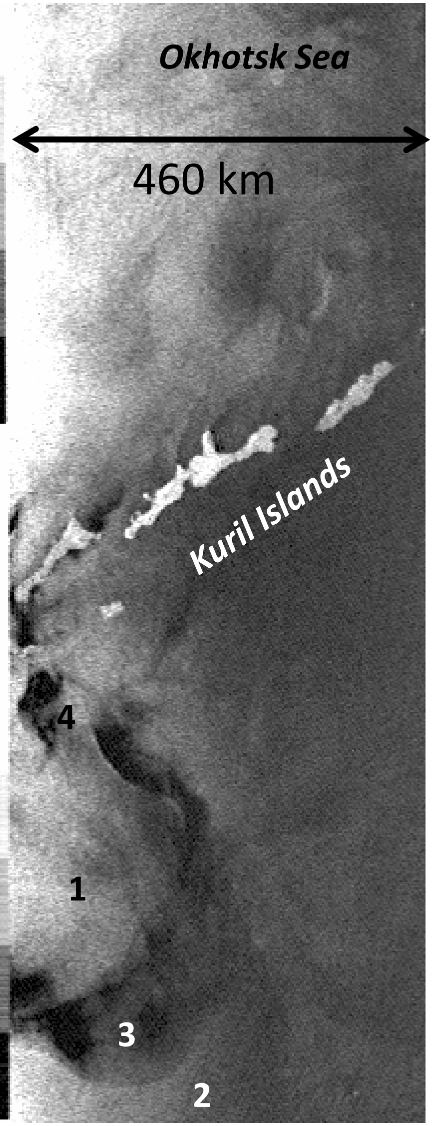

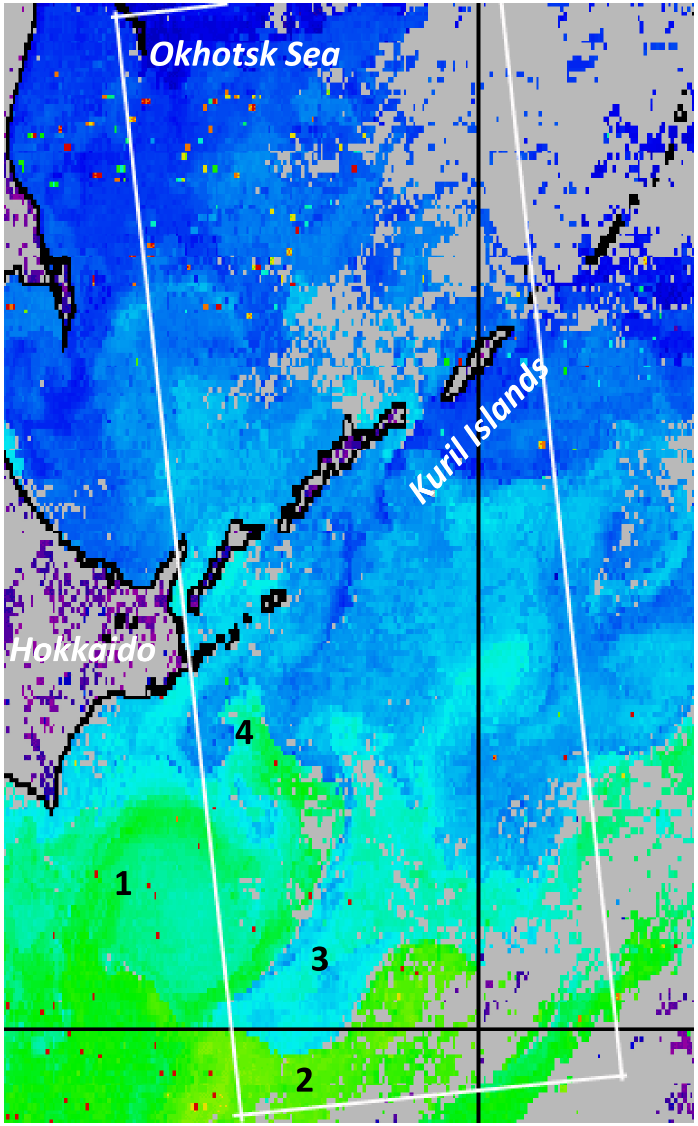

Resolution 1-2 km

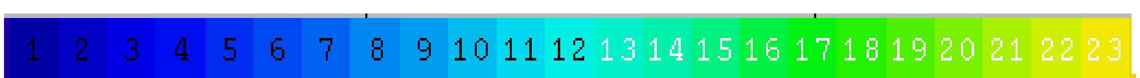

Okean-7 X-band Real Aperture Radar (RAR) and NOAA AVHRR-derived SST. 20 November 1999.

White rectangle marks the boundaries of ***RAR*** *image.*

При *W* < 5-6 м/с к югу от Курил значительным РЛ-контрастом обладают АЦ вихрь 1, окружающие его холодные воды Ойясио 2 и теплые воды Куросио 3, ограничивающие их с юга. Из сопоставления с полем ТПО по данным **AVHRR** спутника **NOAA-14** видно, что хорошо отображаются тонкие детали распределения температуры воды такие, как выступ теплых вод в северной части вихря и др. Температурные контрасты на границе вихря достигают 12ºC.

Kuroshio-Oyashio transition zone

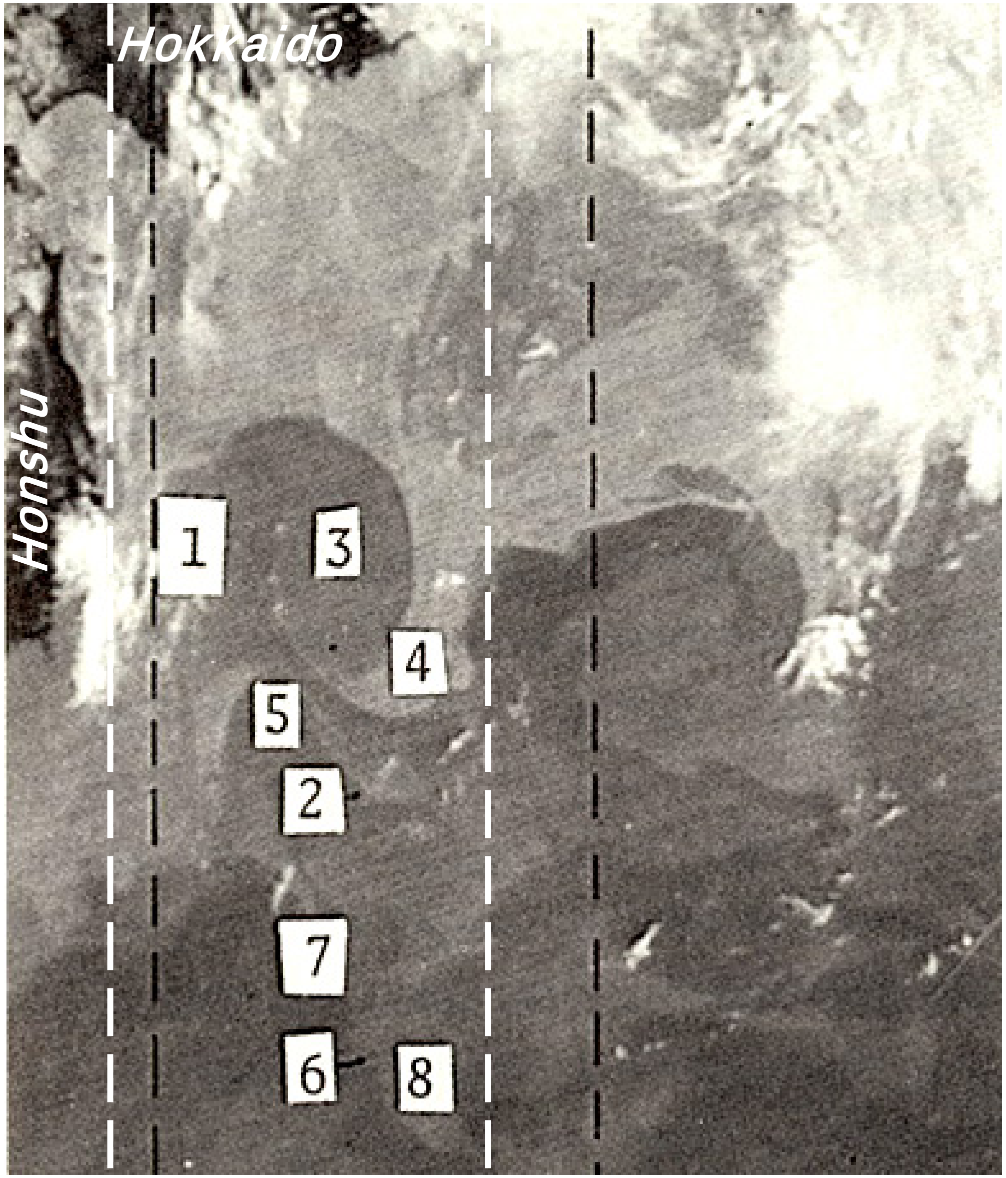

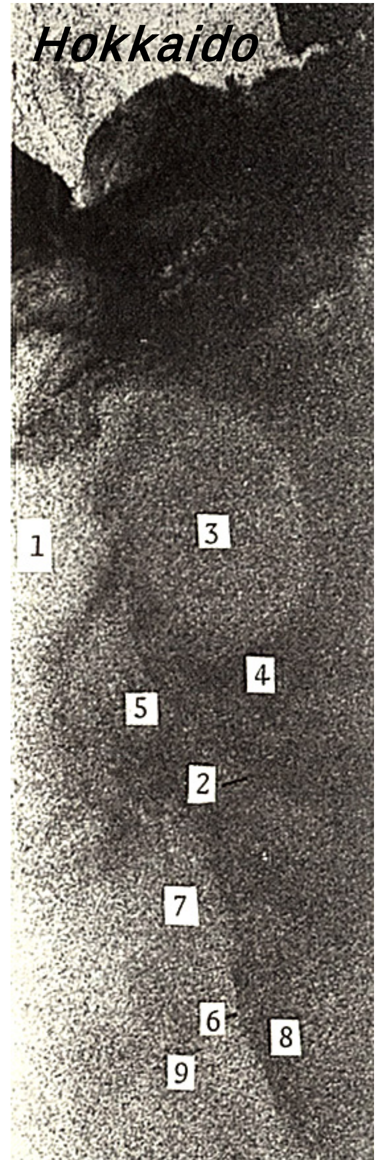

Resolution 1-2 km

NOAA-10 AVHRR infrared image acquired on 30 April 1987 (left) and Kosmos-1500 Real Aperture Radar image

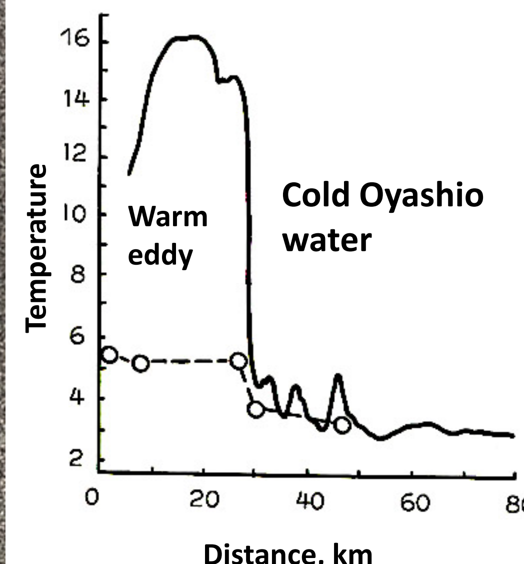

Mitnik L.M. and V.B. Lobanov (1991), Reflection of oceanic fronts on satellite radar images, *Oceanography of Asian Marginal Seas*, Kenzo Takano, Ed., Amsterdam, Elsevier, pp. 85-101.

ALOS PALSAR. Anticyclonic eddy

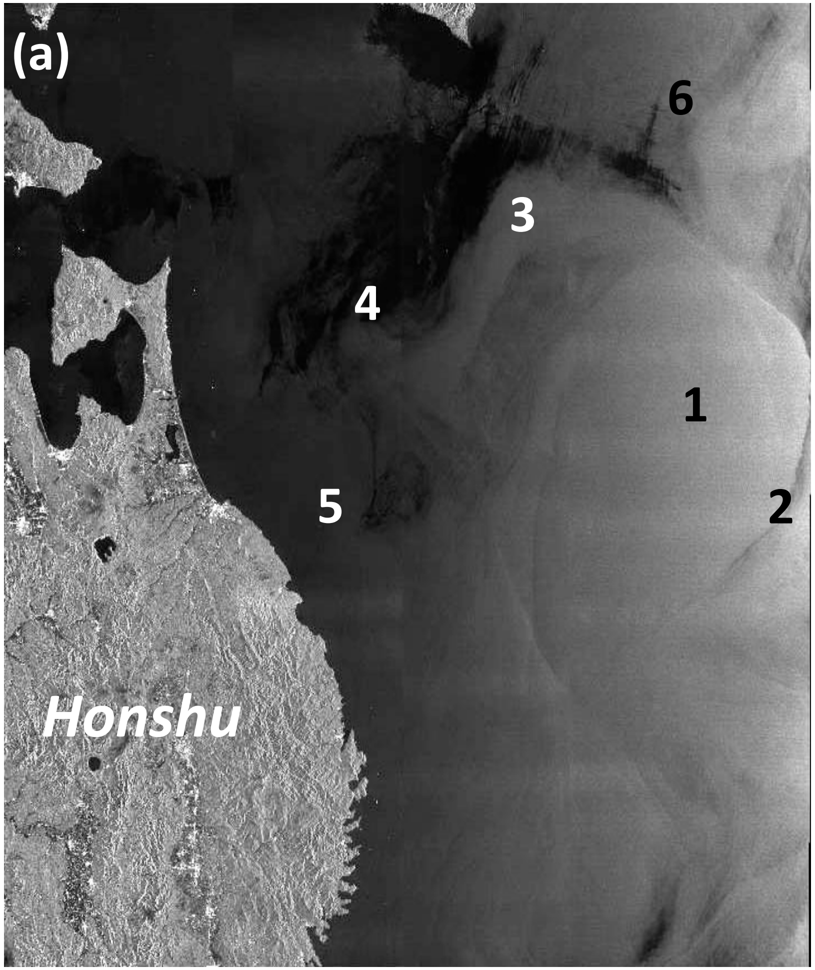

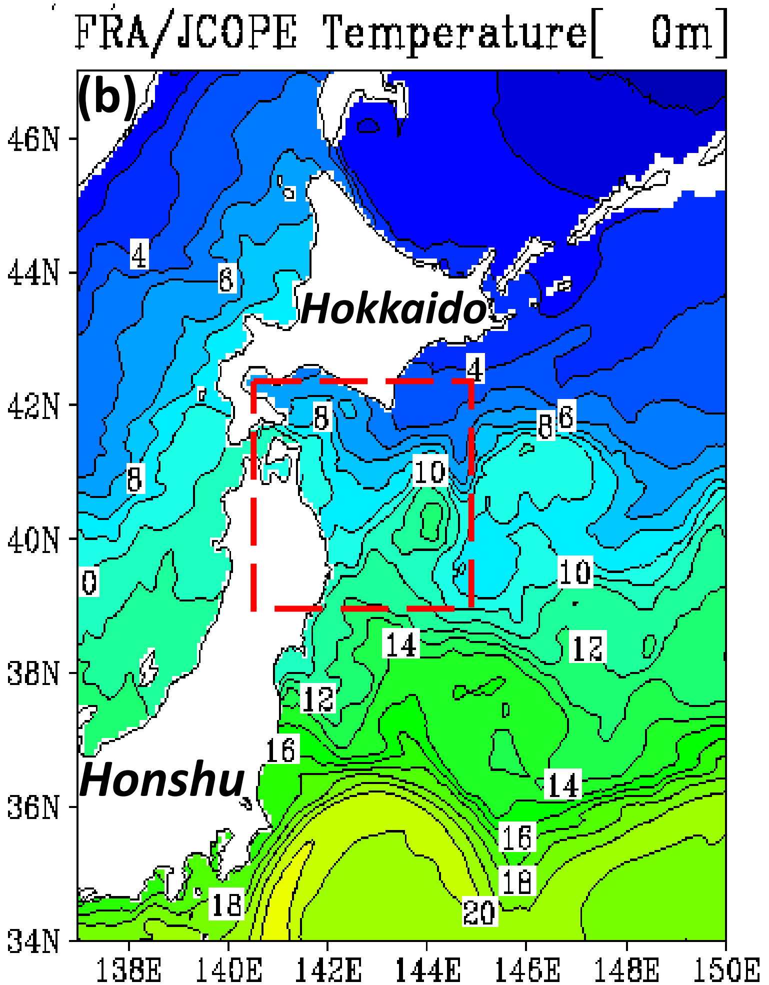

PALSAR image acquired on 18 April 2009 at 01:10 UTC; (b) sea surface temperature map for the same day submitted by Fishery Research Association. Red rectangle marks the boundaries of PALSAR image. 1 – warm waters, 2- cold waters , 3 – warm streamer, 4-6 and 5 – cold small eddies, 6 – warm small eddy.

Aqua MODIS. 19 April 2009, 03:40 UTC

(c) Infrared image (31-st channel) and (d) chl-a field

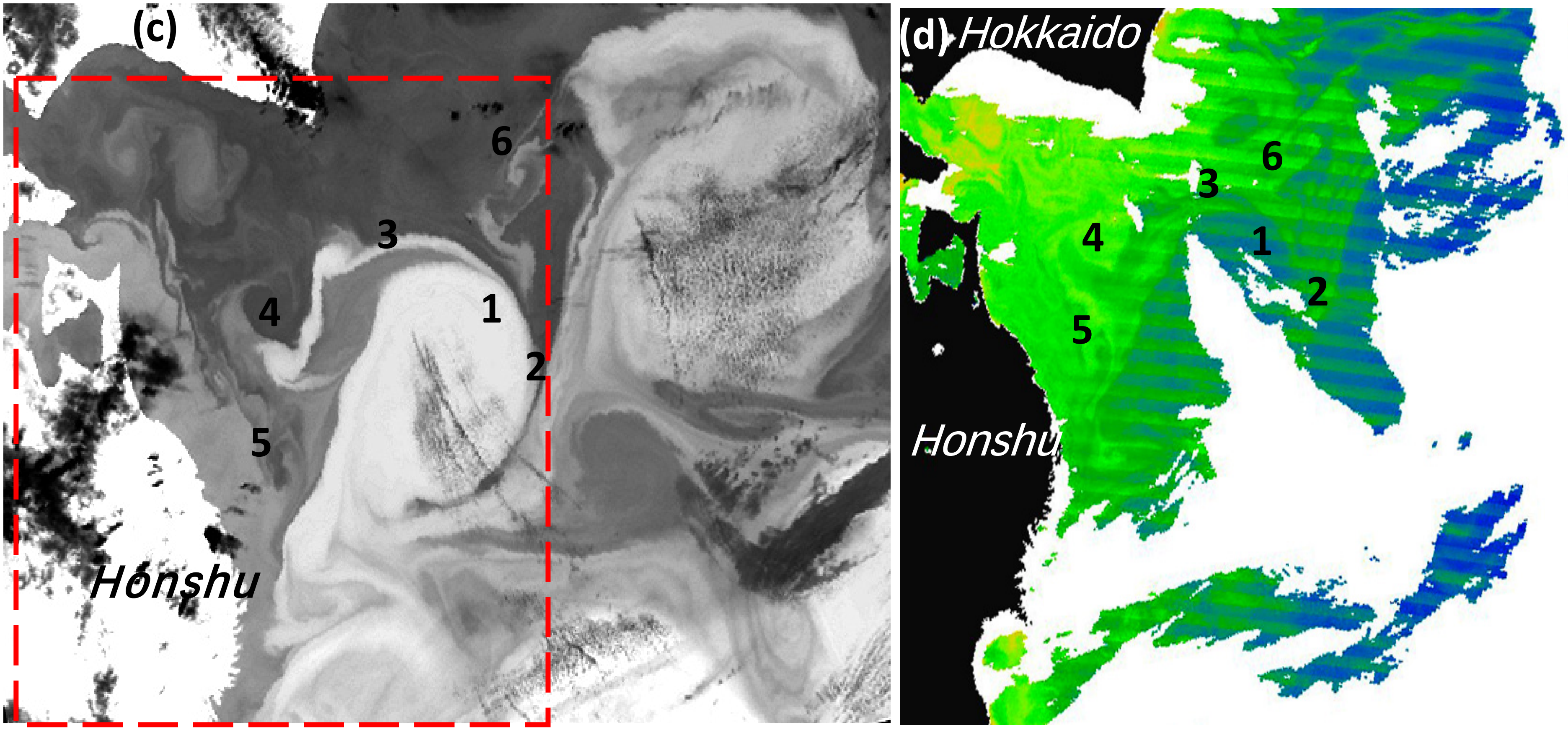

1 – warm waters, 2- cold waters , 3 – warm streamer, 4 and 5 – cold small eddies, 6 – warm small eddy. Red dotted rectangle marks the boundaries of PALSAR image.

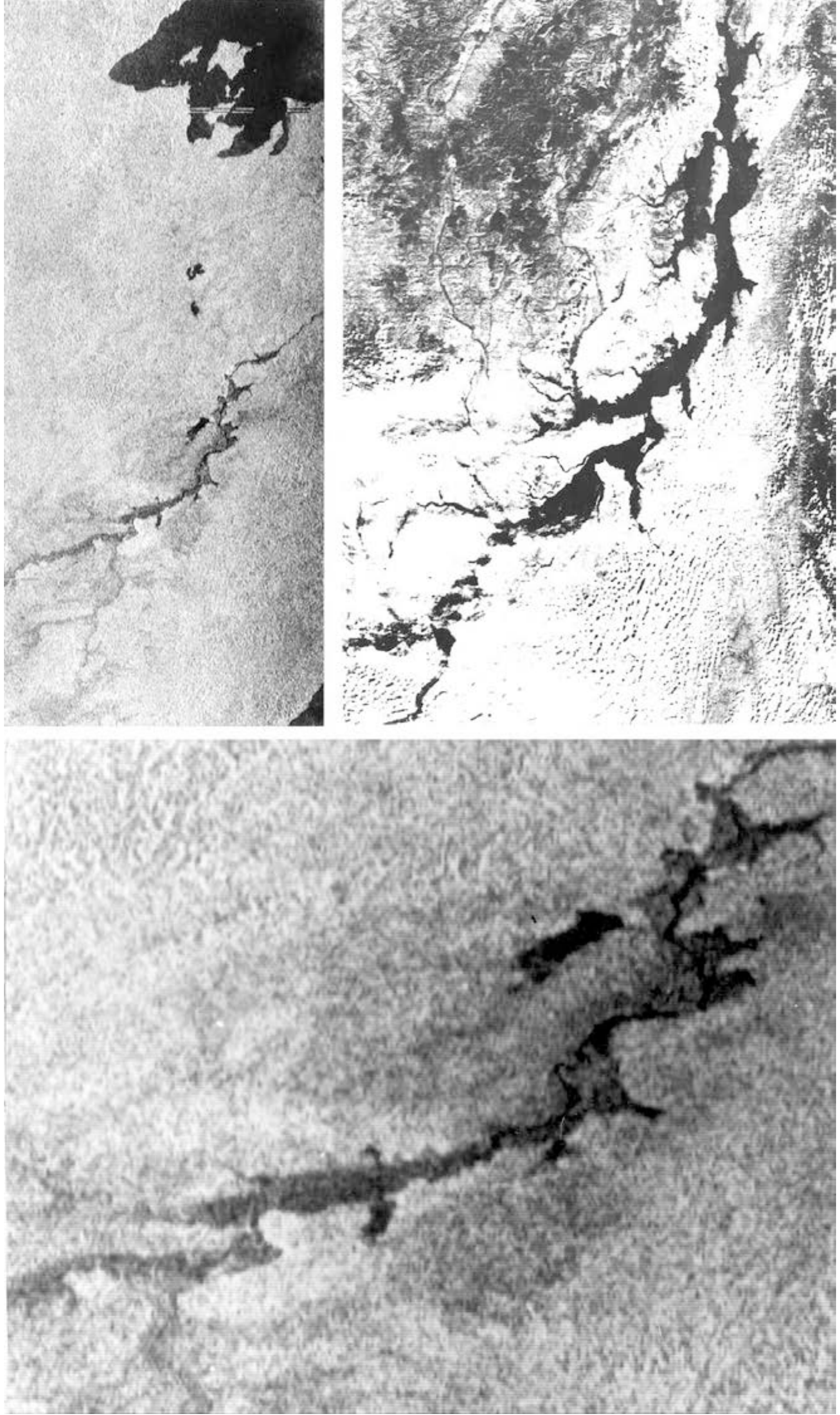

Rain flood in Amur area on radar and visible images

On possibility of usage of passive microwave techniques to control dynamics of flooding . In: Remote Estimates of areas total moisture content . 1984. Moscow. P. 97-102.

Use of satellite data in study of Amur River rain flood. Water resources. 1988. 1988. No. 5. P. 102-107.

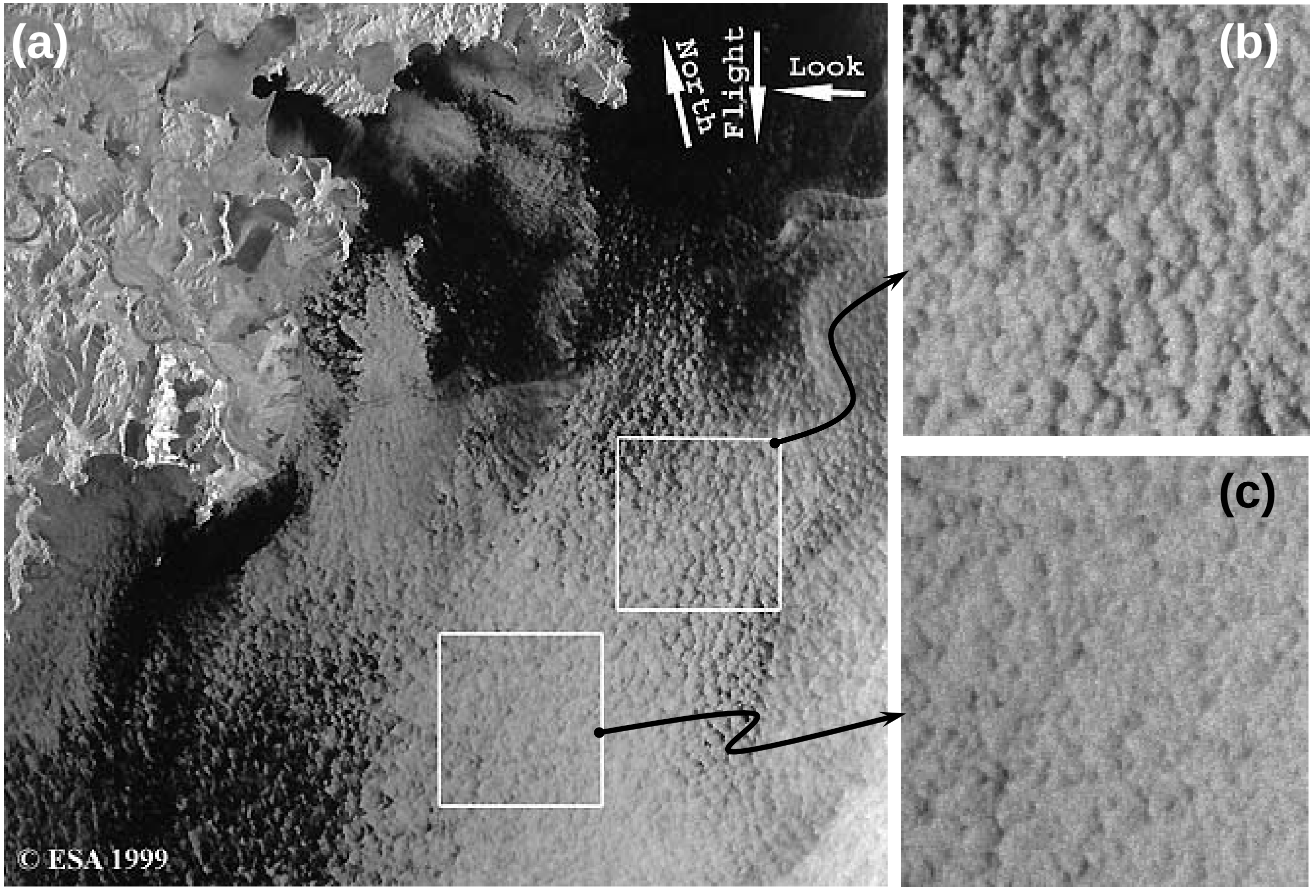

ERS-2 SAR image of the Japan Sea. 20.03.1999, 02:03 UTC.

Sea surface temperature t_s increased from about 1°C (at the bottom left) to about 3°C at the right of the image. Coastal stations reported the air temperature t_a = – (2-5)°C.

Brightness variations are due to cellular convection in the boundary layer of the atmosphere 90 km x 90 km south of Vladivostok, pixel size of 100 m. White squares outline the enlarged fragments with a pixel size of 50 m. The cloudless weather with weak winds was observed during SAR sensing.
The mesoscale convective cells of 1-2 km size resulting from unstable atmospheric conditions (t_a - t_s < 0°C) manifest themselves on the image as the regulated brightness (sea surface roughness) variations which generate so named mottle structure. Convection looks less organized and the cell size is larger in the fragment (*c*).
The average σ° is –12.6 dB for area (b) and –11.7 dB for area (c). The wind speed values were calculated with a CMOD4 model [*Stoffelen and Andersen*, 1997]: W_{avr} = 2 m/s and 2.5 m/s. Wind direction (320°) was determined from the streak orientation at the top of the image near a coast.

cyclones

Passive microwave at λ = 0.8 cm (a), X-band radar (b) and visible (c) images taken on 9 March 1996

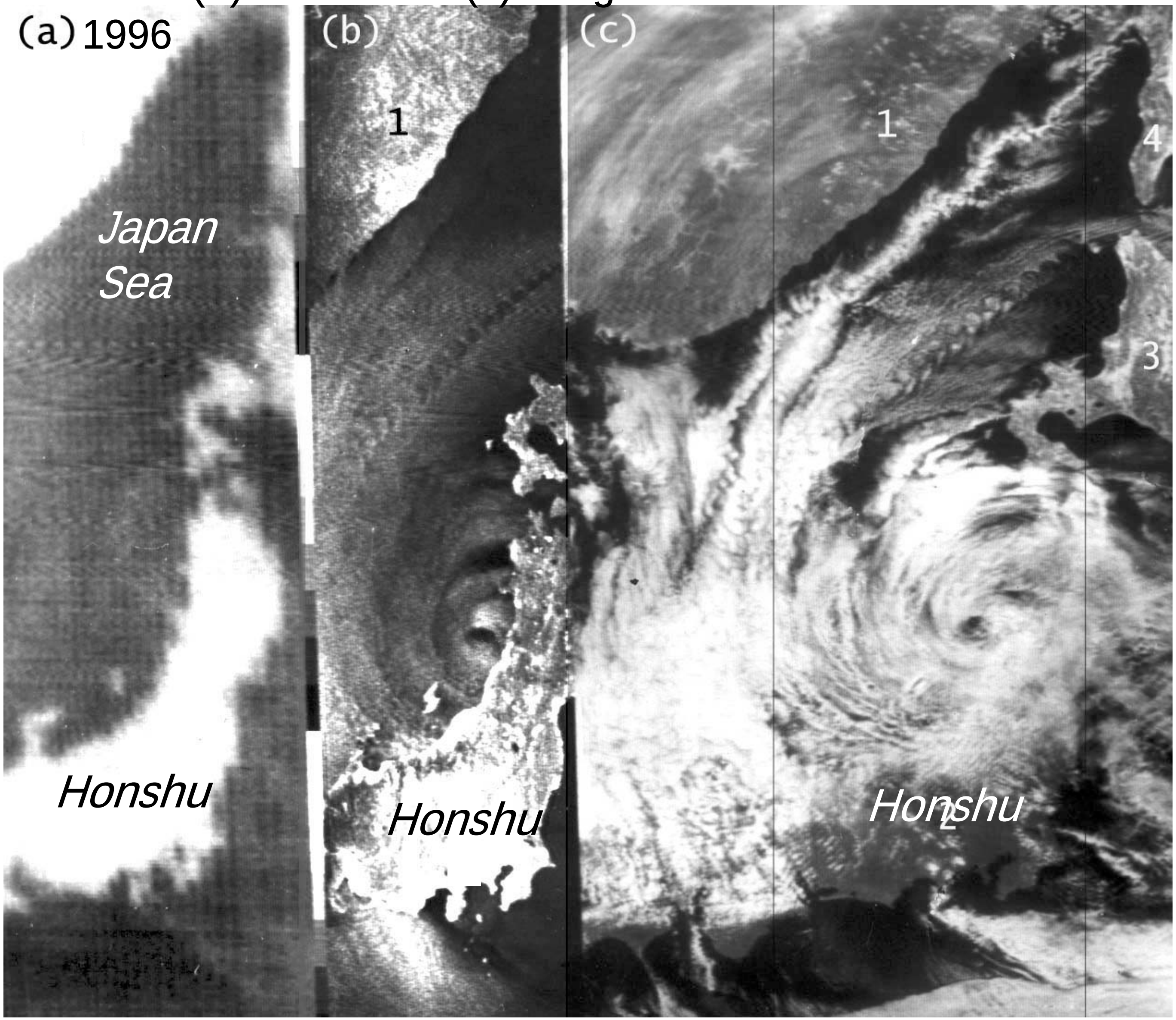

24 December 1994

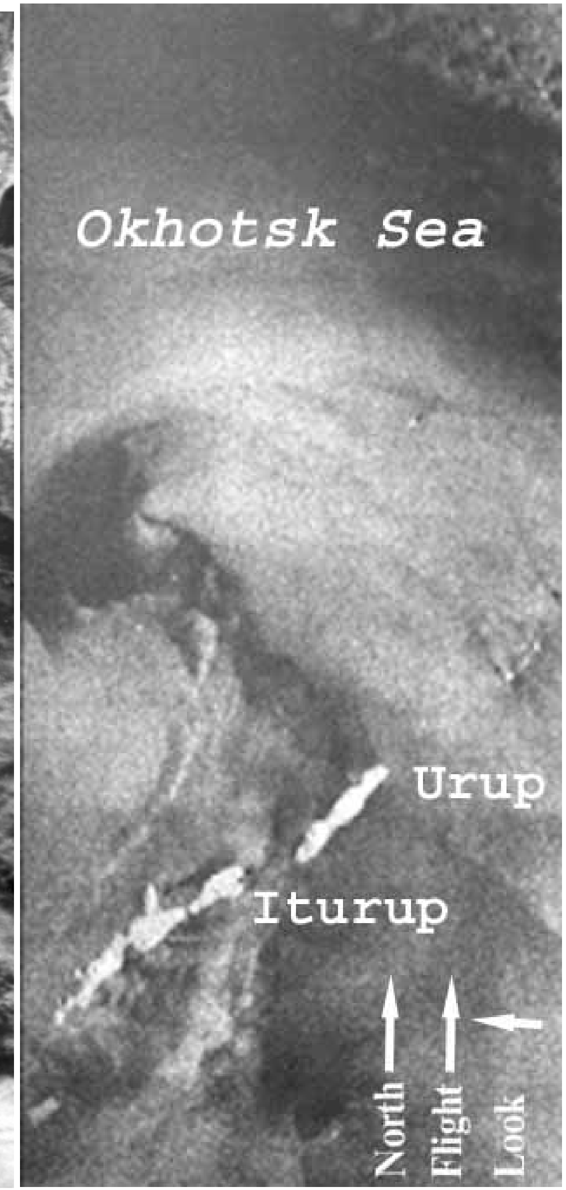

Cell and roll convection

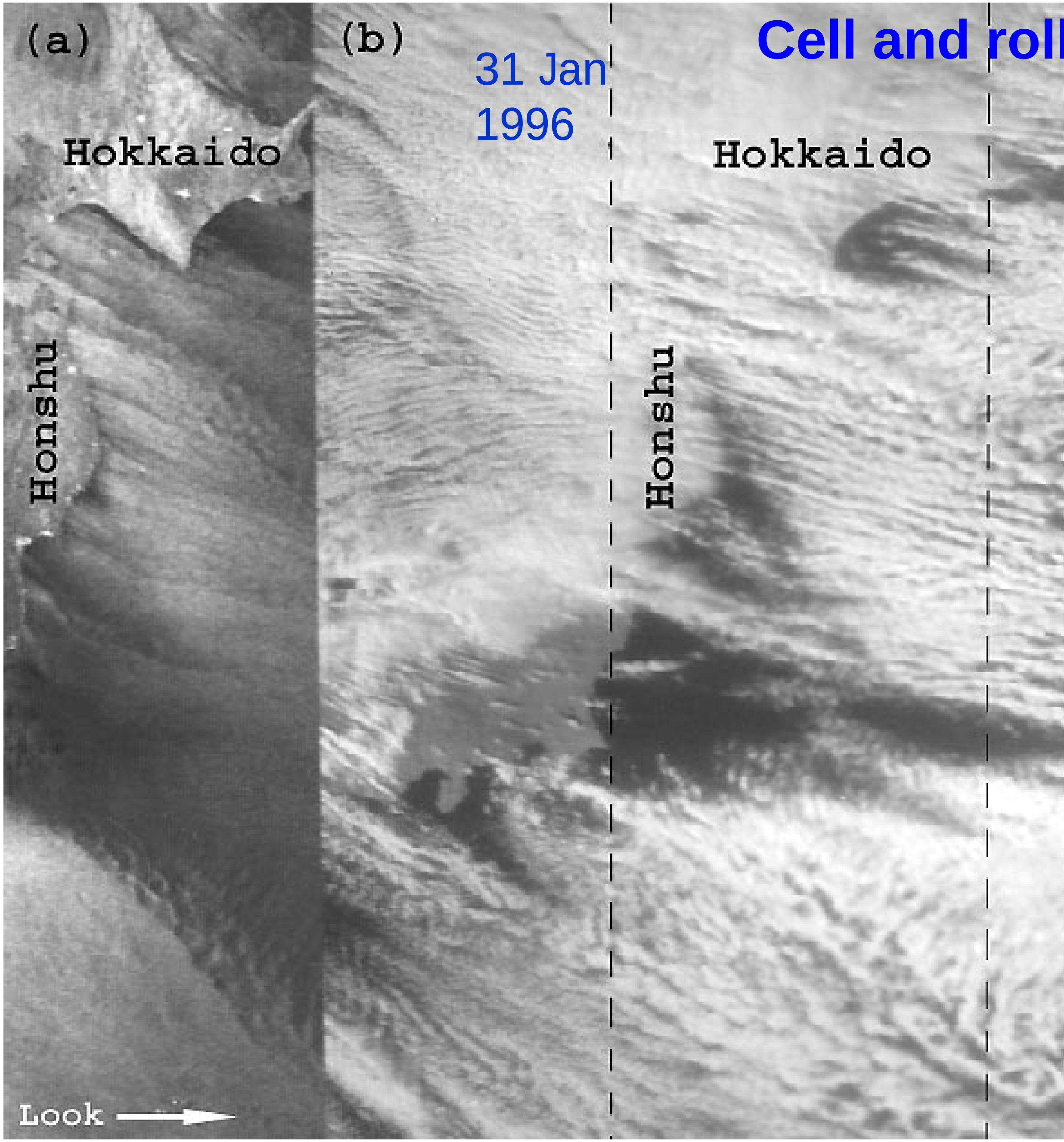

Okean-7 RAR (a) and visible (b) images of the Pacific Ocean east of Japan during the cold air outbreak

27 Jan 2000

8 February 2000

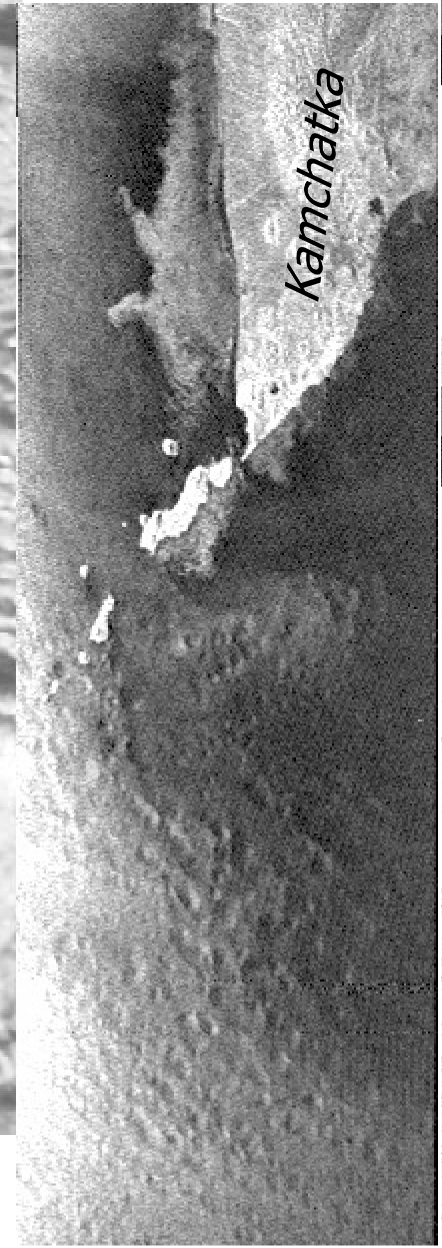

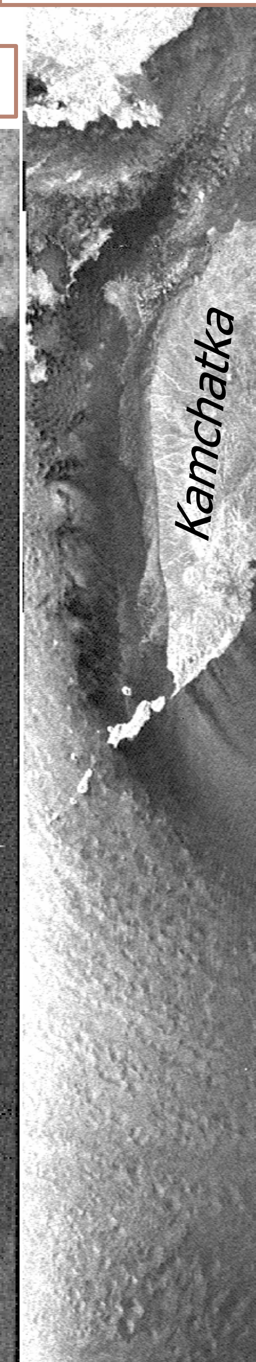

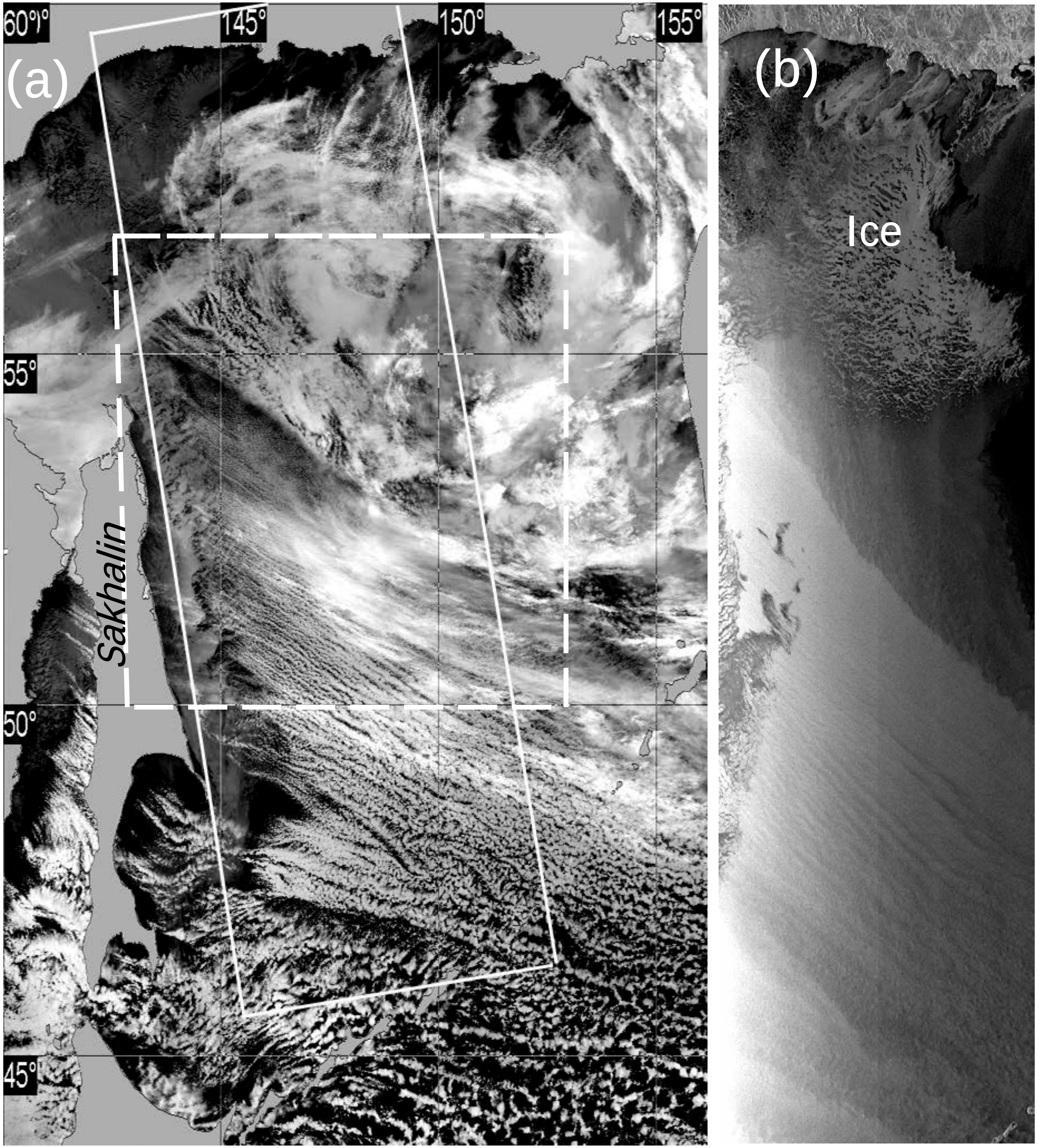

convectio
n

Okhotsk Sea
10 January
2007

Mesoscale convective rolls and cells on satellite images acquired by (a) NOAA-17 AVHRR at 11:39 UTC and (b) Envisat ASAR at 11:46 UTC

Roll convection. 10 January 2007

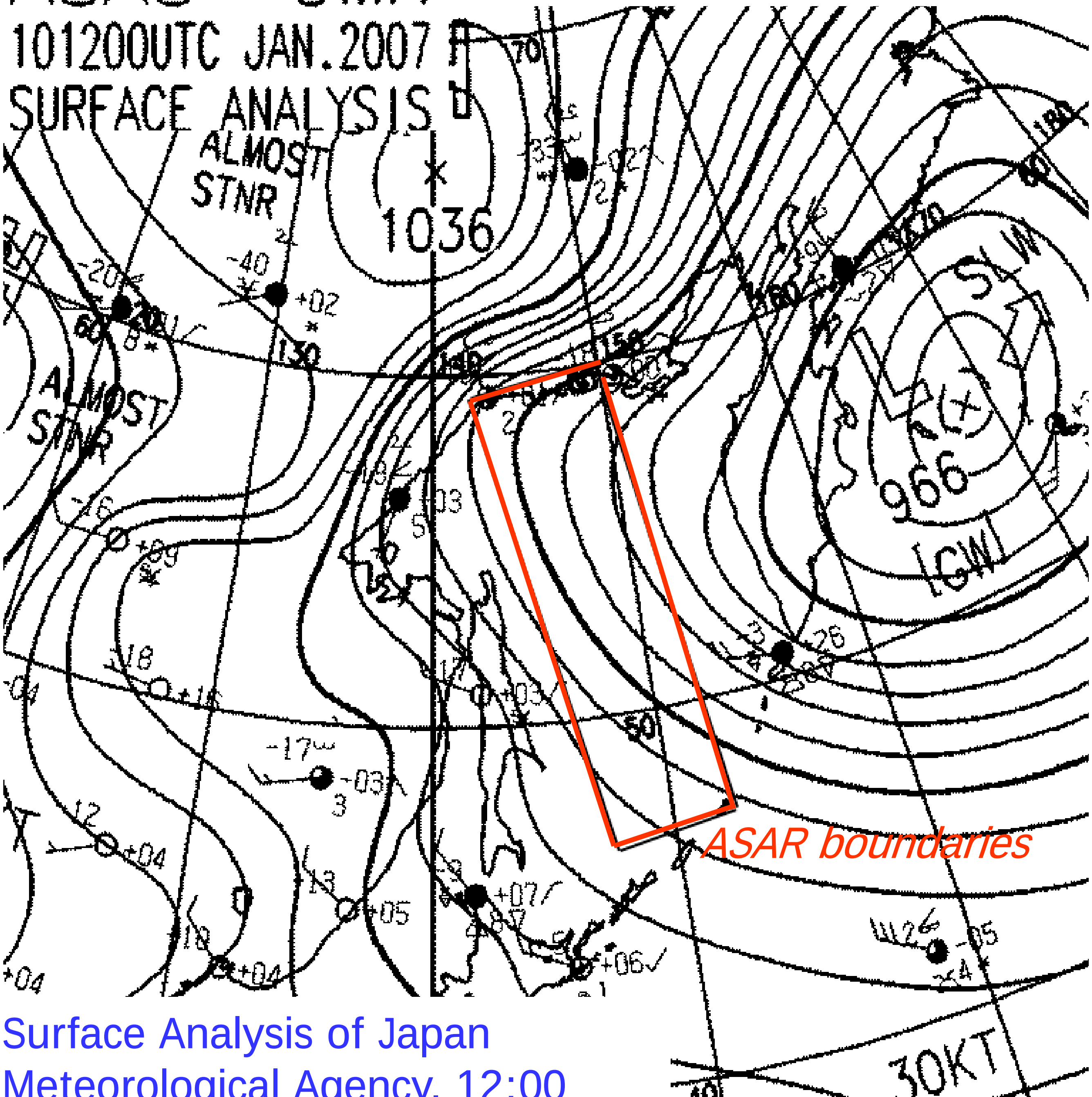

Surface Analysis of Japan Meteorological Agency. 12:00

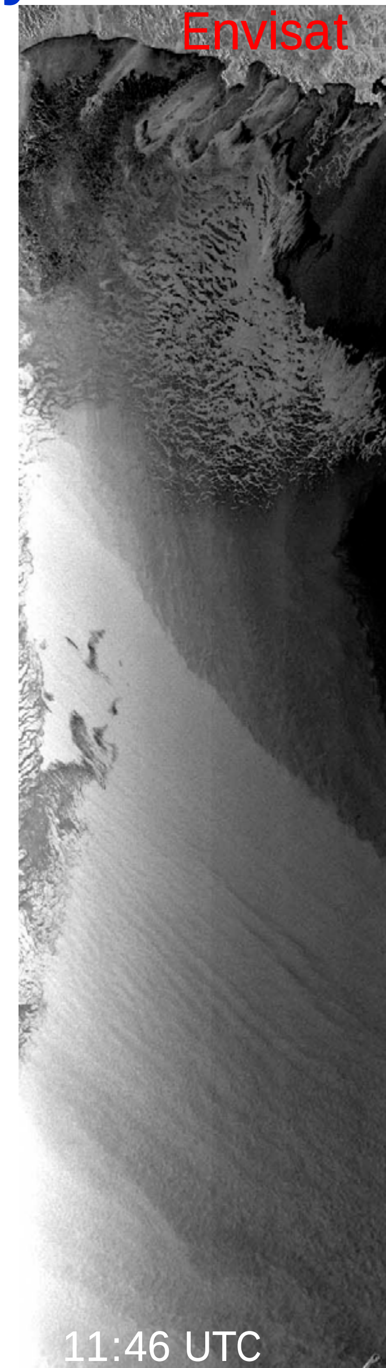

Roll convection. 10 January 2007

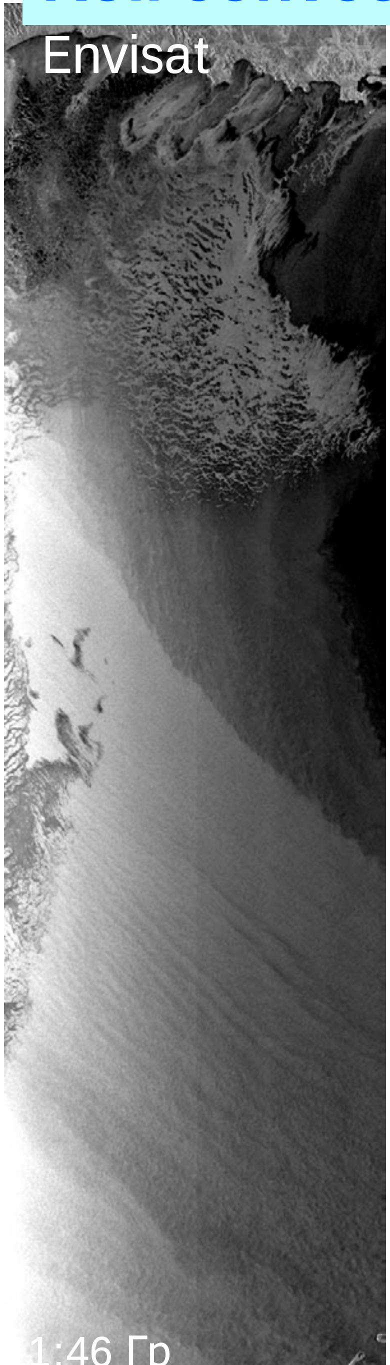

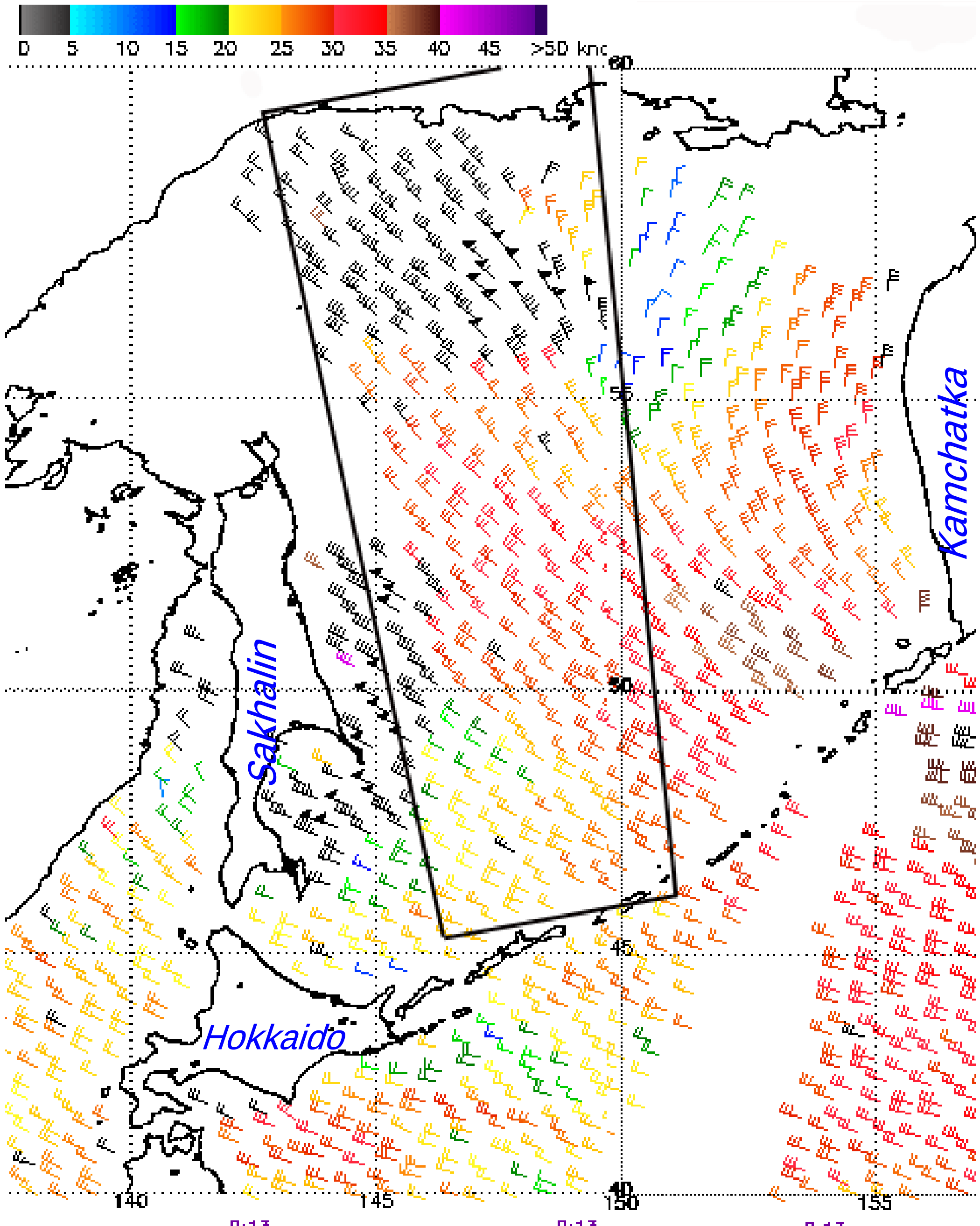

QuikSCAT-derived wind field acquired on 09:13 UTC.

Dark lines mark the boundaries of Envisat ASAR image taken at 11:46 UTC.

Roll convection. 10 January 2007

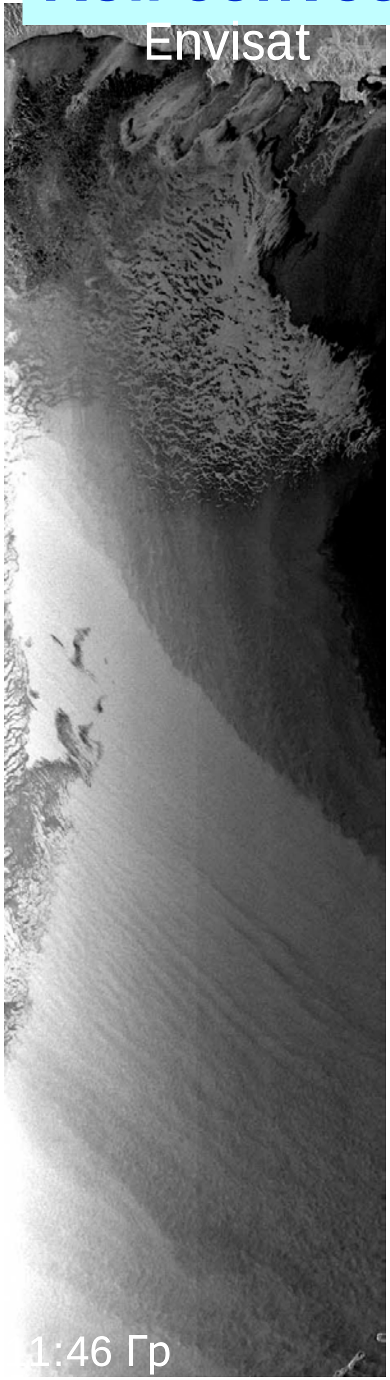

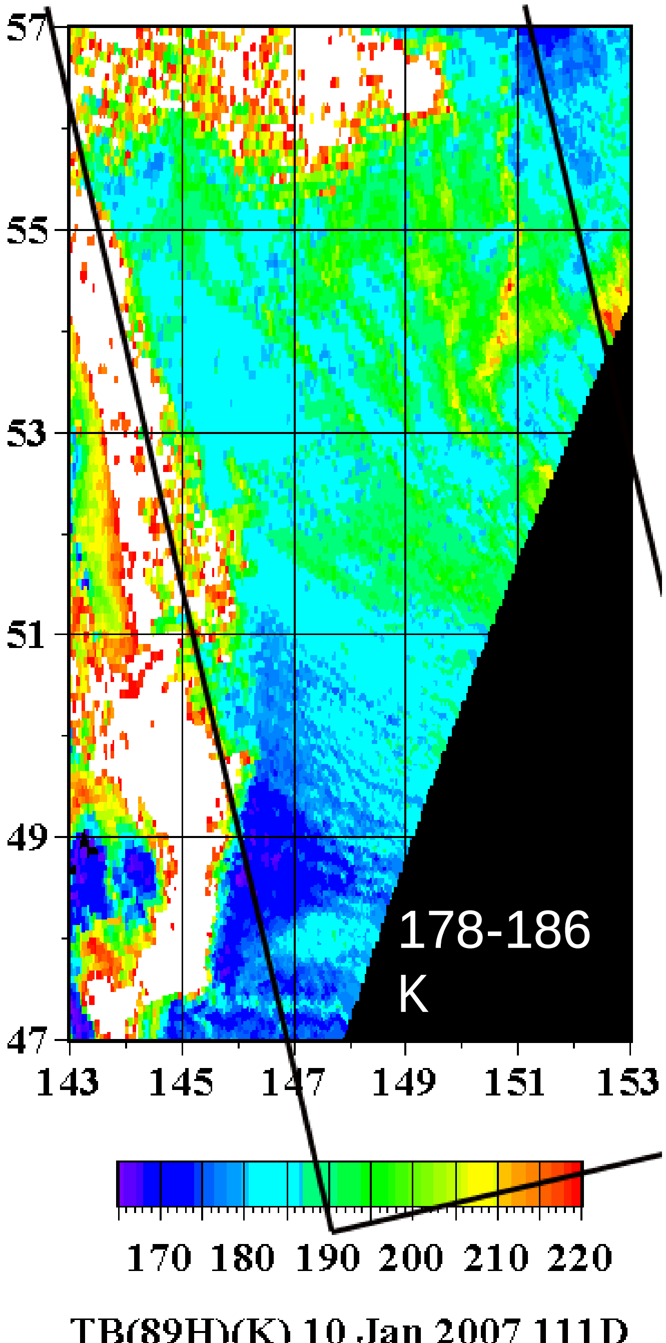

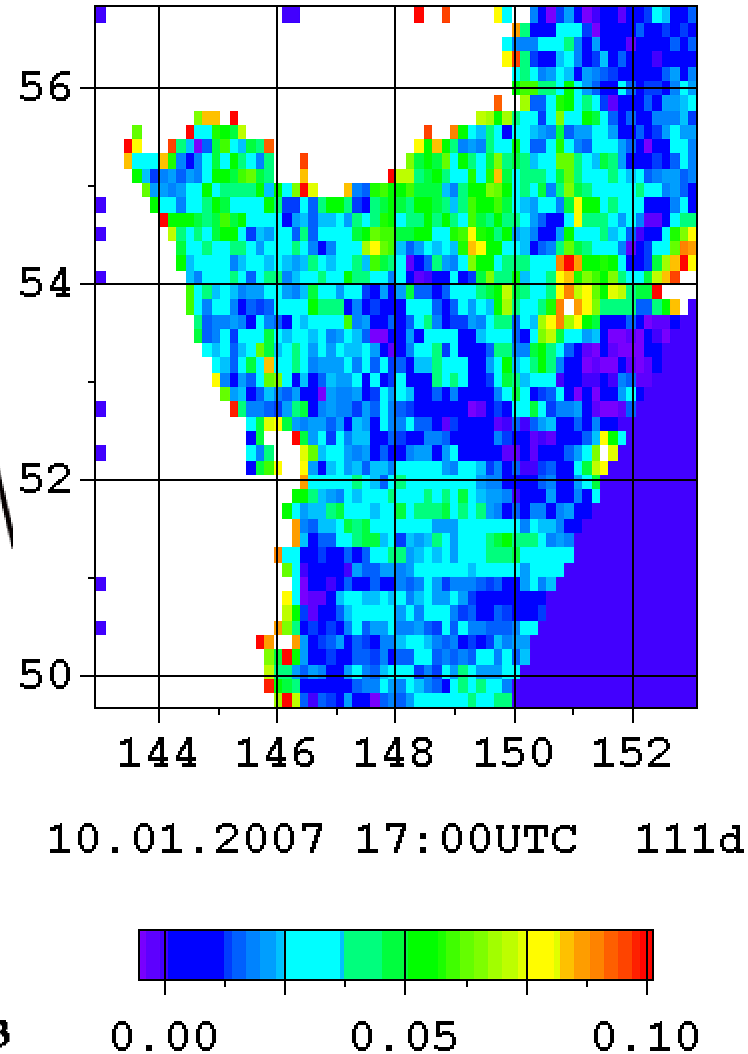

Cloud liquid water, kg/m2

Water vapor content 4-6 kg/m2

Cold air outbreak on 20 December 2002

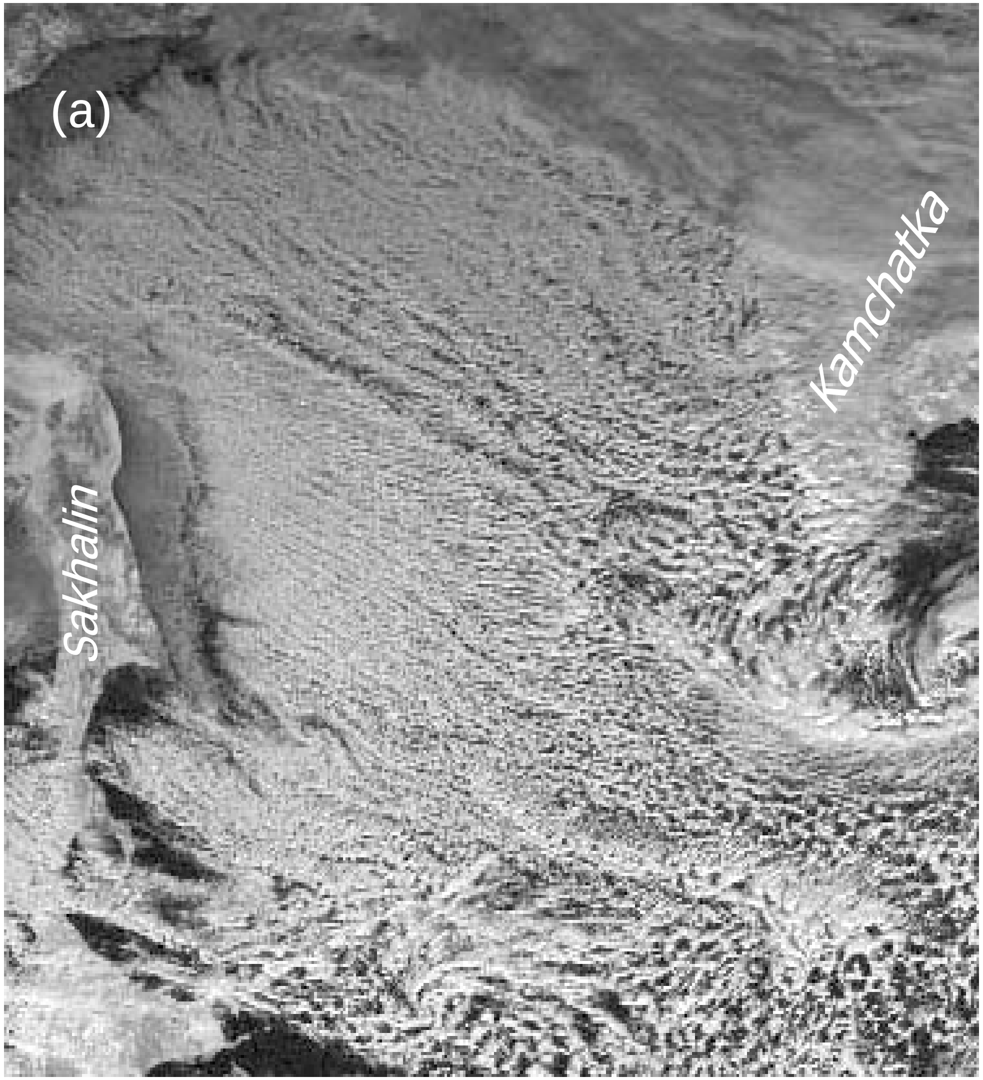

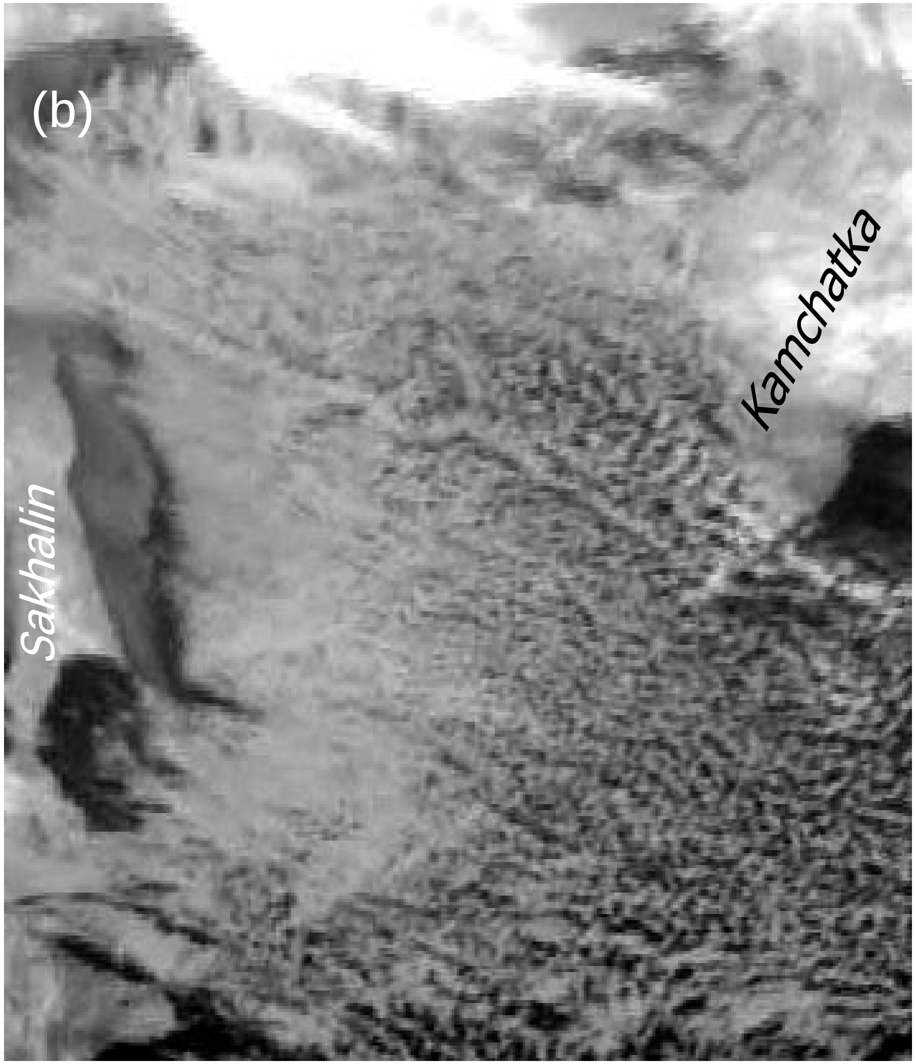

GMS-5 visible (a) and infrared (b) images of the Okhotsk Sea taken on 20 Dec 2002 at 02 UTC (a) and at 12 UTC (b) showing the organization of convection into 2D roll clouds over and downstream of the MIZ of the Okhotsk Sea.

Brightness temperatures at 89 GHz, H-pol during cold air outbreak on 20 December 2002

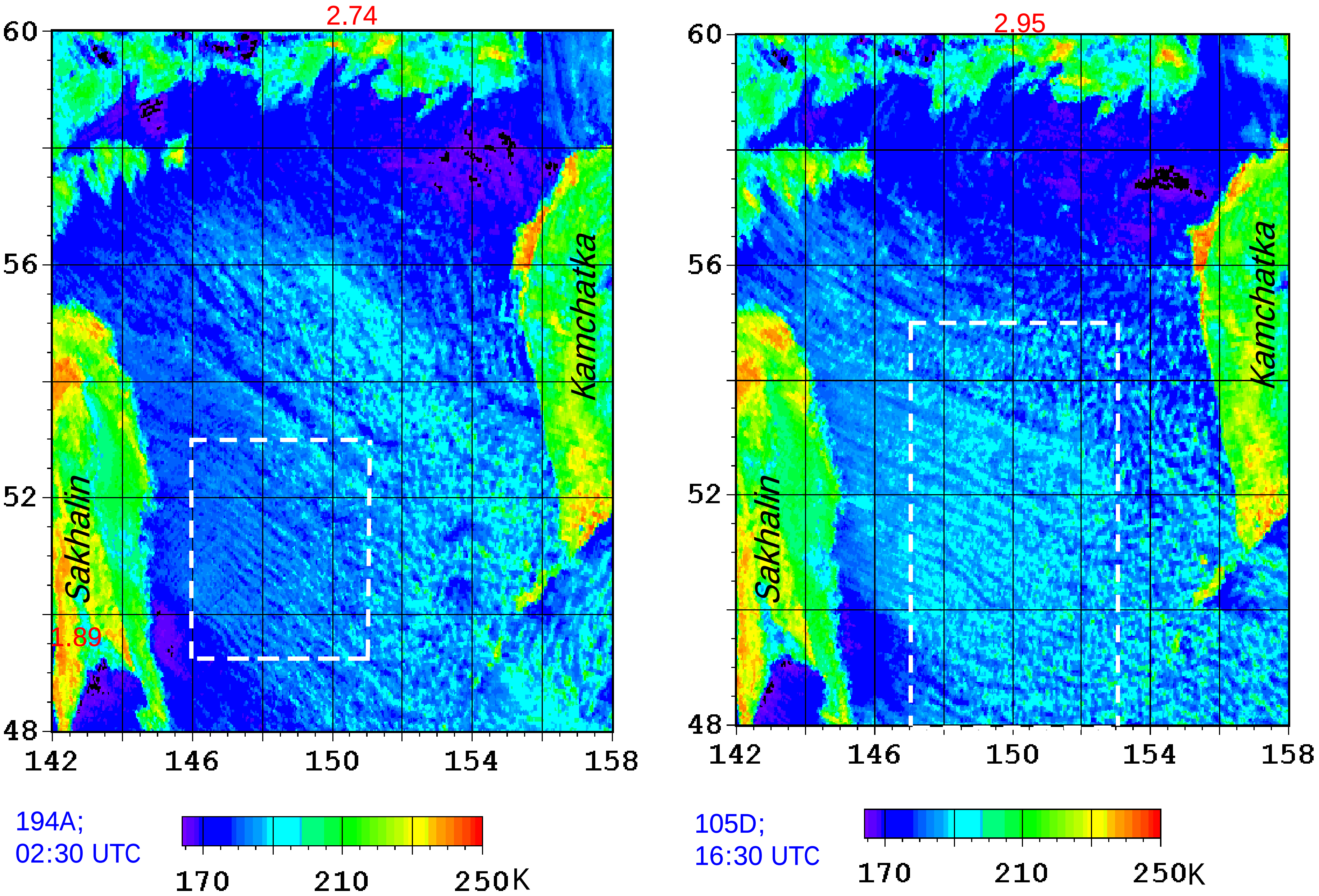

Total water vapor content

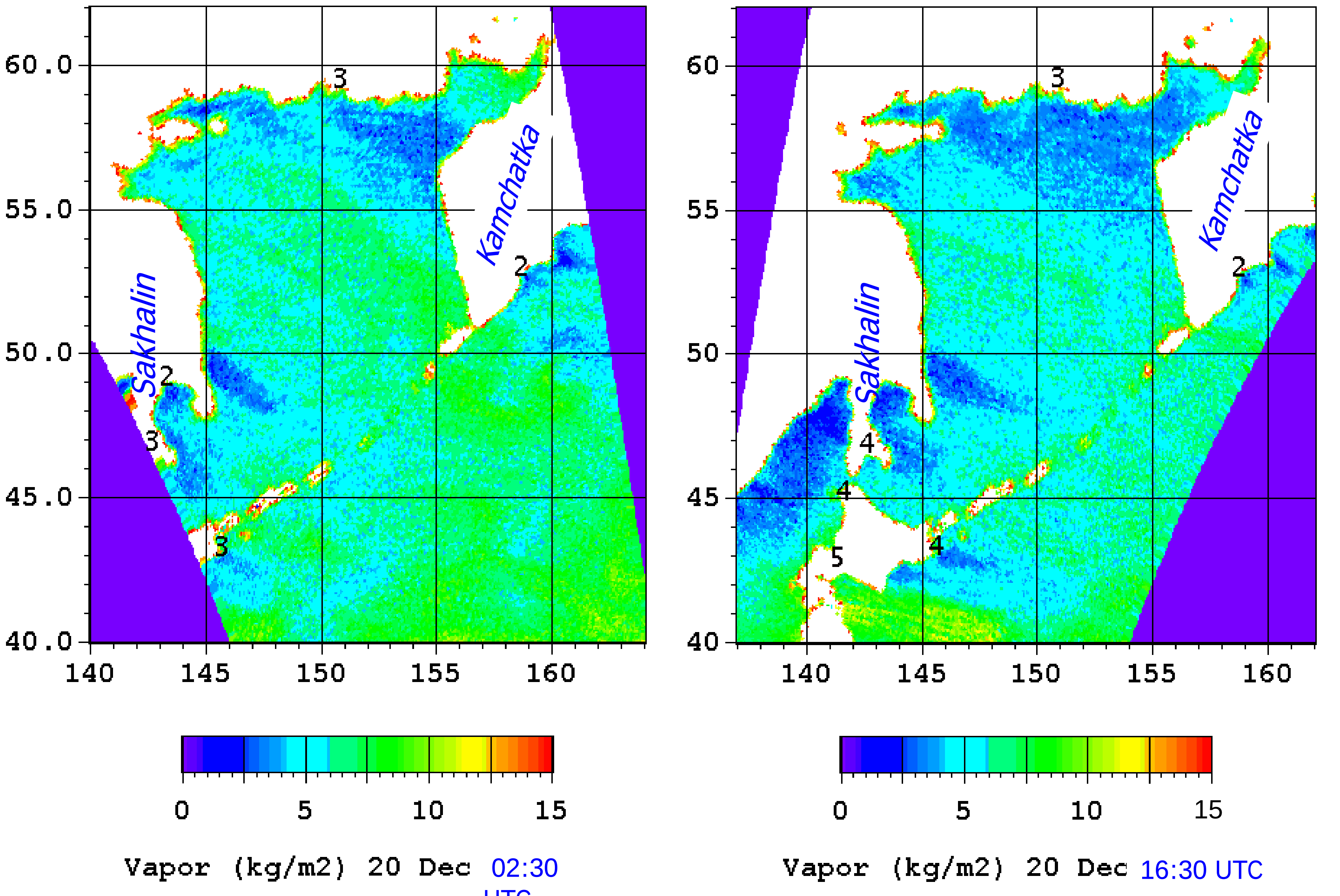

ALOS
PALSAR

26 January
2008 01:02 UTC

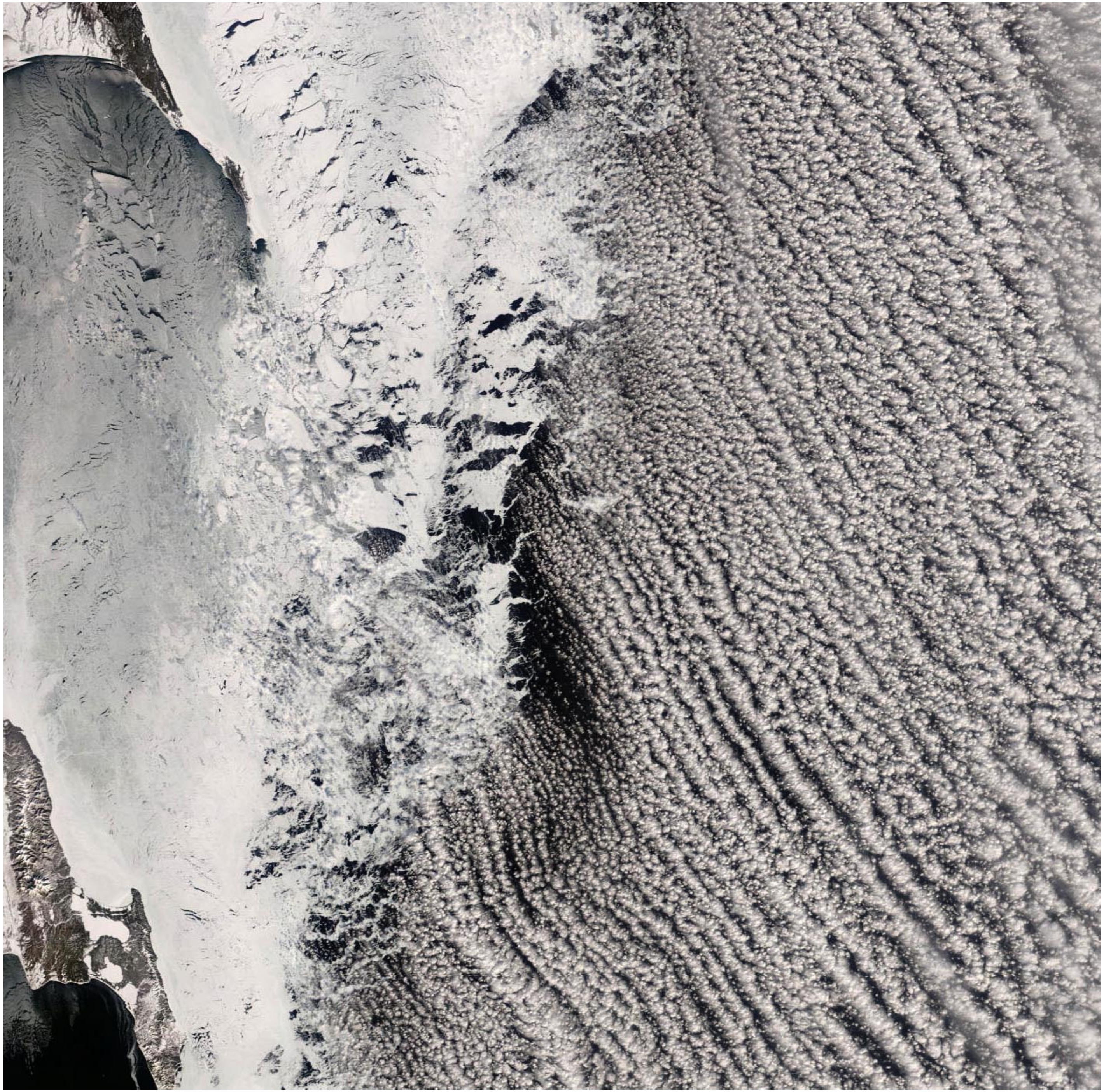

Terra MODIS

01:10 UTC

QuikSCAT-derived wind at 09:30 UTC

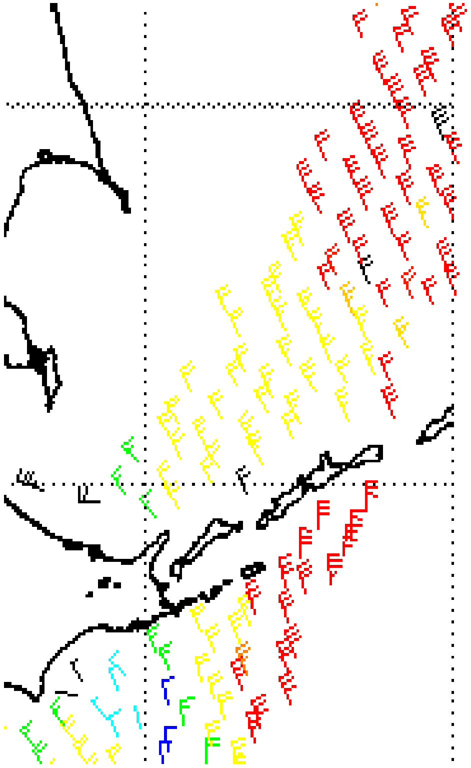

ALOS PALSAR

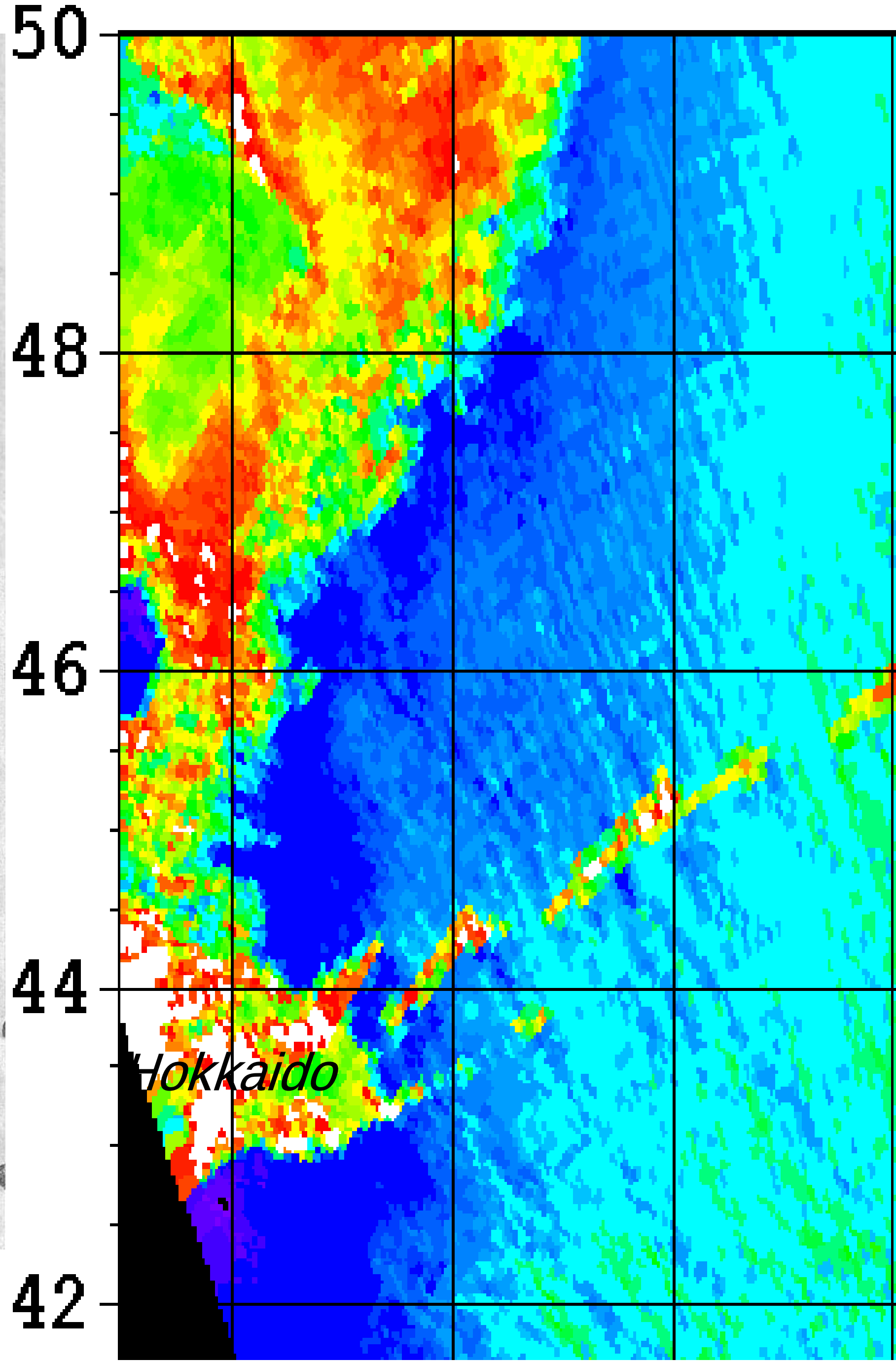

Roll convection

Aqua AMSR-E

26 January 2008

02:30 UTC

Numerical model

The CReSS (Cloud Resolving Storm Simulator) model was developed at Nagoya University. Prognostic variables are 3D velocity components, perturbation pressure and potential temperature as well as the mixing ratio for water vapor, and five species of hydrometeors (rain, cloud water, cloud ice, snow and graupel) (Tsuboki and Sakakibara, 2002). The model has been successfully used to simulate convective roll clouds during a cold-air outbreak over open water (Liu, A. Q., Moore, G. W. K., Tsuboki, K., and Renfrew, I. A.: 2004, 'A High-resolution Simulation of Convective Roll Clouds during a Cold-air Outbreak', *Geophys. Res. Lett.* 31, L03101, dio:10.1029/2003GL018530.

The model domain used in these simulations was 400 km in the along roll (*x*) direction, 100 km in the cross roll (*y*) direction and 12 km in the vertical (*z*) direction; the horizontal grid interval was 500 km. In the vertical, grid stretching was applied with the interval varying from 25 m near the surface to approximately 1 km near the top of the top of the domain. This resulted in a computational grid that was 800×200×60 grid points In the *x* direction, the first 50 km of the domain was specified to be land with a fixed temperature of −23^{o}C; the next 100 km was specified to be the sea-ice zone; while the remaining 250 km was specified to be open water with a fixed SST of 3^{o}C.
A.Q. Liu, G.W.K. Moore, et al. The effect of the sea ice zone on the development of boundary-layer roll clouds during cold air outbreaks. *Bound.-Layer Meteorol (2006) 118: 557–581.*

model

Development of boundary-layer roll clouds

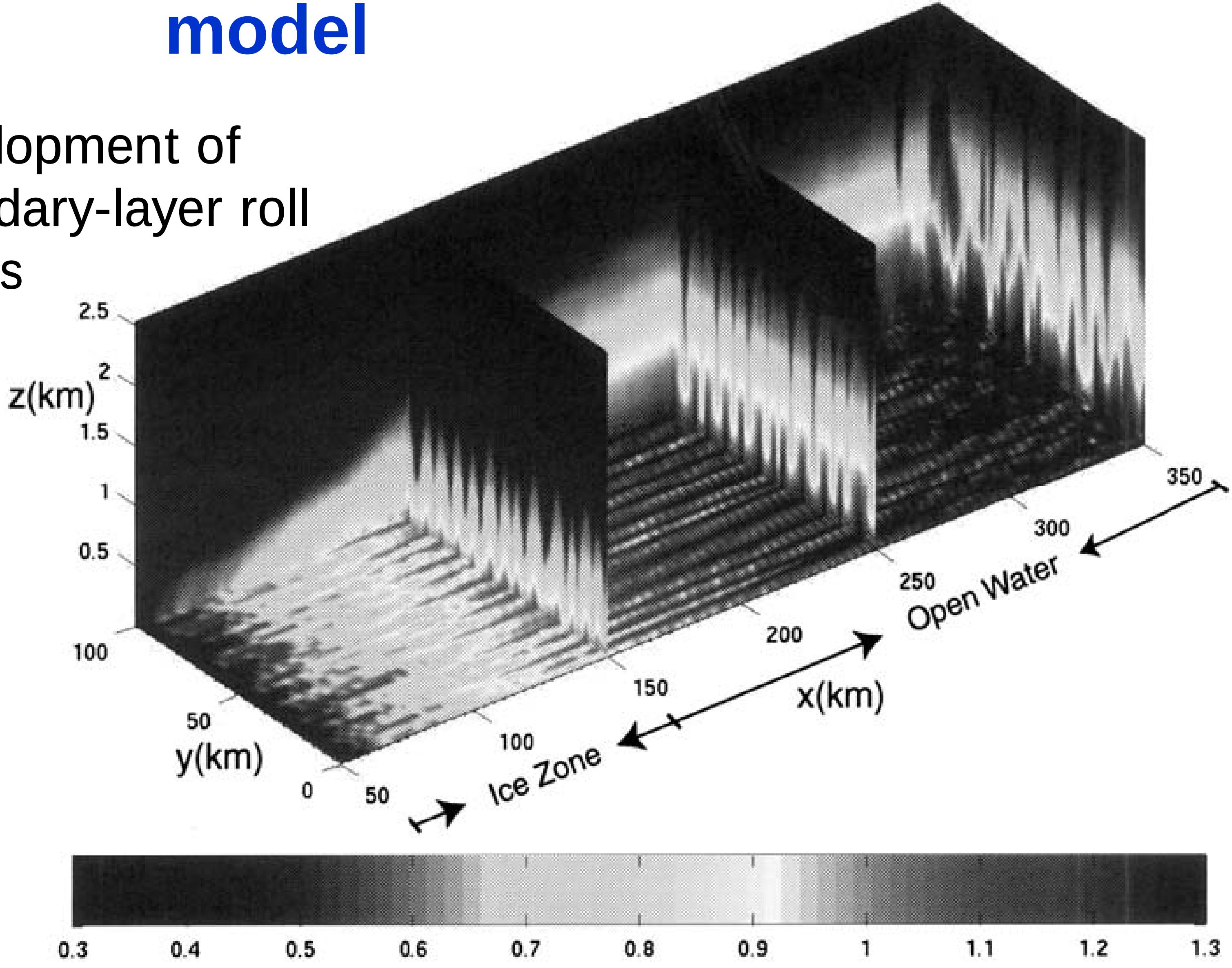

Three-dimensional display of the specific humidity (g/kg) field from the simulation at 10 h. The x–z plane is at y = 100 km; the x–y plane is at z = 25 m; three y–z planes are at x = 150 km, x = 250 km and x = 350 km separately.

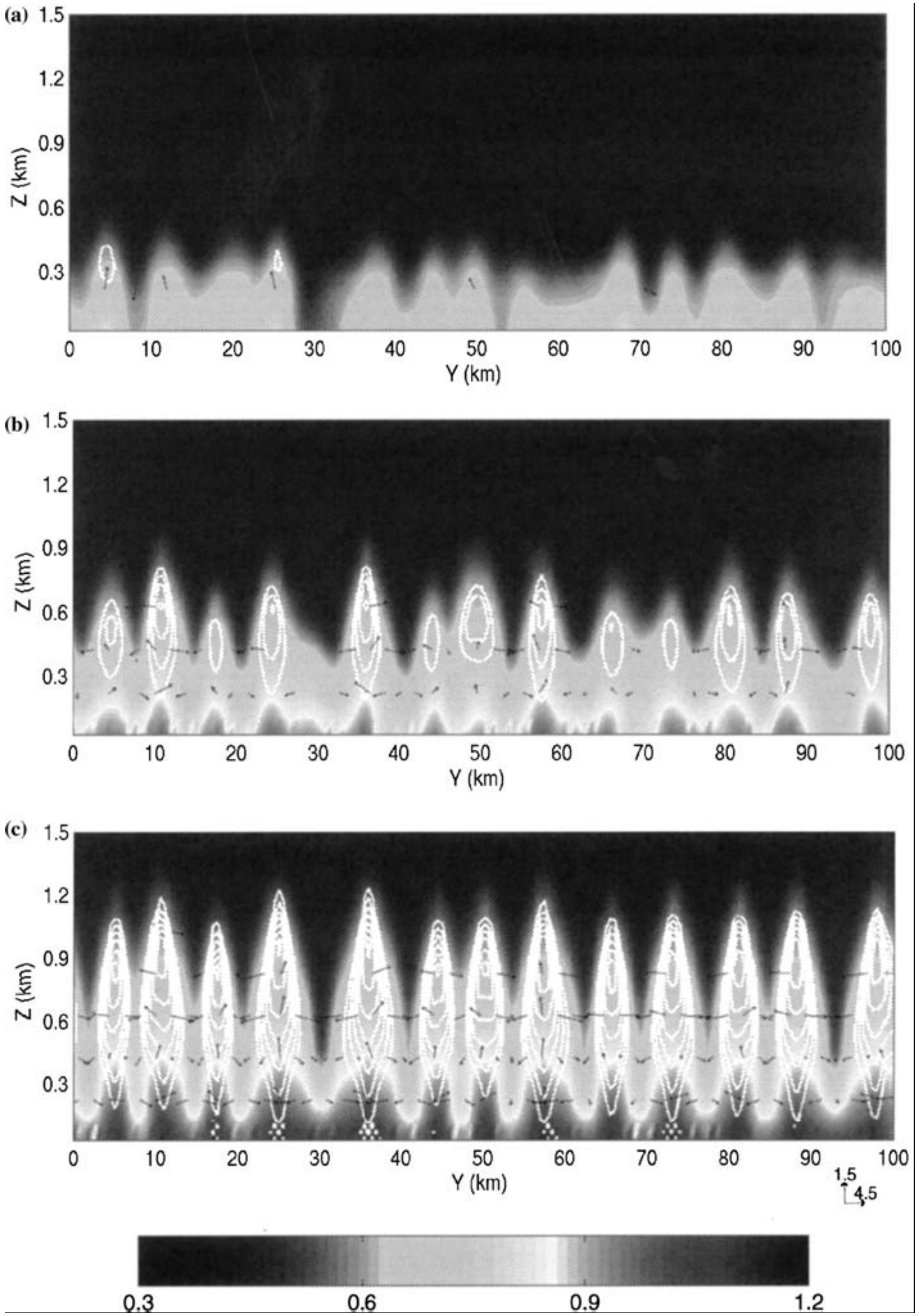

Numerical model

Secondary flow development at 10 h over the sea-ice zone at (a) $x = 90$ km (45% sea ice), (b) $x = 130$ km (18% sea ice) and (c) $x = 170$ km (open water). The specific humidity field (g/kg) is shaded, the cloud liquid water mixing ratio (g/kg) is contoured with contour interval 0.05 g/kg and the velocity in the $y-z$ plane is indicated by the vectors (only plotted every fourth grid in y direction and every third grid in z direction with abs

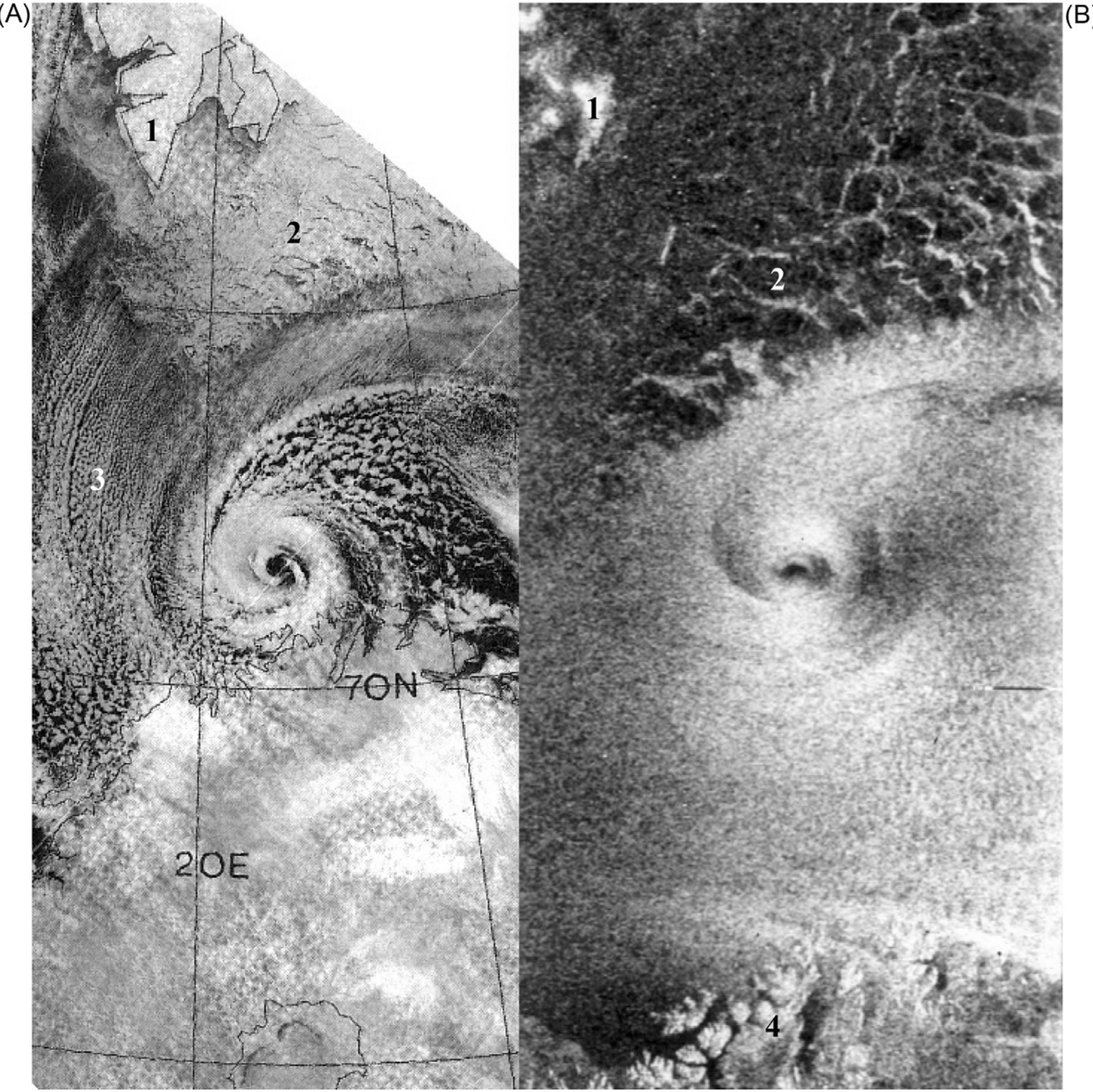

Polar low over the Barents Sea on the images obtained by: NOAA-9 AVHRR (infrared channel) at 0409 UTC on Feb. 26 (A) and Kosmos-1766 RAR at 18:45 UTC on Feb. 27, 1987 (B).

1 - Svalbard,
2 - sea ice,
3 - area of cold air outbreak,
4 - Scandinavian Peninsula

Envisat ASAR images of mesoscale cyclones

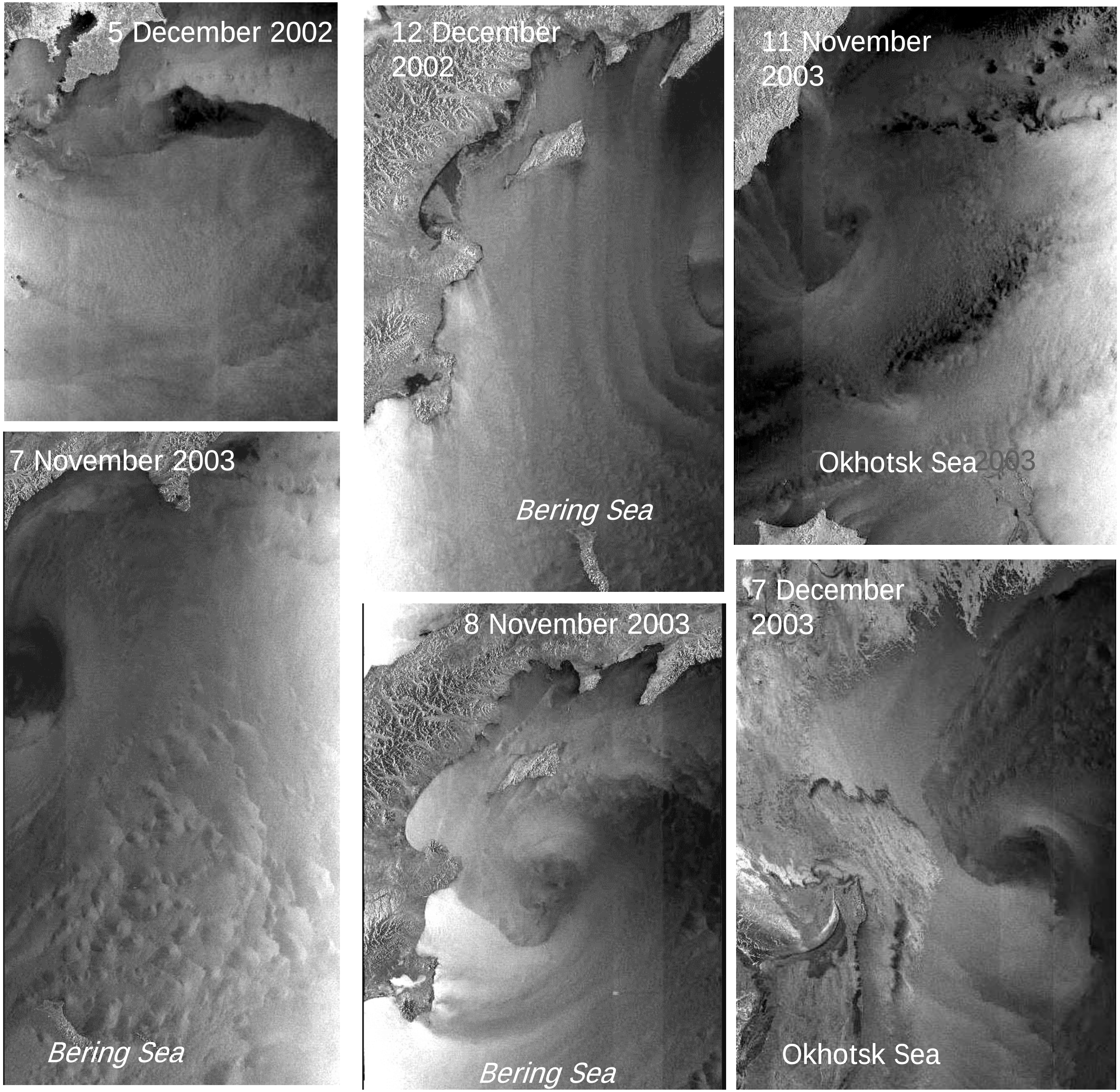

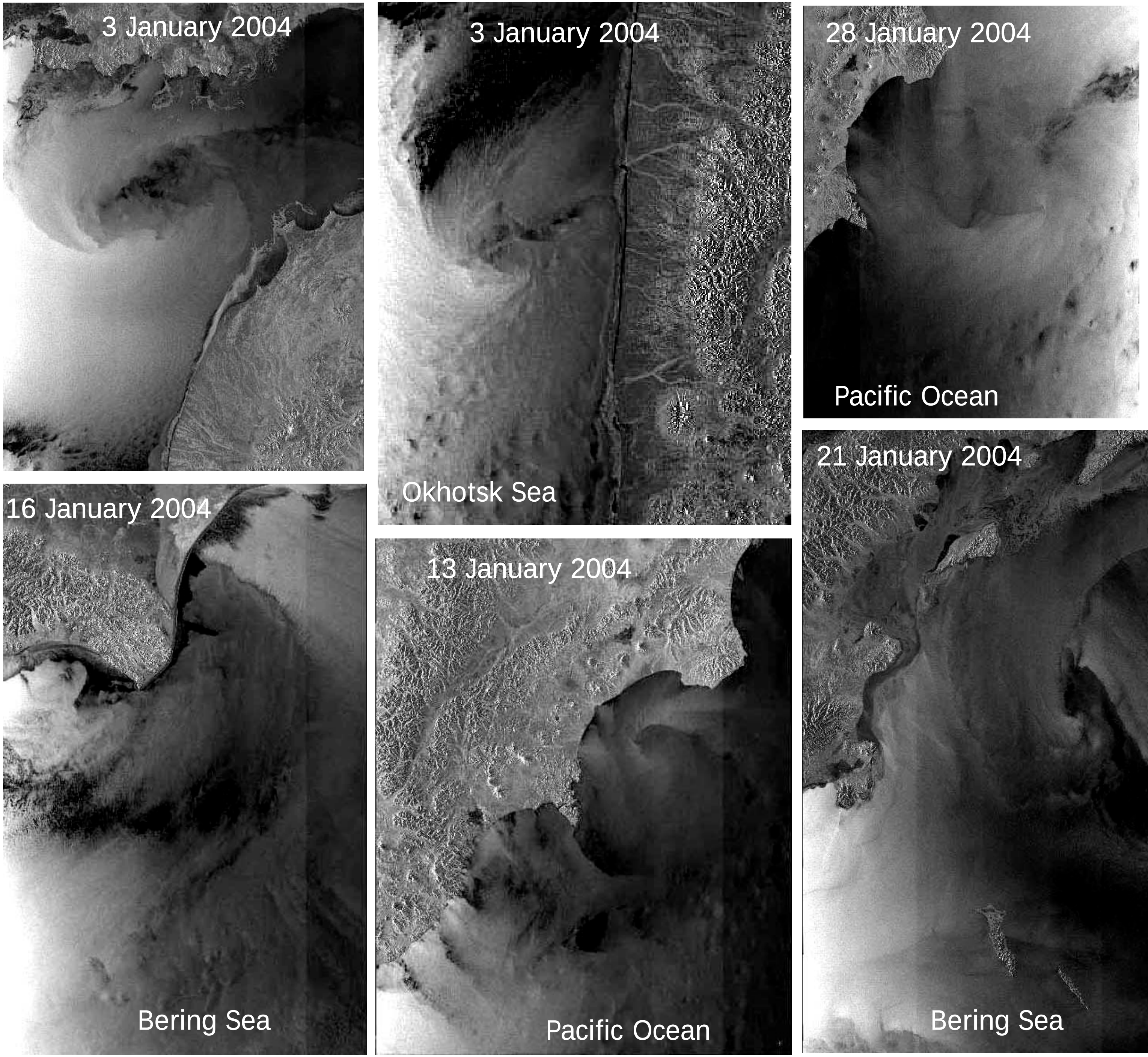

ASAR images of mesoscale cyclones

Envisat ASAR images of mesoscale cyclones

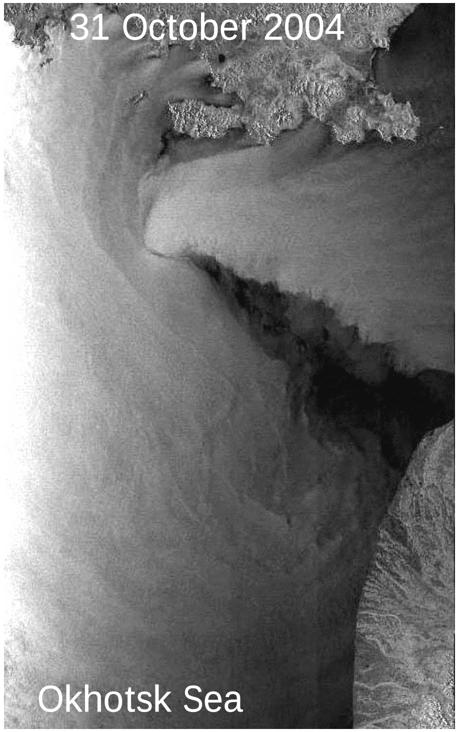

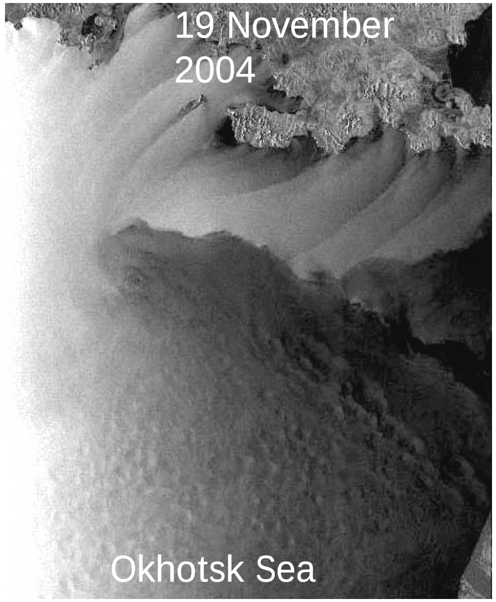

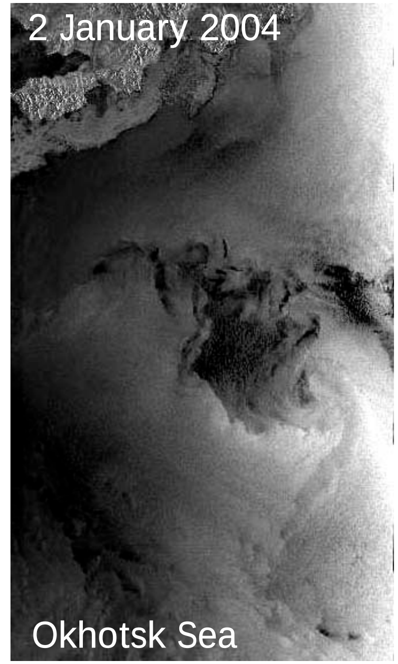

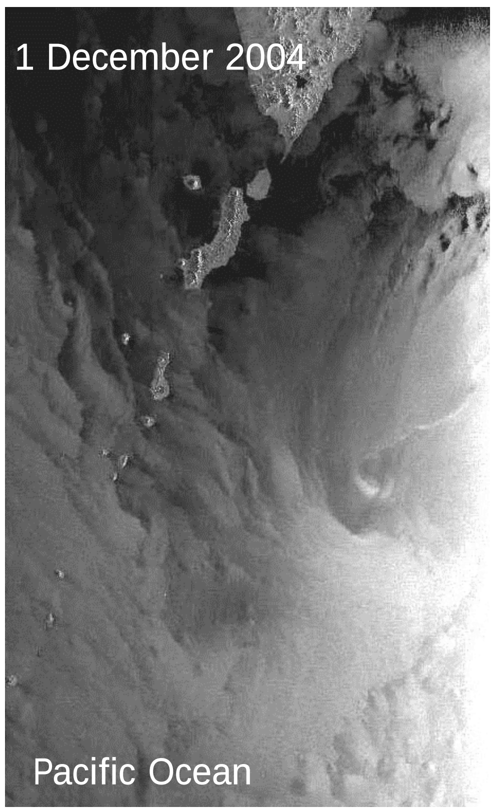

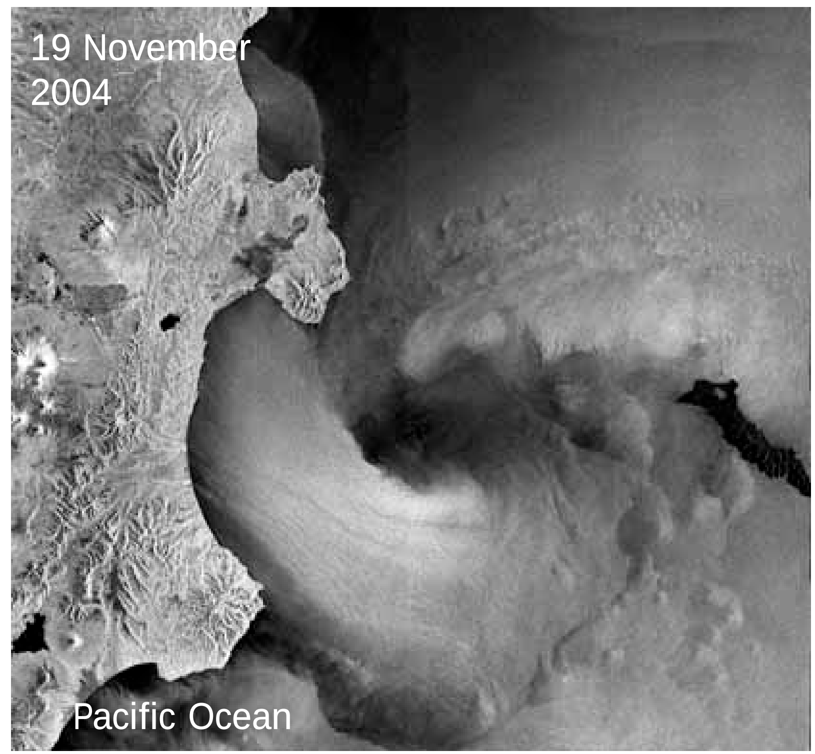

mesoscale cyclones

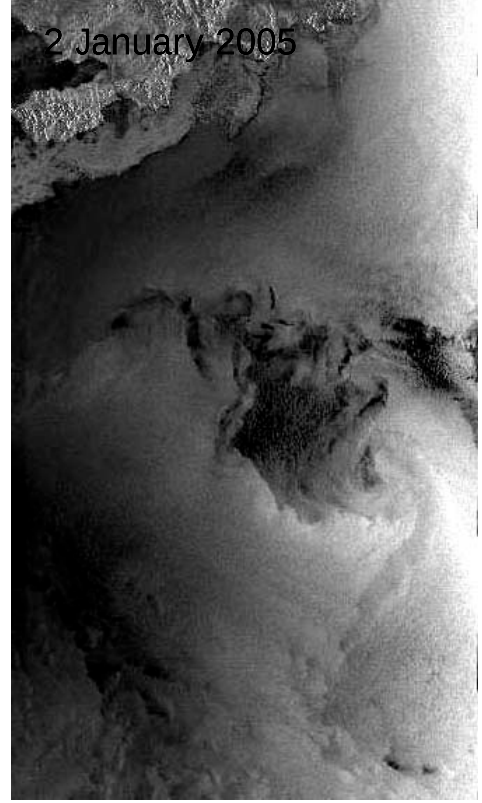

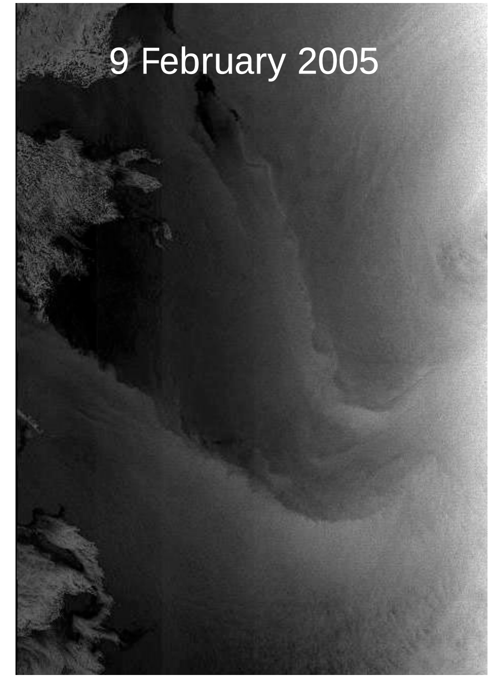

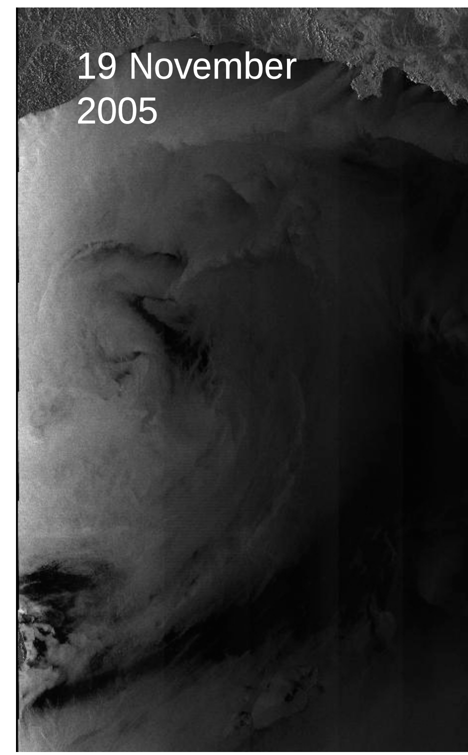

Envisat ASAR images of mesoscale cyclones

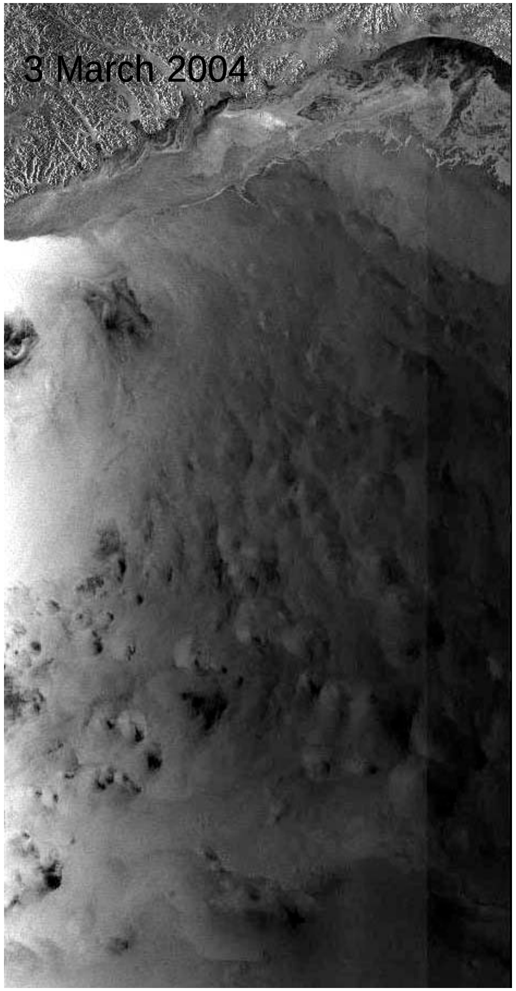

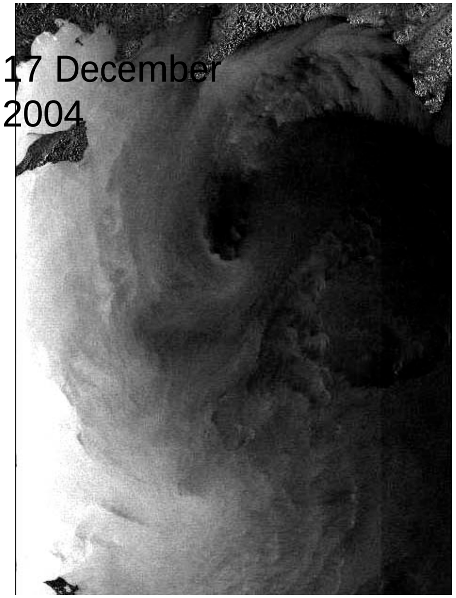

mesoscale cyclones

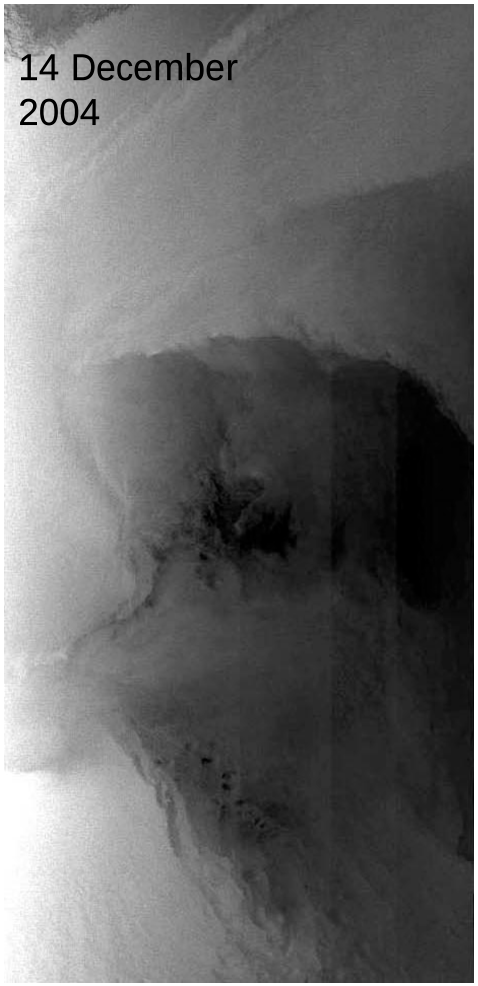

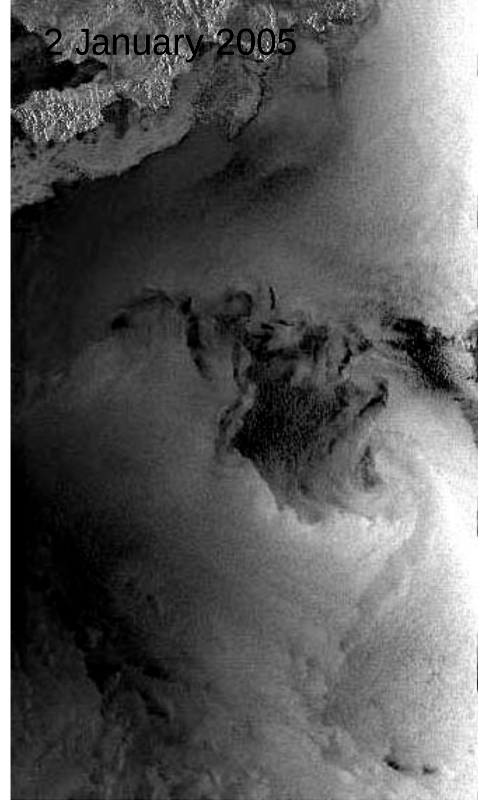

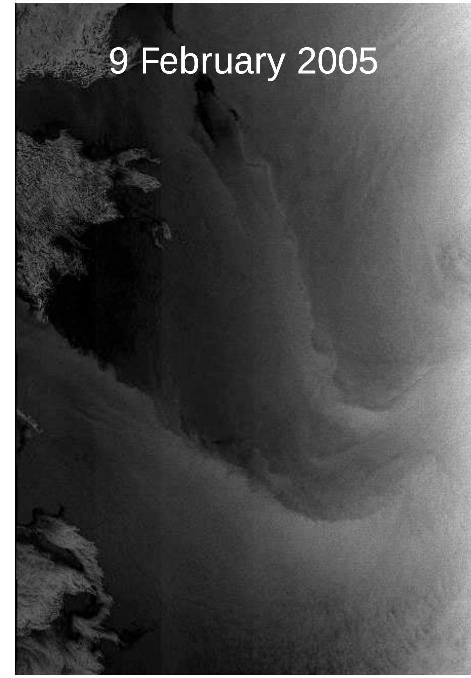

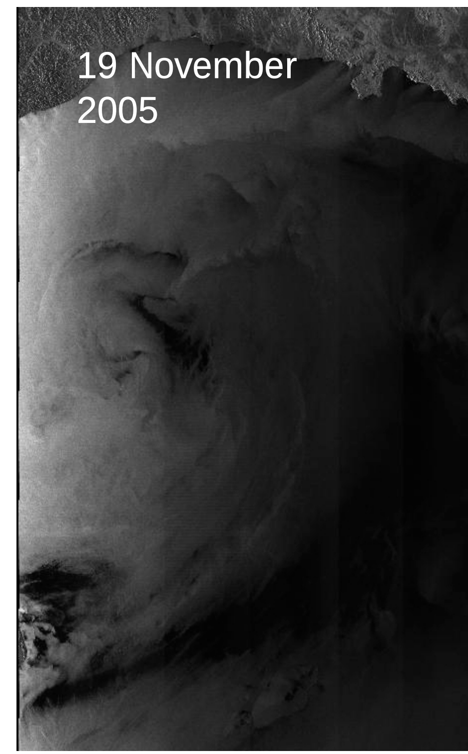

30 December 2004
Envisat, Aqua

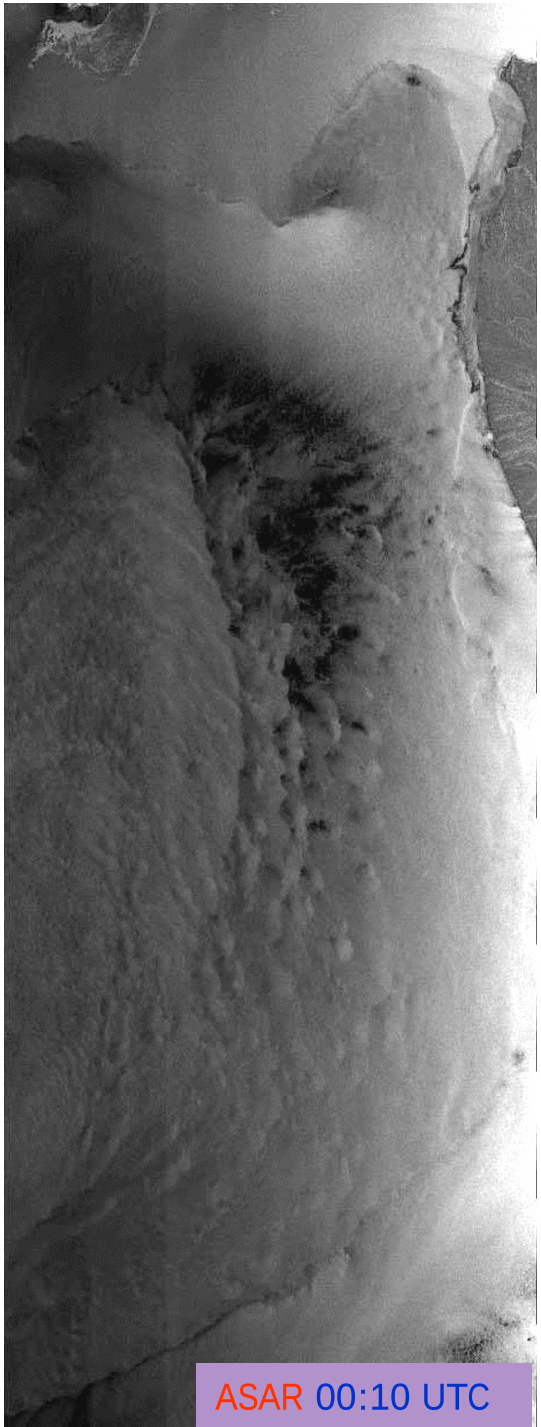

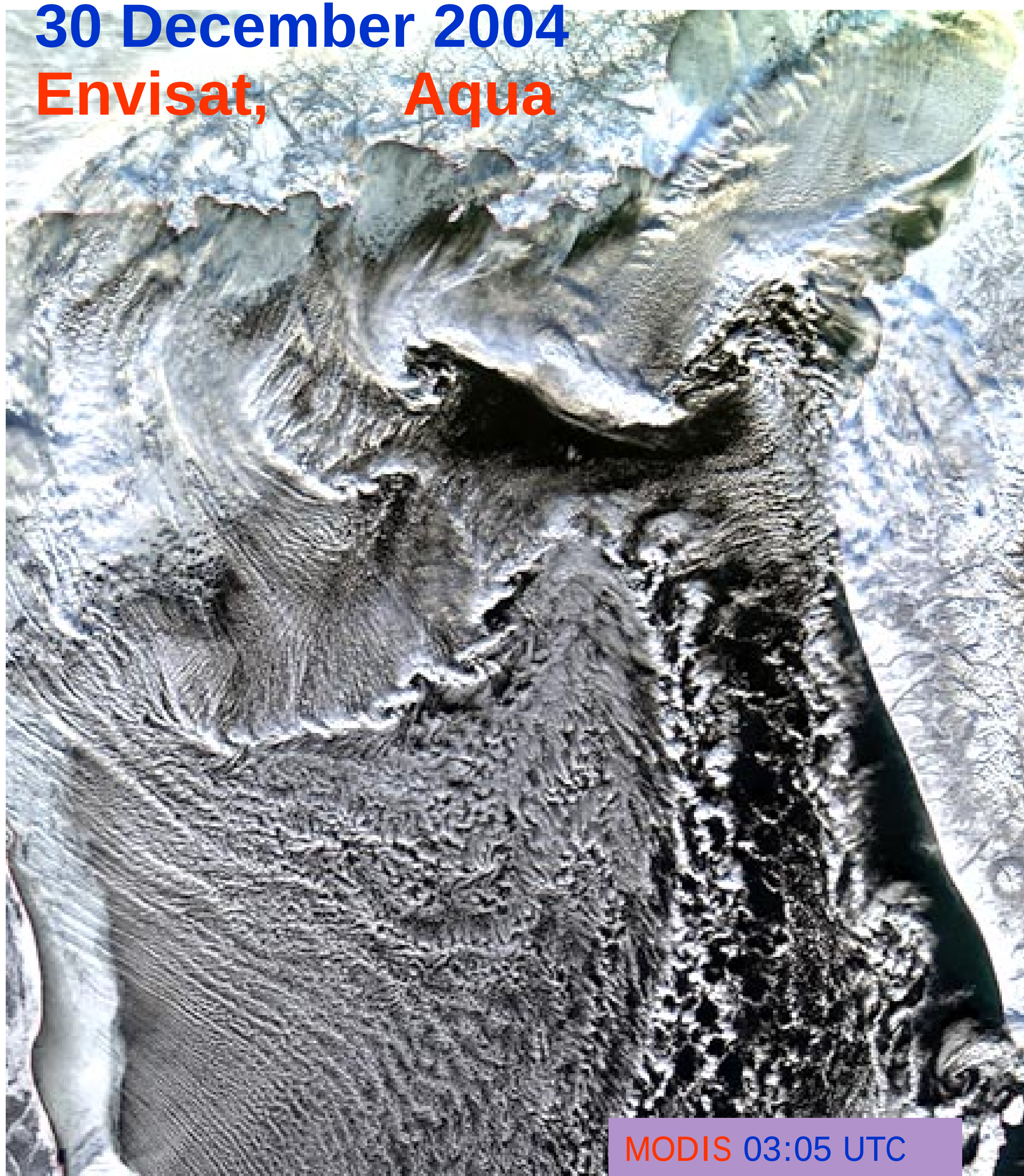

30 December 2004, Aqua AMSR-E

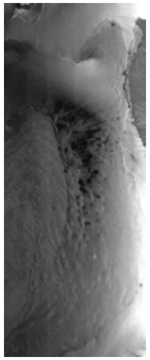

03:05 UTC

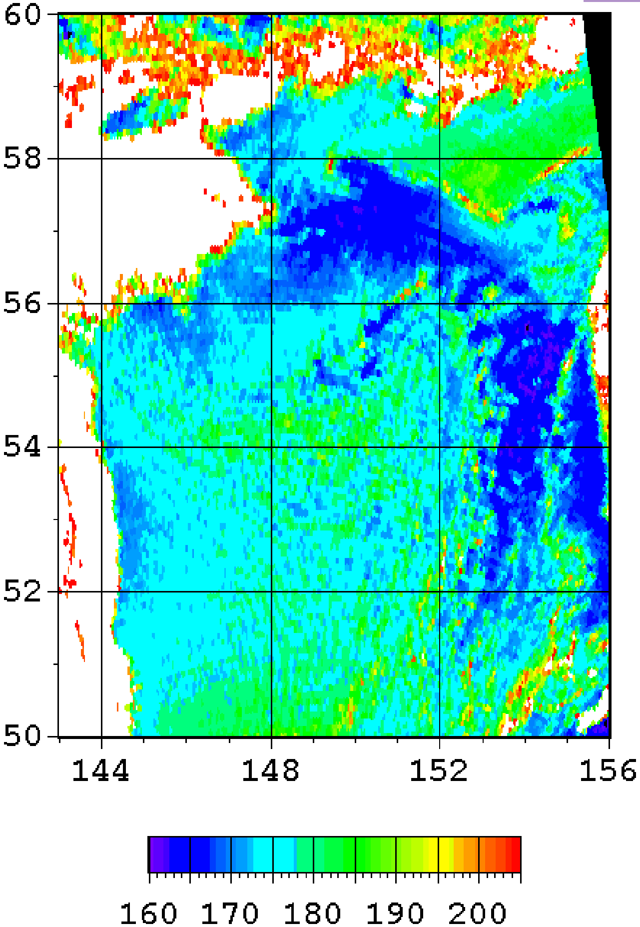

Brightness temperature 89H (K)

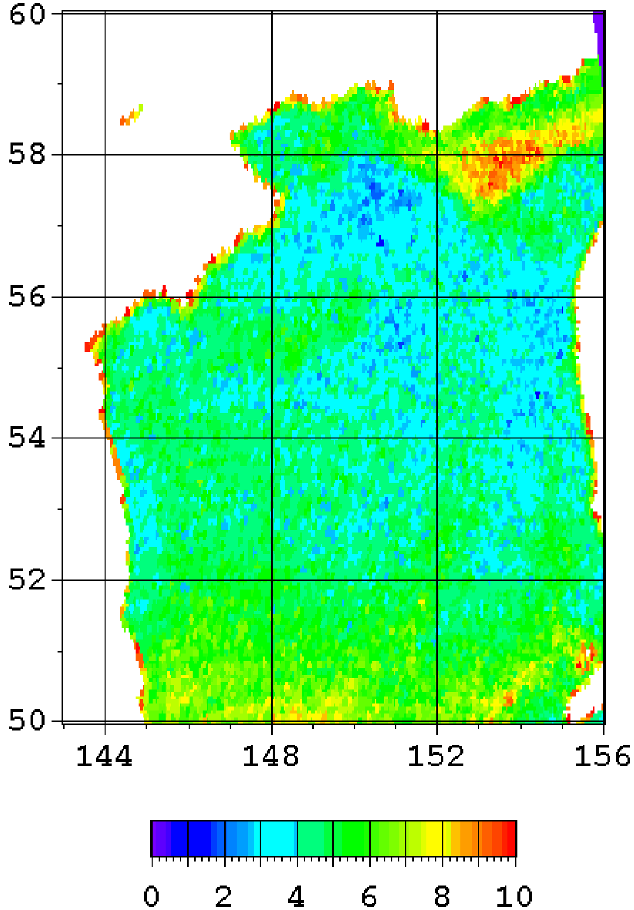

Total water vapor content (kg/m2)

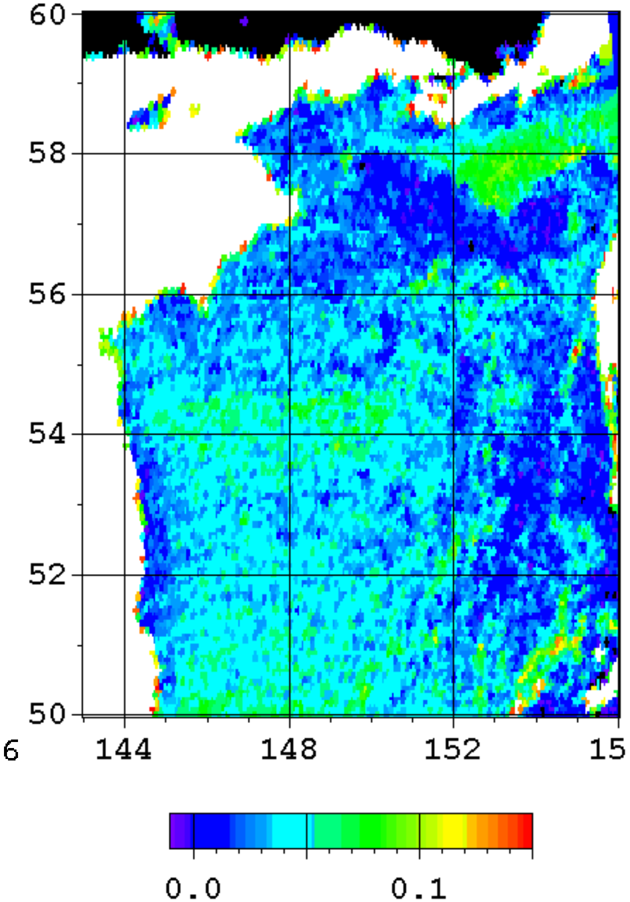

Total cloud liquid water content (kg/m2)

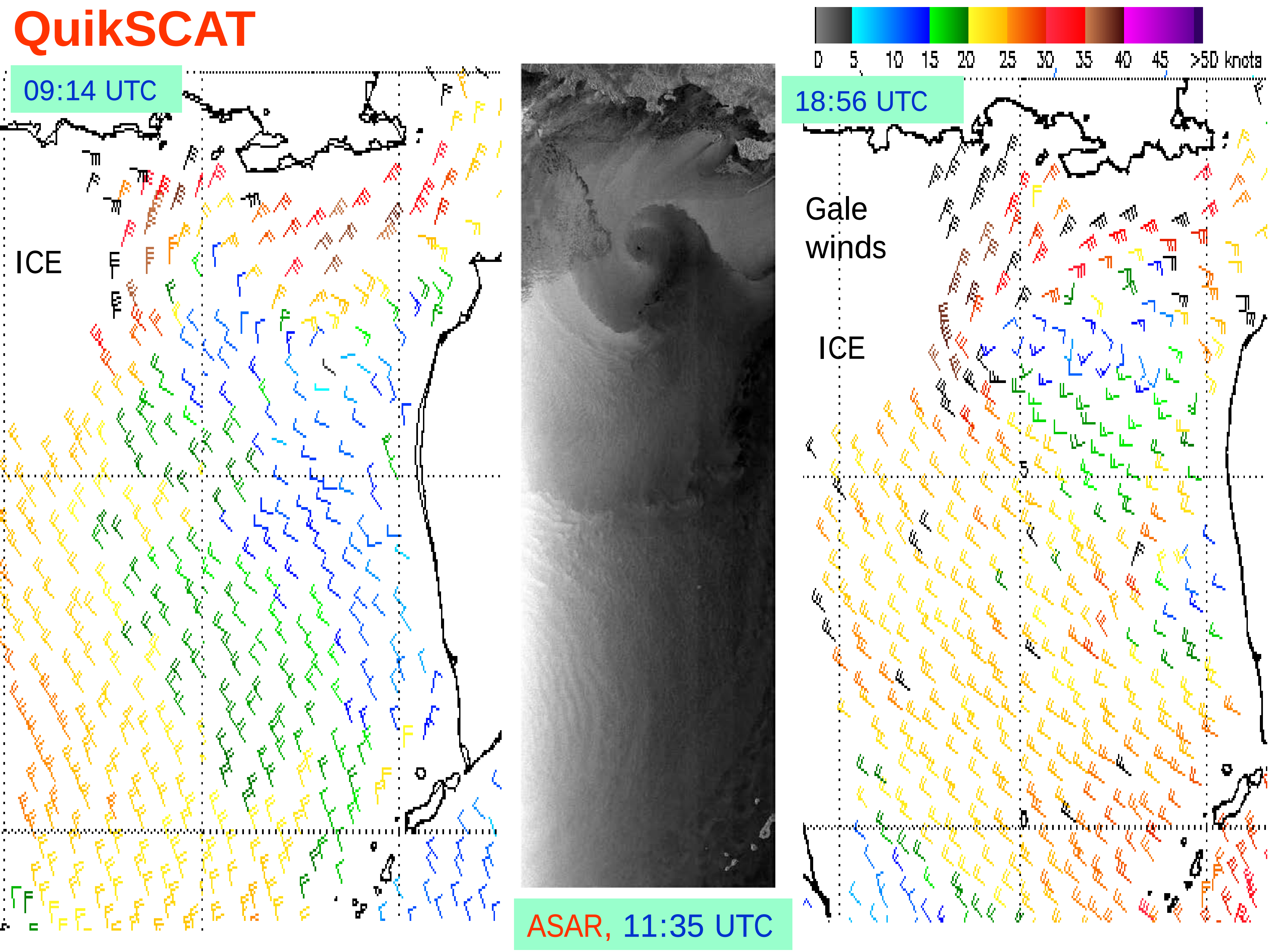
QuikSCAT
0 5 10 15 20 25 30 35 40 45 >50 knots
09:14 UTC
ICE
ASAR, 11:35 UTC
18:56 UTC
Gale winds
ICE

30 December, Envisat, Aqua

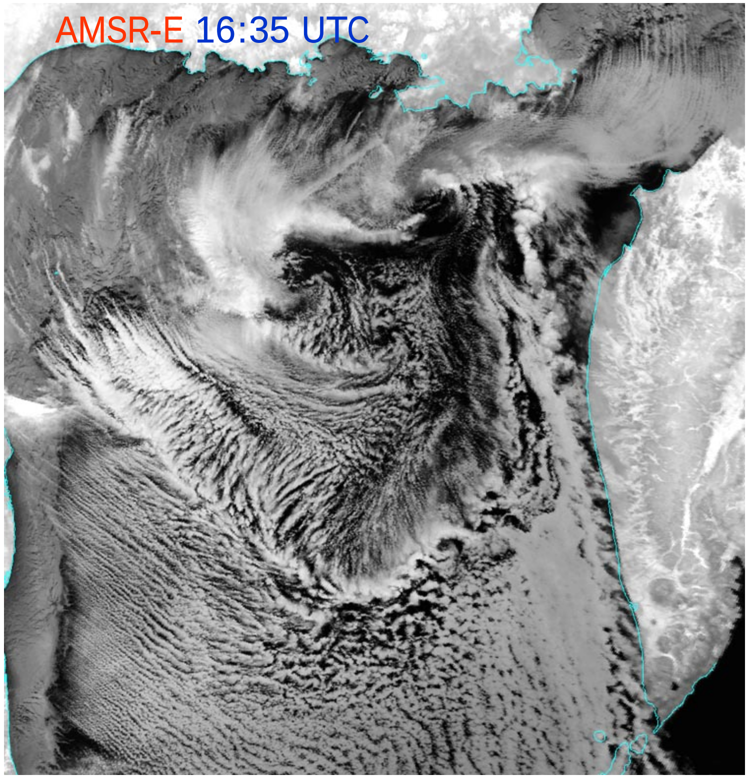

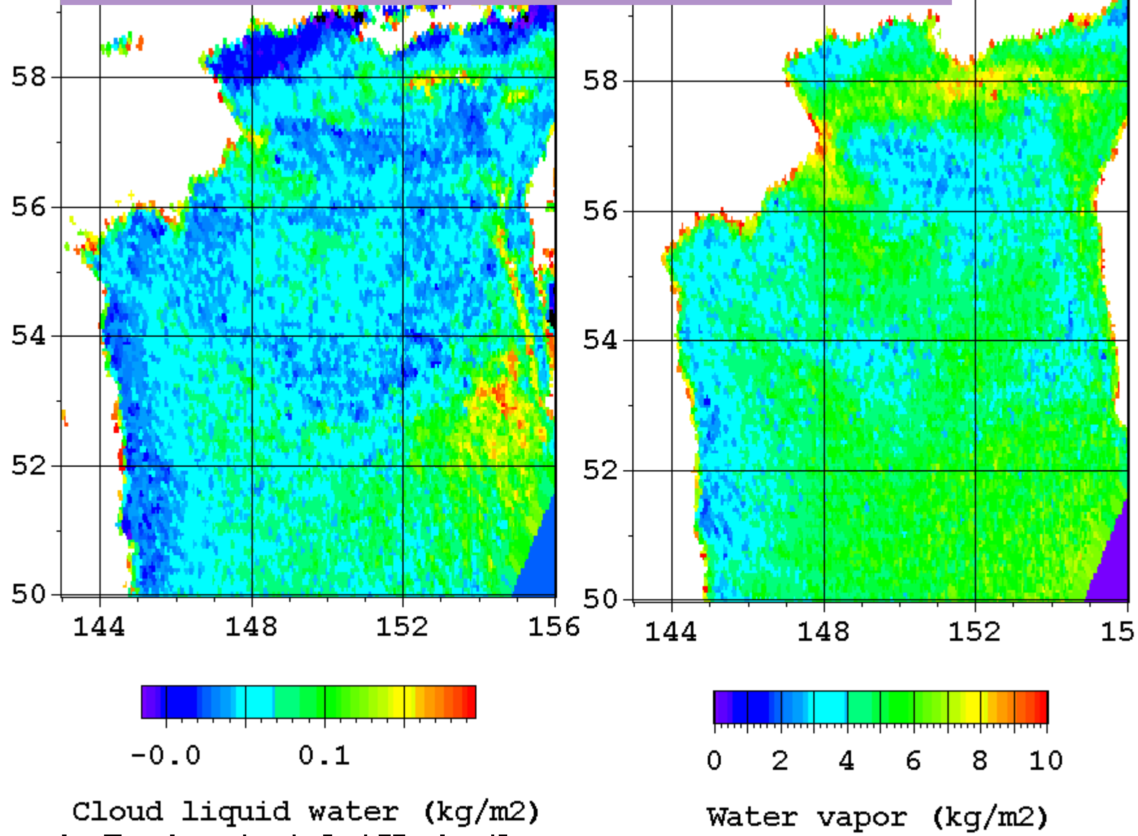

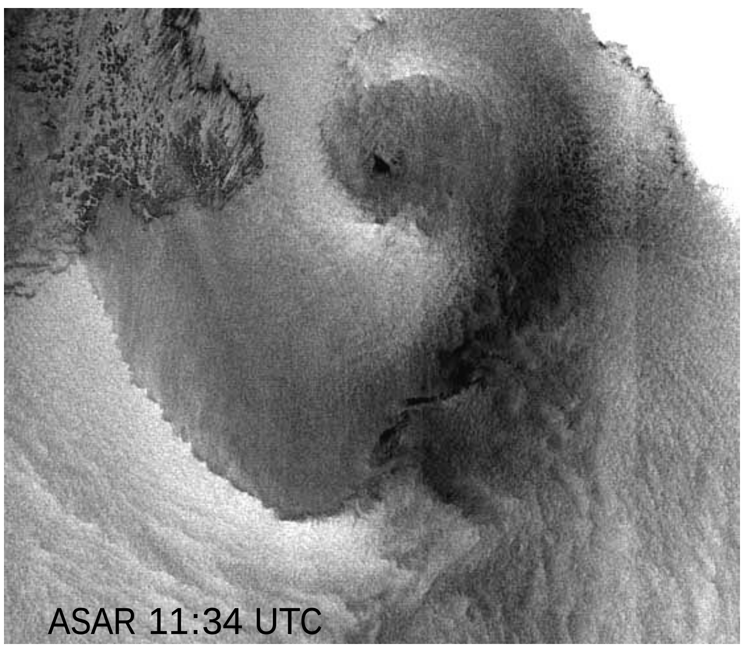

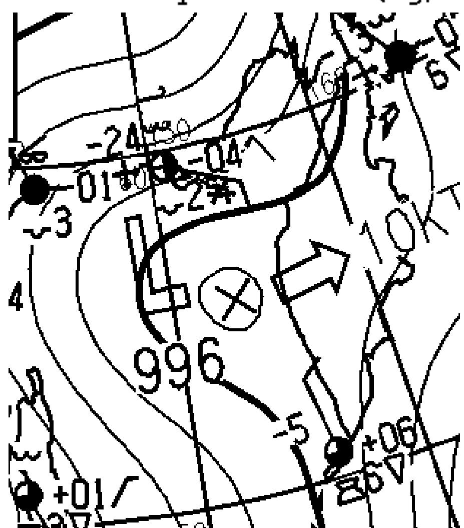

Surface analysis map of the JMA for 12 UTC

2 January 2005

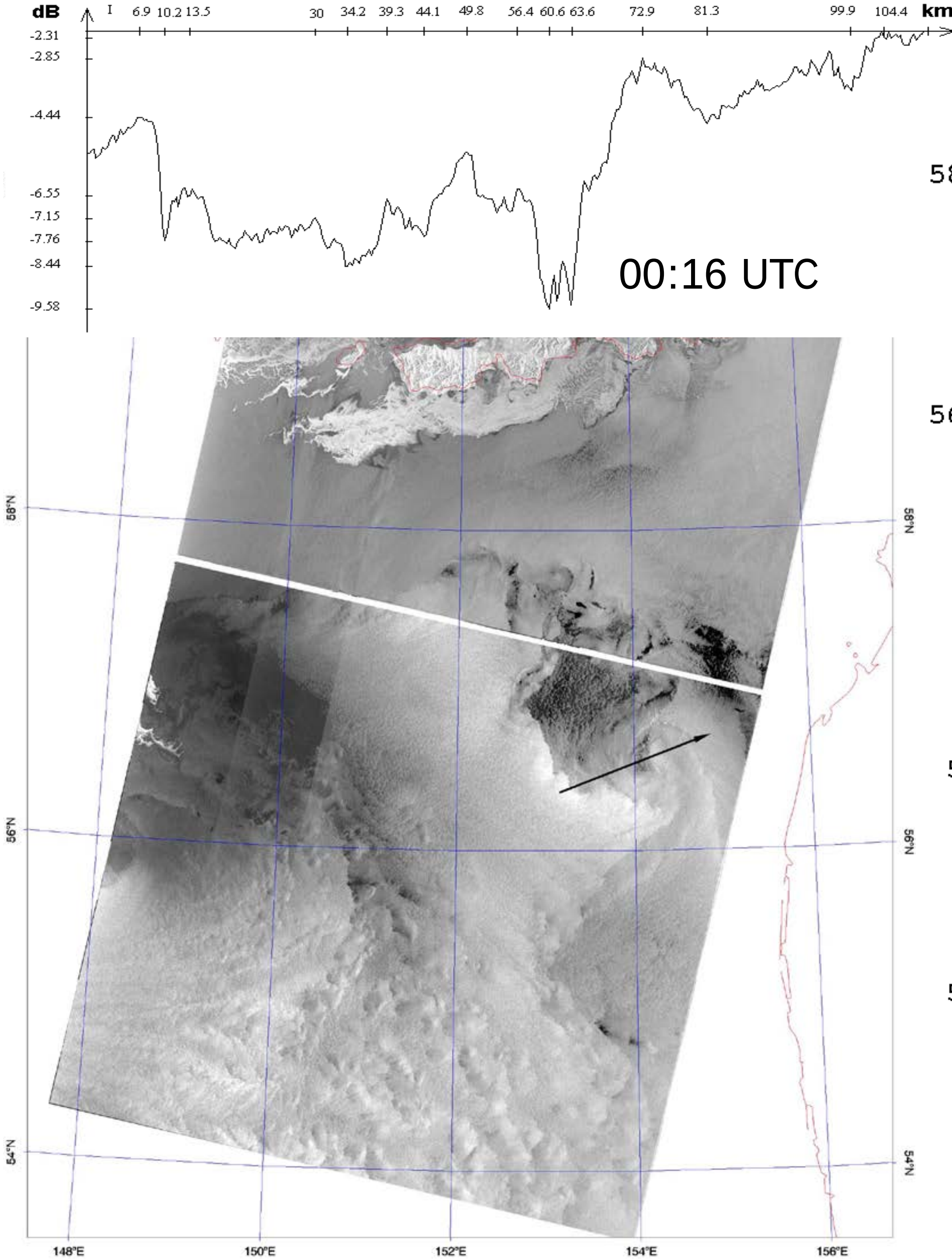

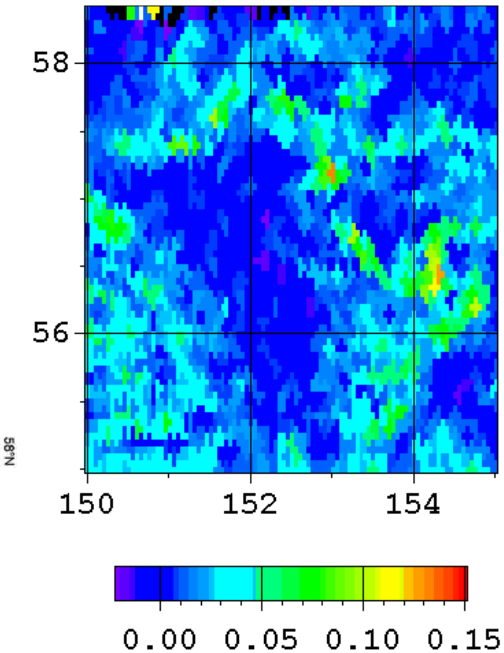

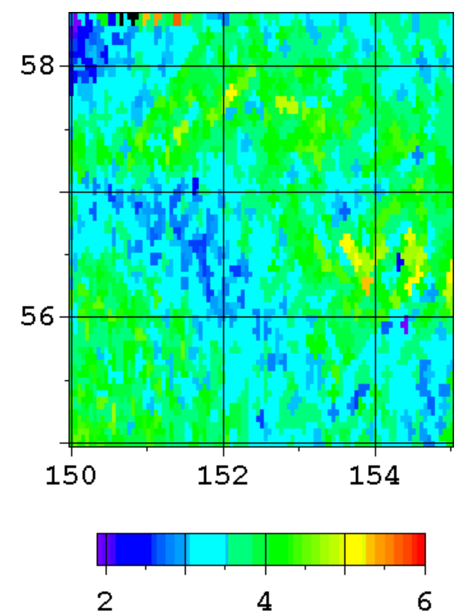

UTC

Aqua MODIS

Aqua AMSR-E

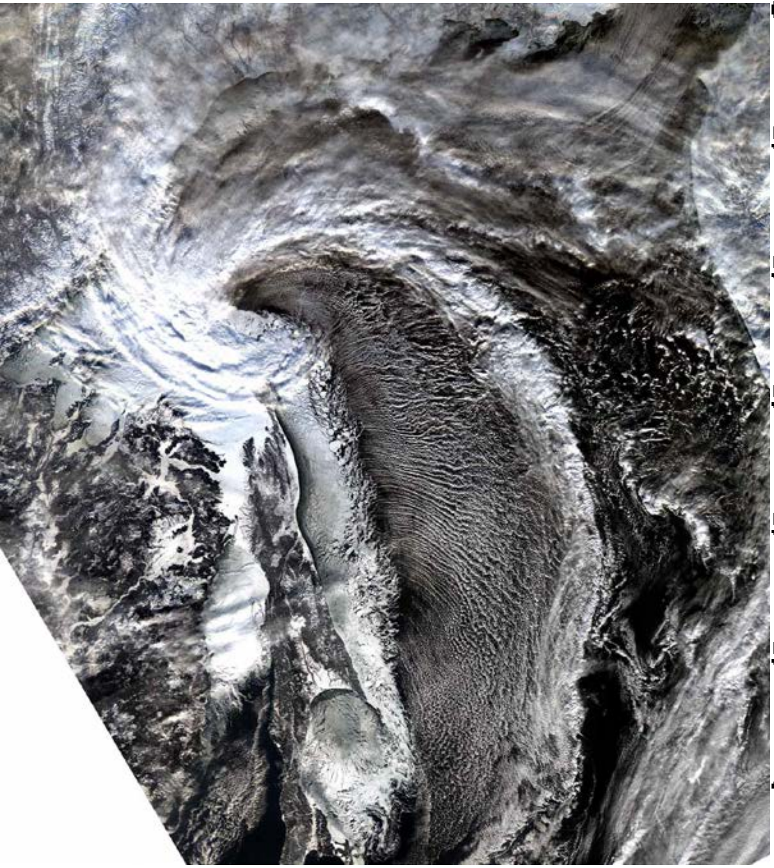

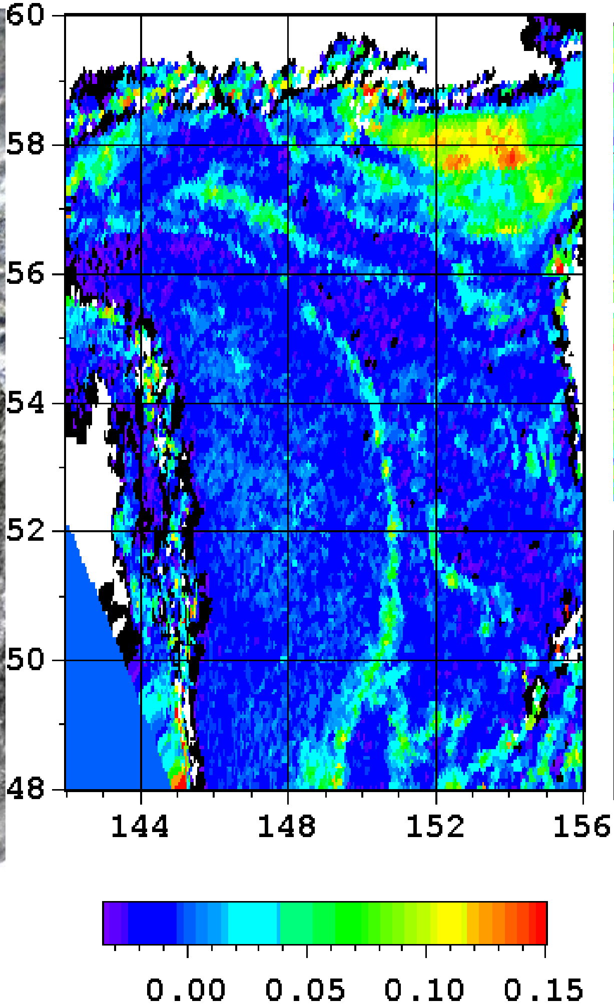

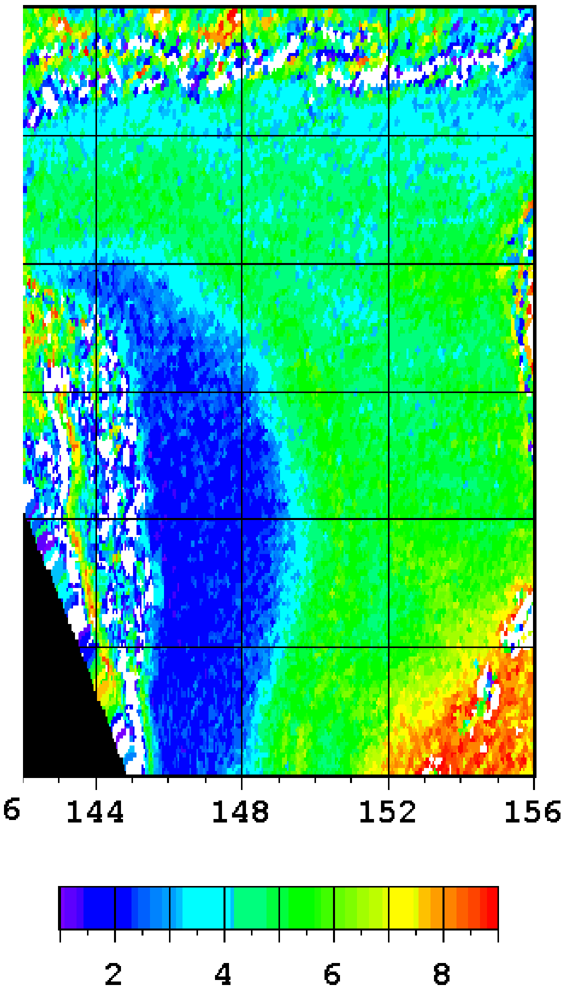

Clouds (kg/m^2)

Water vapor (kg/m^2)

15 January 2006

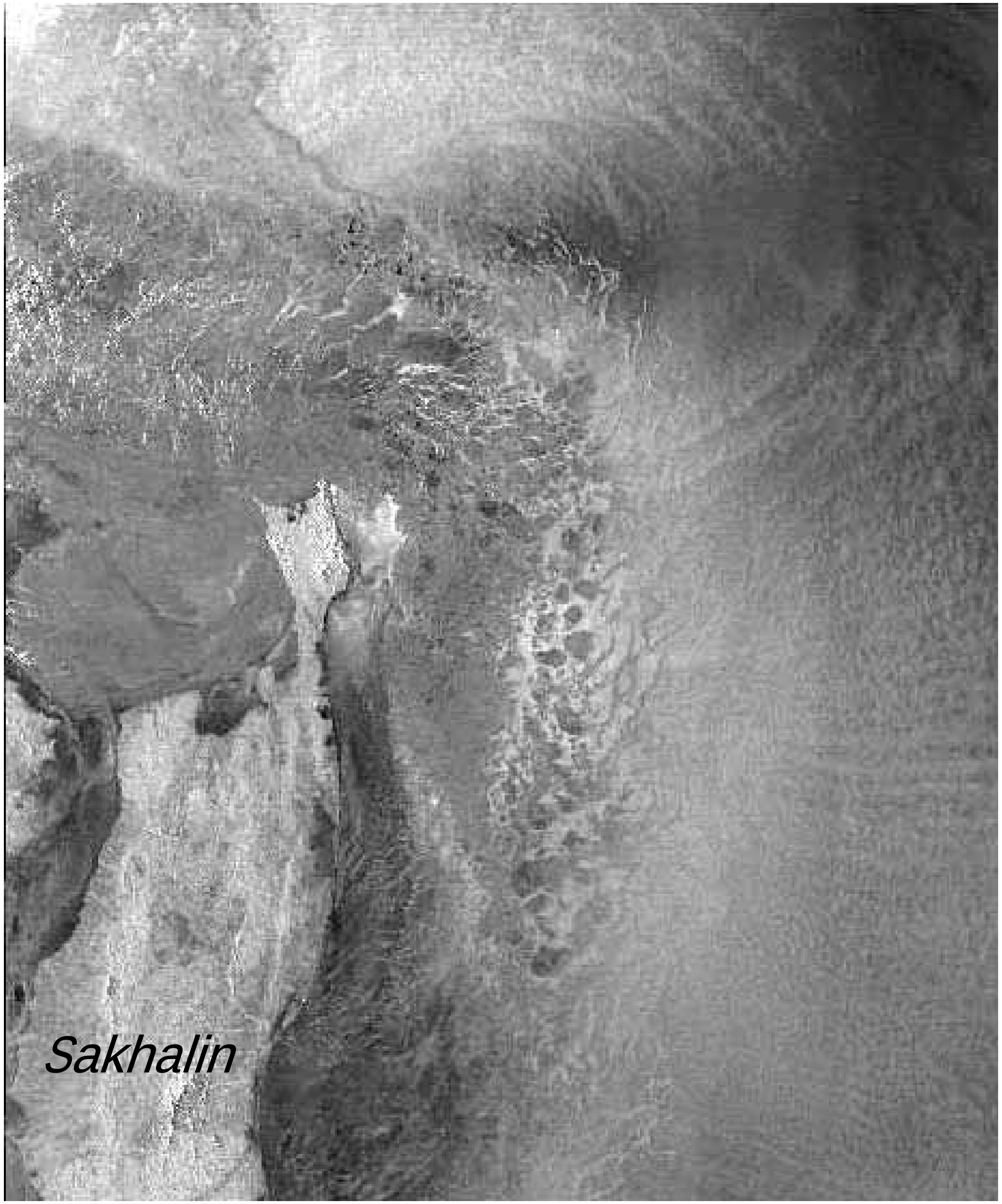

Envisat ASAR image at 12:02 UTC

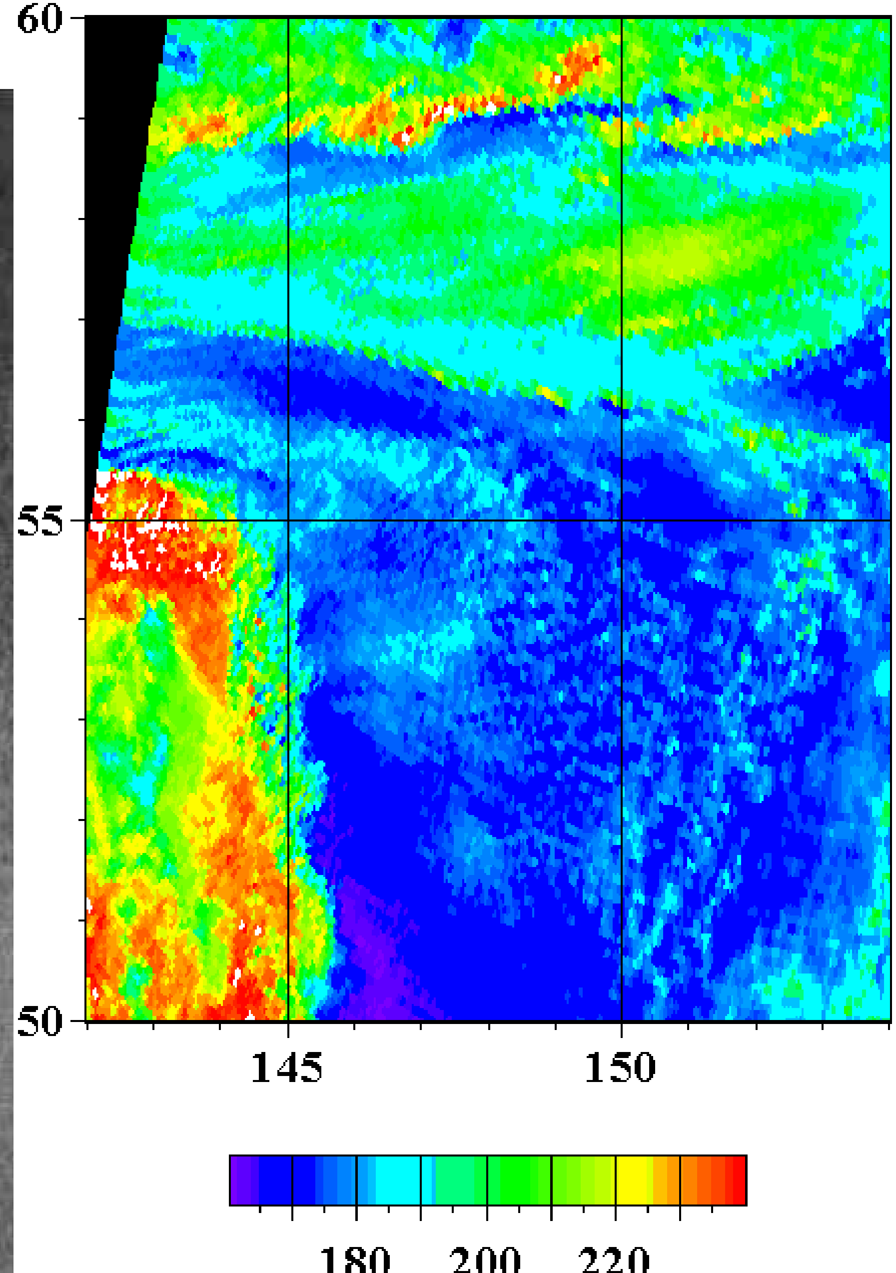

TB(89H) (K) 16:20 UTC

Bering Sea, 15 January 2006

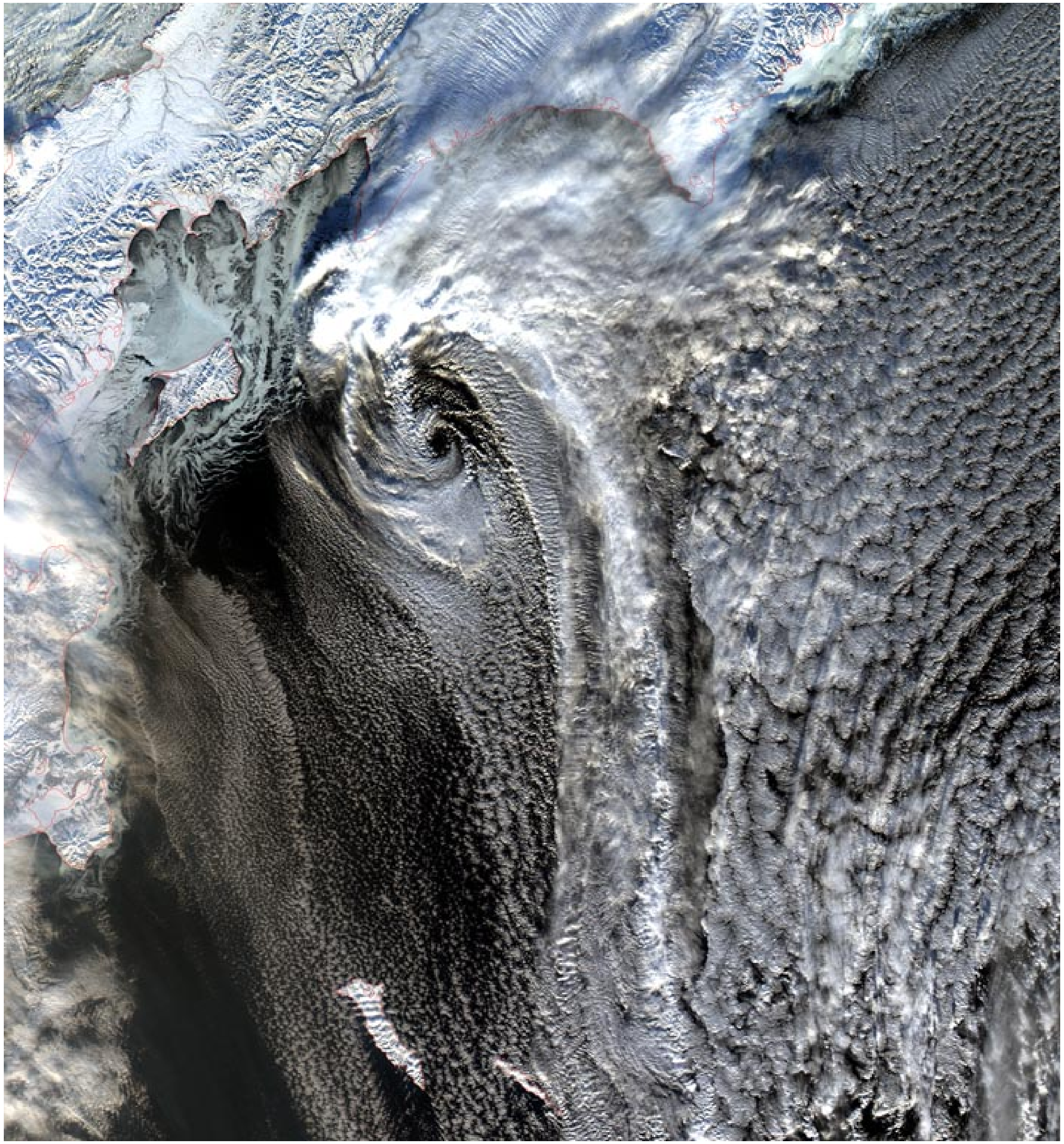

Aqua MODIS at 00:55 UTC

Envisat ASAR at 10:21 UTC

Bering Sea, 15 January 2006, 00:55 UTC Aqua

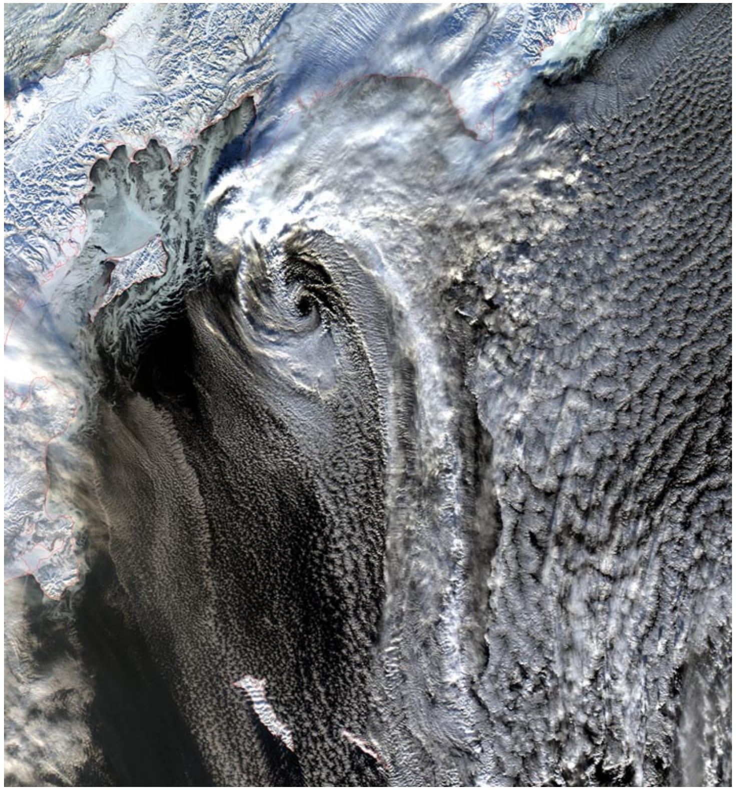

MODIS

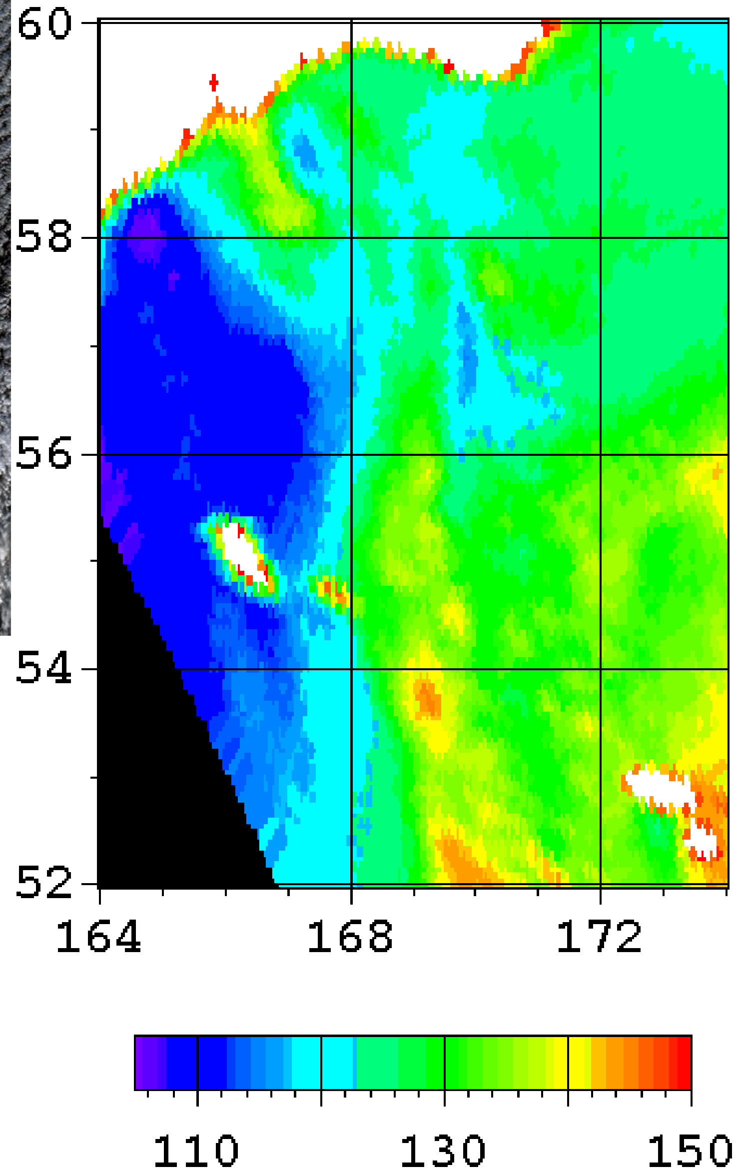

TB(24H) (K)

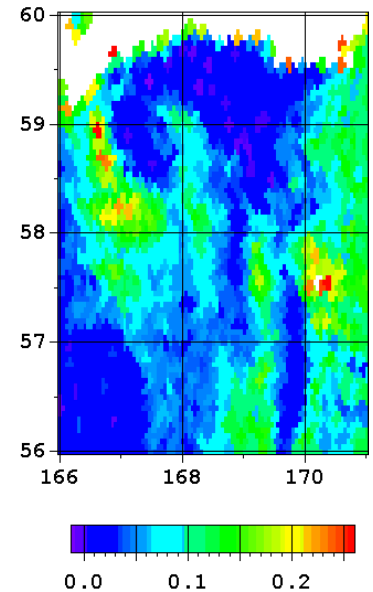

kg/m2

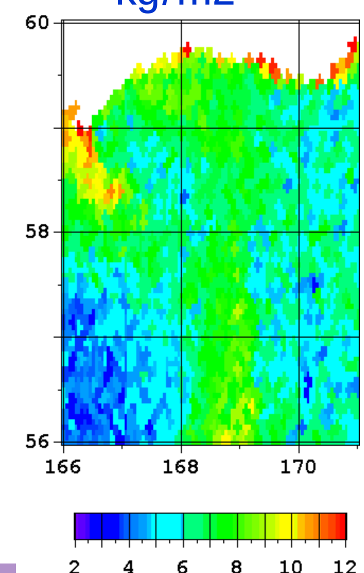

kg/m2

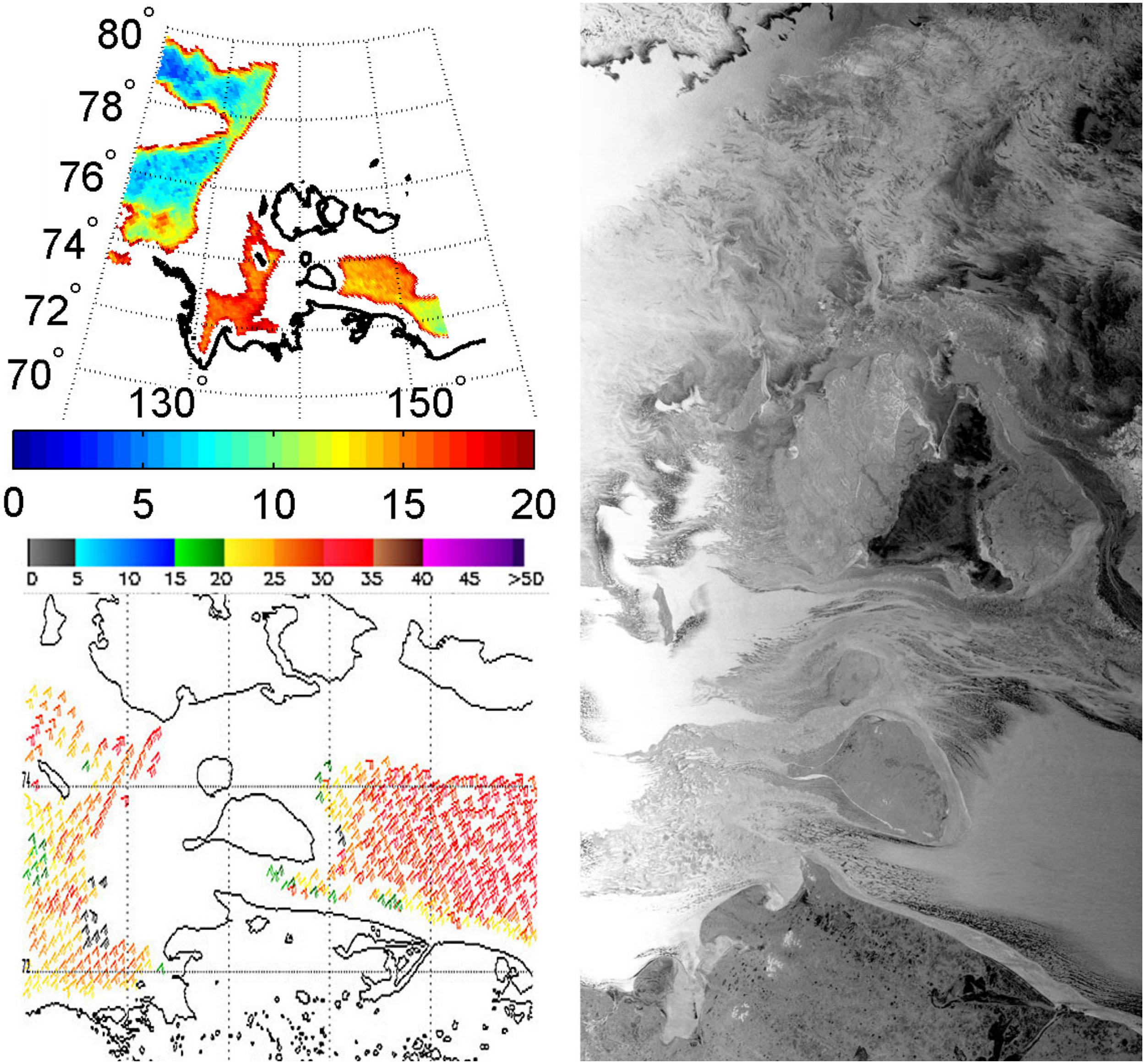

Спутниковое зондирование СМП в районе Новосибирских о-вов 23.10.2014: приводный ветер по данным радиометра AMSR2 за 02:23 Гр. в м/с (а) и скаттерометра MetOp-A за 4:19 Гр. в узлах (б) и изображение РСА SAR-C на ГГ-пол. со спутника Sentinel-1A за 07:40 Гр. (в).

Изображение
РСА SAR-C
на ГГ-пол. со
спутника
Sentinel-1A
19 октября в
08:10 Гр.

PALSAR interferogram indicating crustal deformation (left) and PALSAR amplitude image observed after the earthquake (March 20, 2011) (right).

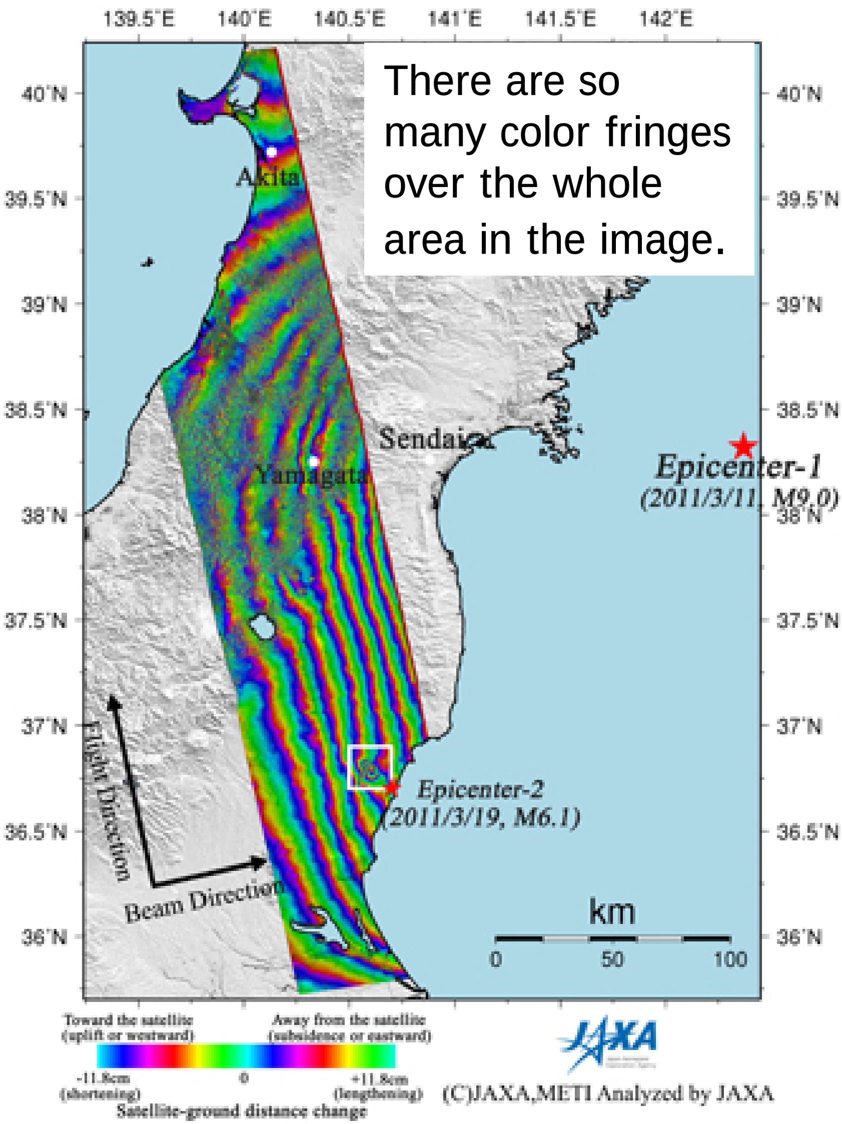

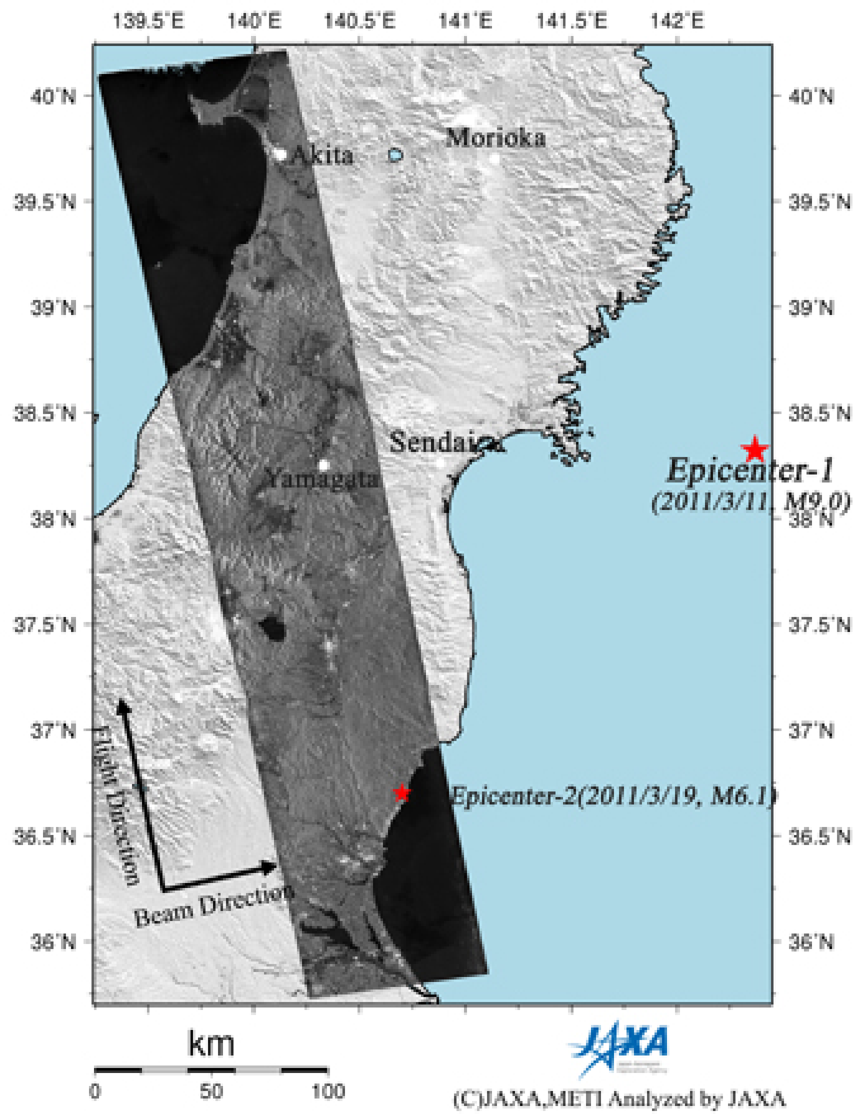

Epicenter-1 and epicenter-2 indicate those of the M9.0 earthquake on March 11 and the M6.1 earthquake on March 19, respectively.

Авария на нефтяных платформах в Жёлтом море

msn 産経ニュース

ニュース検索 bing

トップ 速報 事件 政治 経済・IT 国際 スポーツ エンタメ ライフ 科学 地方 オピ

中国・台湾 朝鮮半島 アジア 米州 欧州・ロシア 中東・アフリカ トピックス 写真 ランキン

[国際]ニュース

トピック：資源

ブログに書く 引用ブログ 49 メッセ 印刷

中国の海上油田で原油流出　隠蔽体質に非難集中

2011.7.6 00:02 (1/2ページ)

【北京＝川越一】中国山東省沖の渤海にある同国最大の海上油田で6月上旬に原油が流出していたことが発覚し、国家海洋局は5日、初めて事故を公表し、原油が広がった面積は840平方キロにわたったことを明らかにした。汚染拡大が懸念されているにもかかわらず、発生から約1カ月も事故を隠蔽した当局や企業の姿勢に、国民の不信感が高まるのは必至だ。

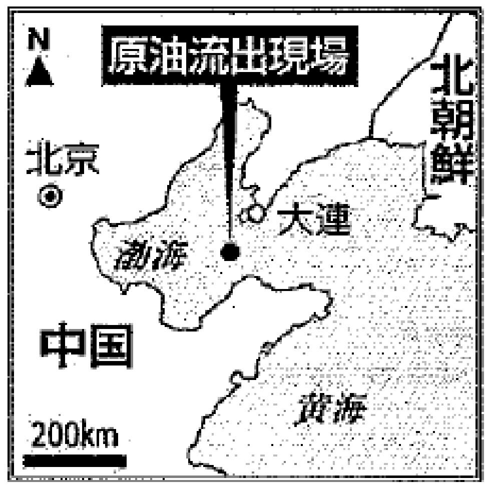

クリックして拡大する

同油田は、中国国有石油大手、中国海洋石油と米石油大手コノコフィリップスが共同開発した。原油が流出したのは6月4日。同月20日ごろ、インターネット上の書き込みで発覚した。中国海洋石油関係者による内部告発とみられている。

中国メディアからの問い合わせに沈黙を守っていた中国海洋石油は1日夕になって流出を認めた。3日には同社関係者が「油漏れの範囲はわずか200平方メートル程度だ。事故処理はすでに完了しており、現場海域の環境への影響は少ない」とコメントしたが、国家海洋局の発表によって、事態を著しく過小評価していたことも浮き彫りとなった。

Oil spill monitoring by remote sensing
http://cearac.poi.dvo.ru

Bohai Bay. Yellow Sea. Penglai 19-3 offshore oil field

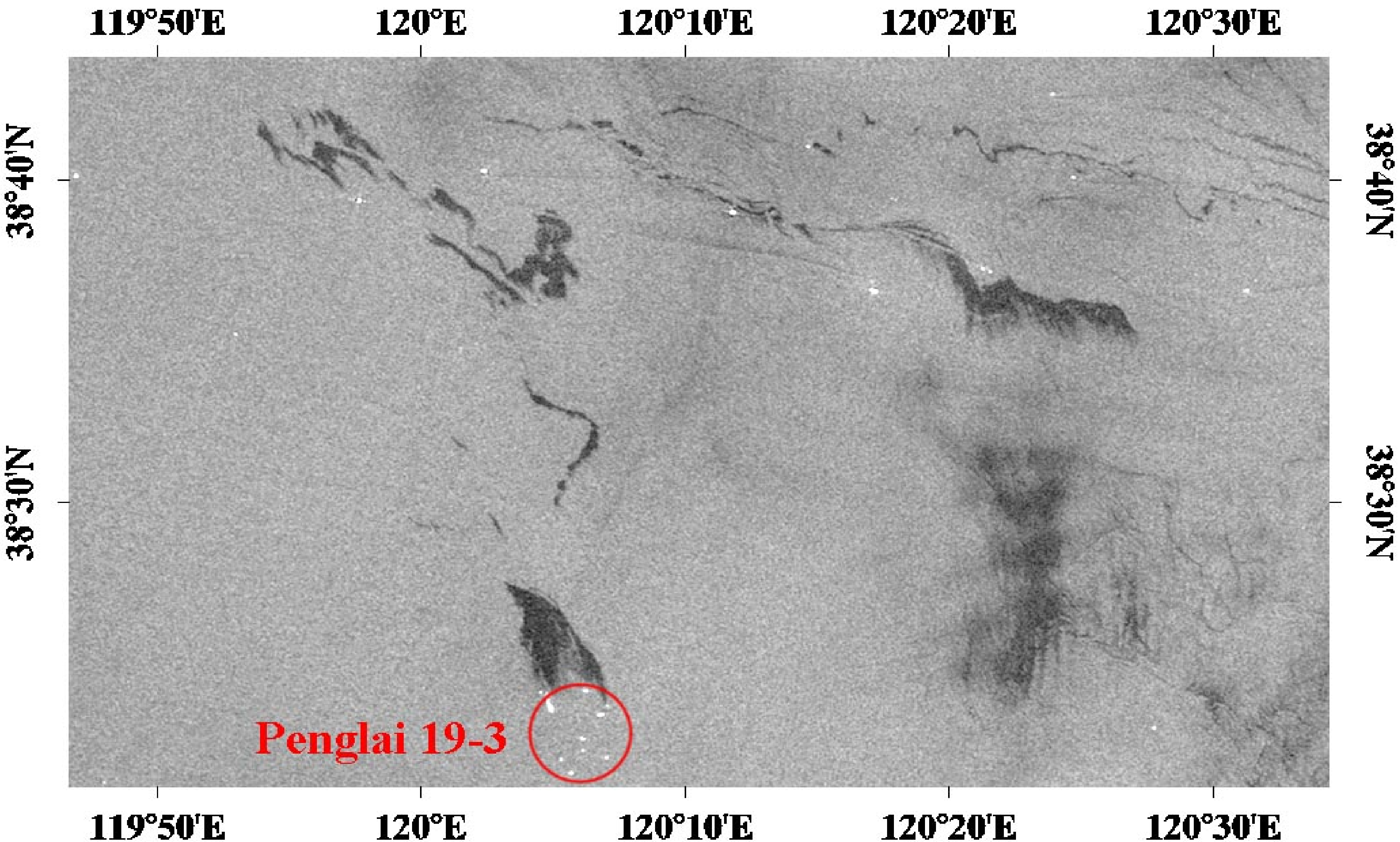

Envisat ASAR. 11 June 2011. Polluted area 65 km²

Image courtesy of ESA - European Space Agency

Sanchi oil spill (China) seen by Sentinel-1 / 2 / 3

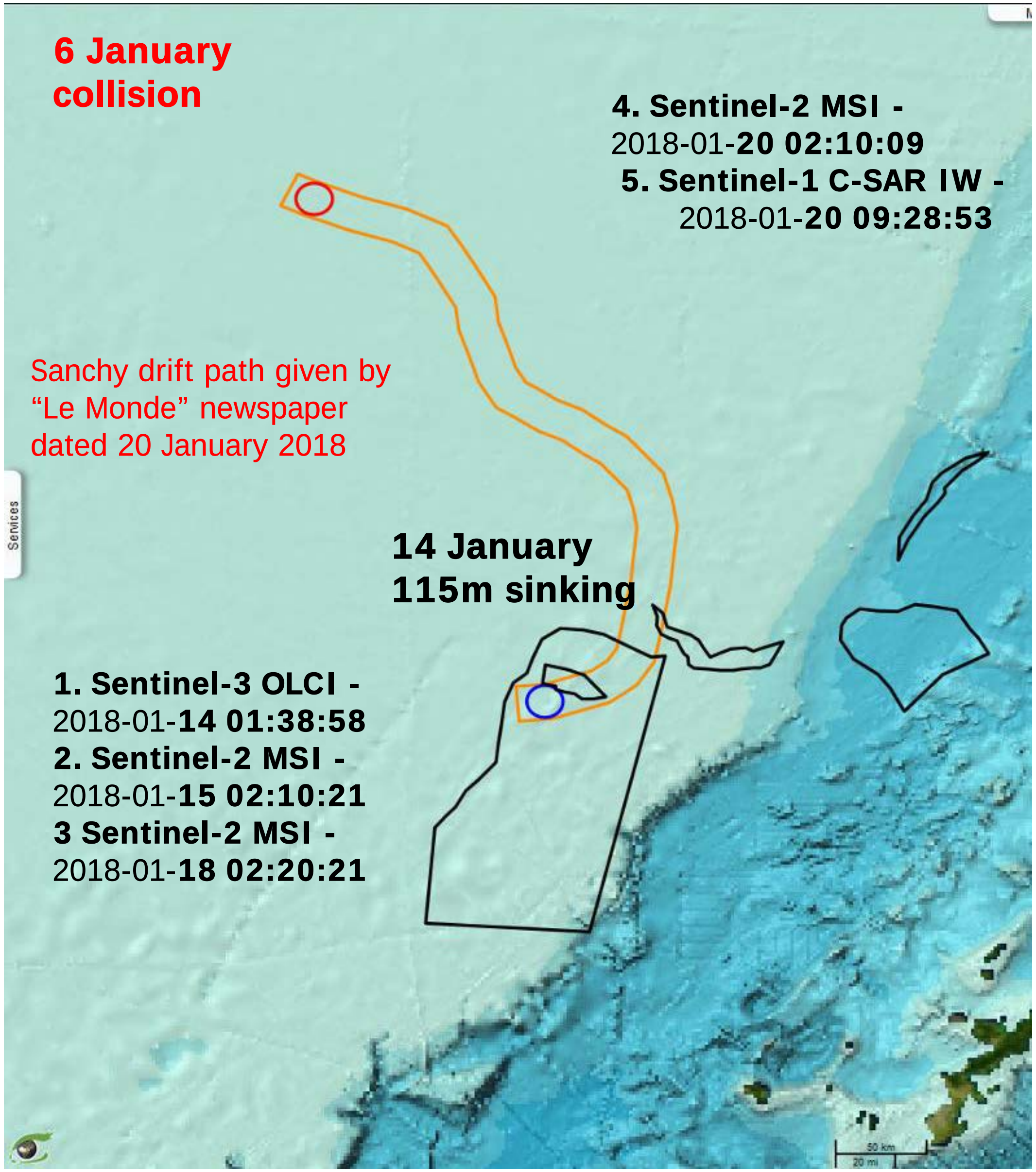

Sanchi oil spill

Sanchi oil spill

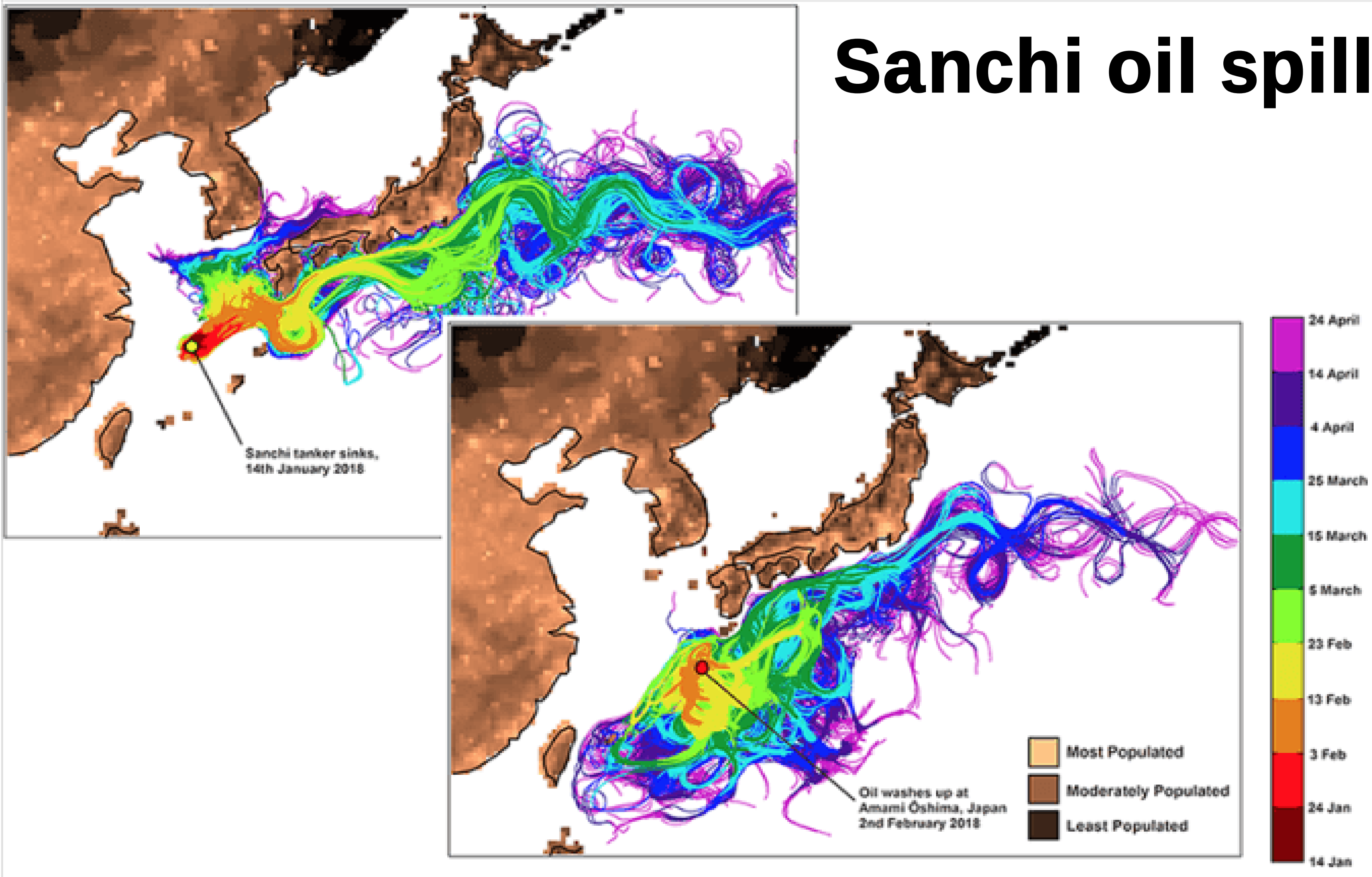

This shows the trajectories of virtual oil particles released from (a) the final resting site of the Sanchi (top-left; 14 January 2018 release) and (b) the vicinity of Amami-Oshima Island (bottom-right; 2 February 2018 release)

ALOS-2
PALSAR
18
January
2018

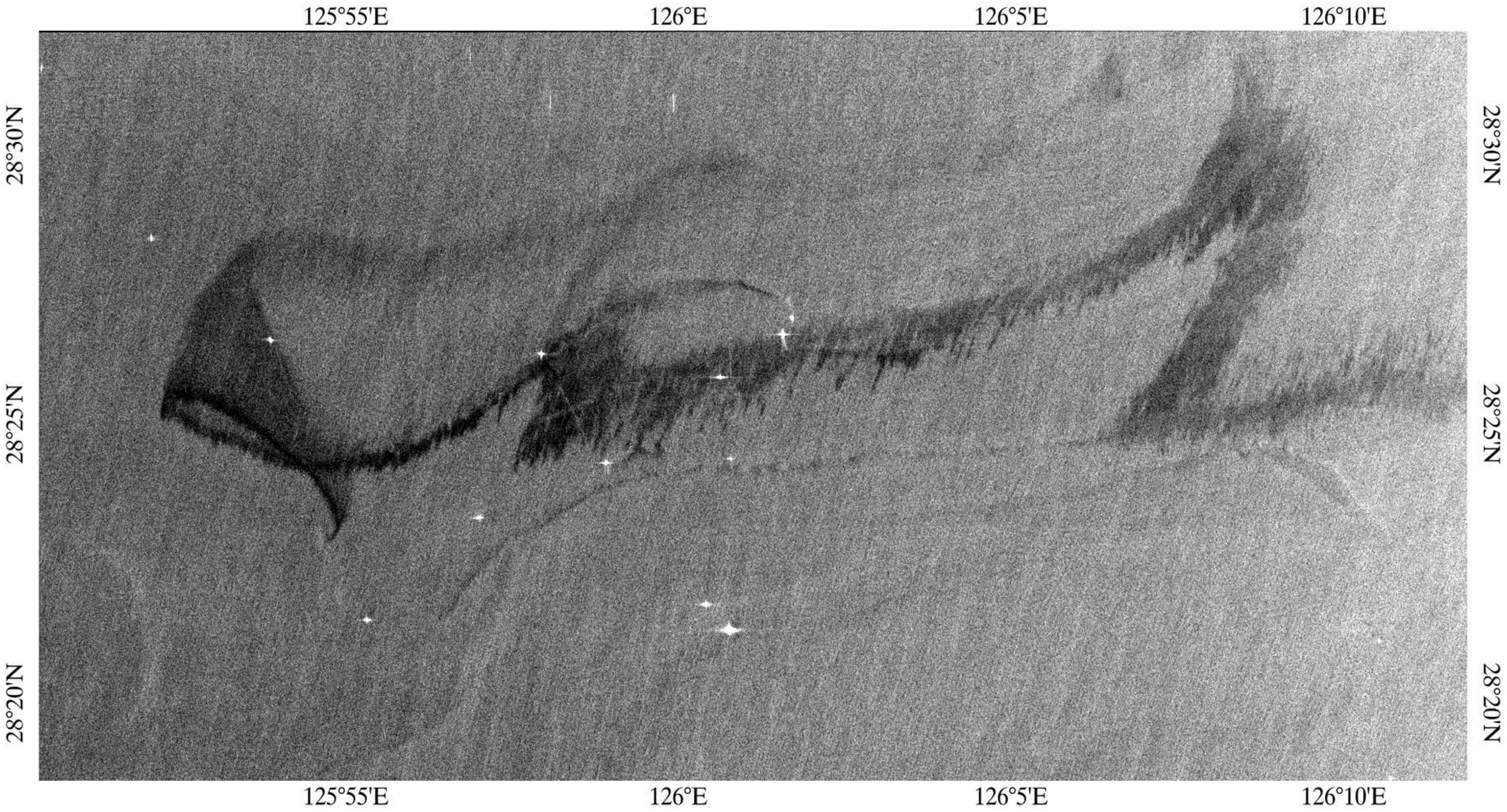

Разлив нефти в Восточно-Китайском море после аварии танкера Sanchi на изображении РСА PALSAR-2 на ГГ поляризации со спутника ALOS-2 18 января 2018 г. в 03:33 Гр.

Sanchi oil spill

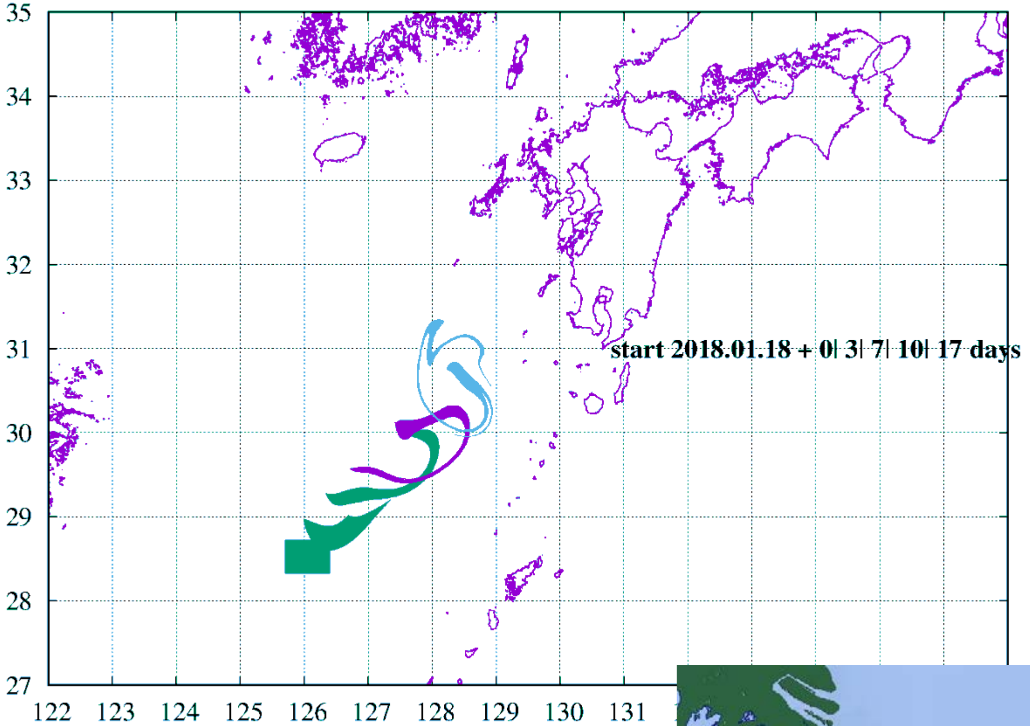

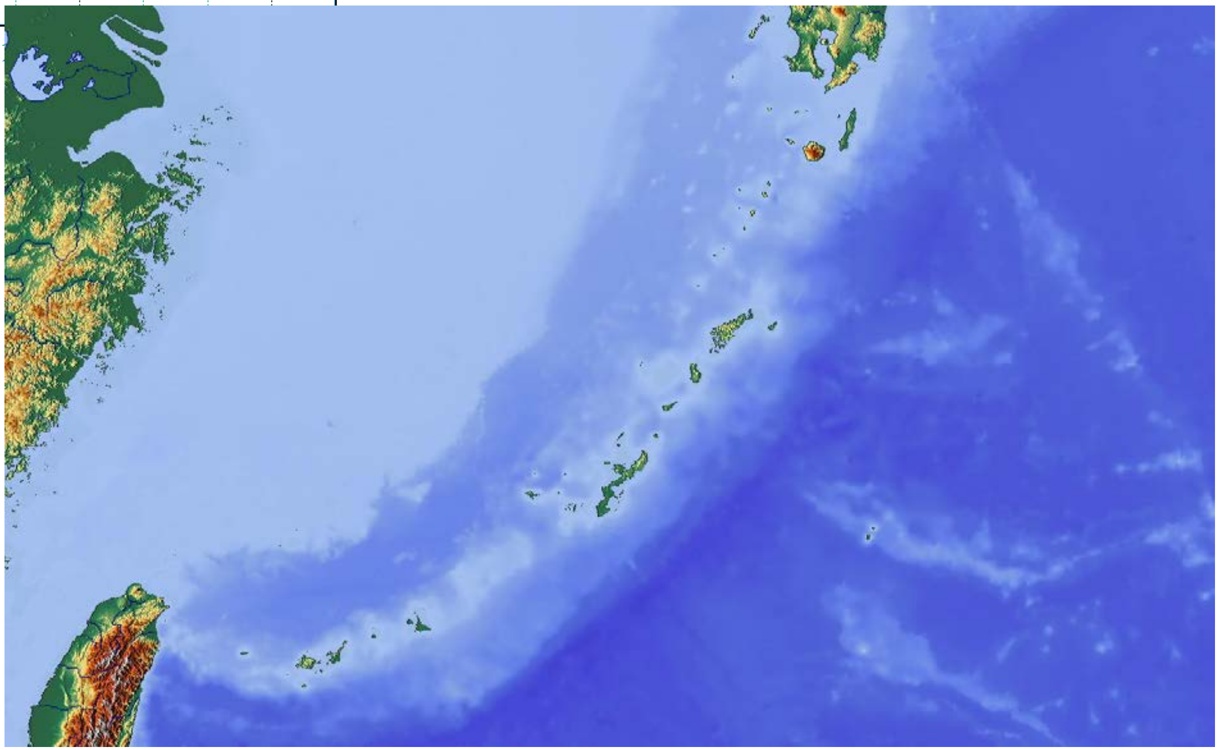

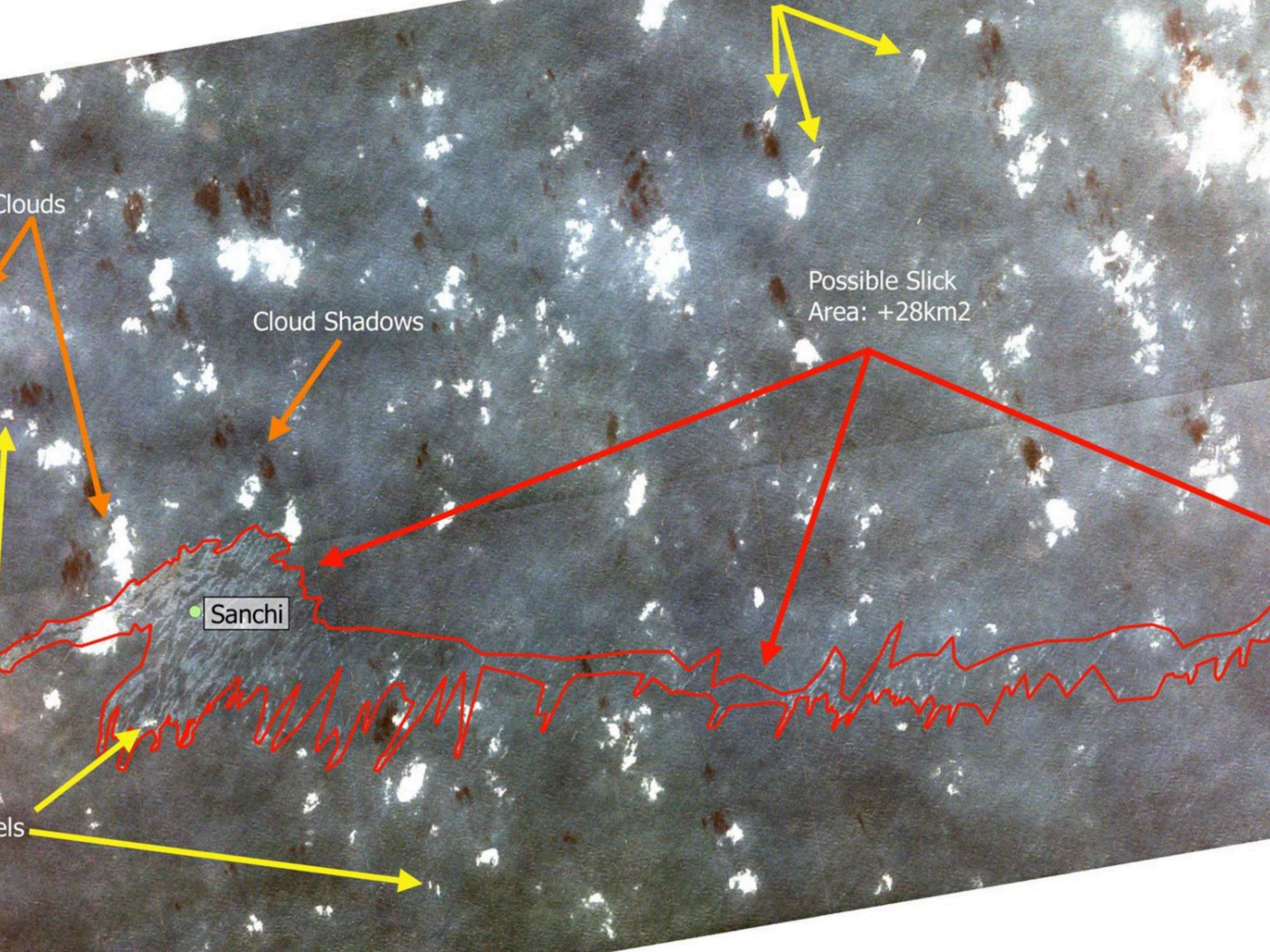
Clouds
Cloud Shadows
Possible Slick
Area: +28km2
Sanchi
els

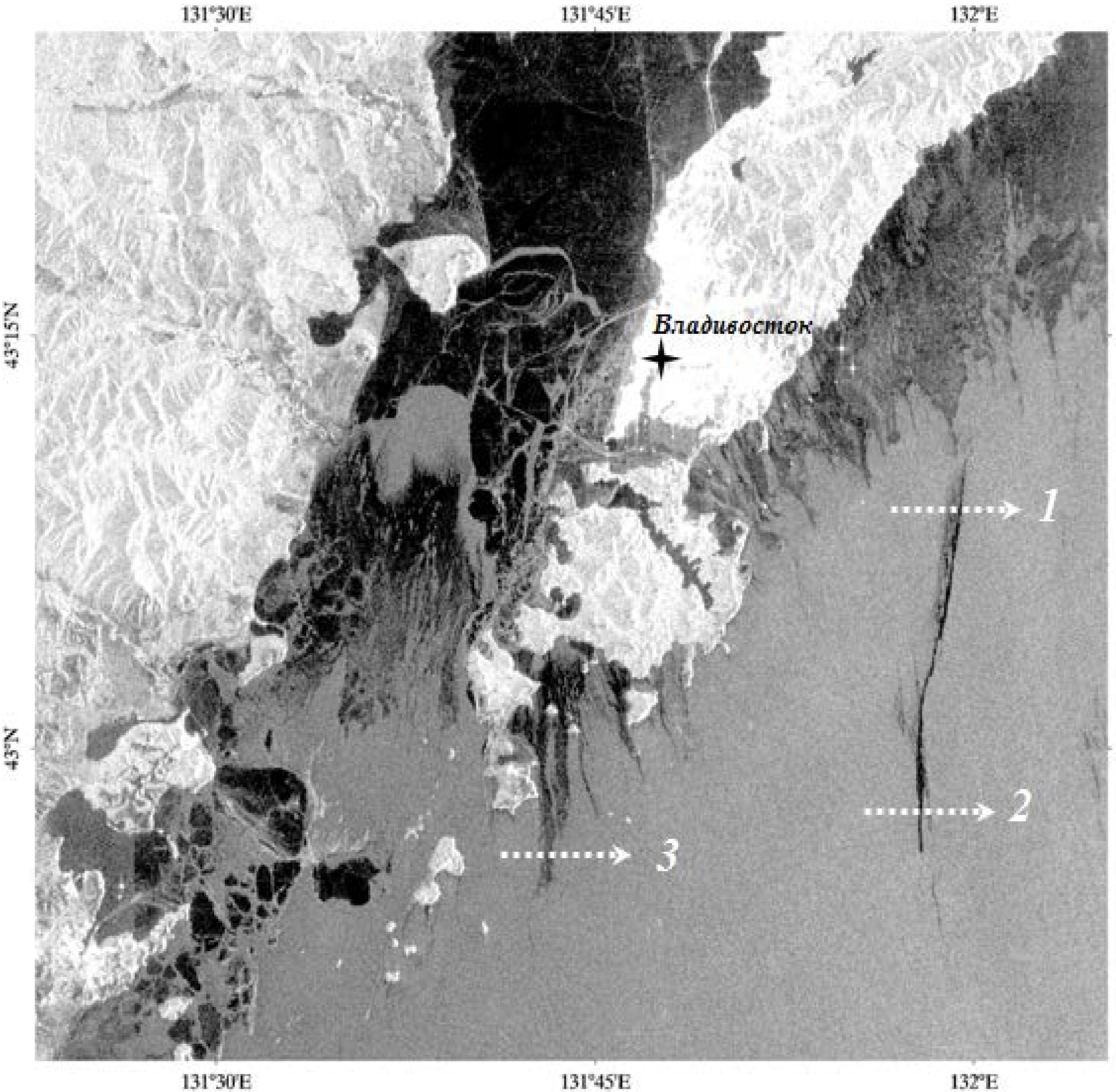

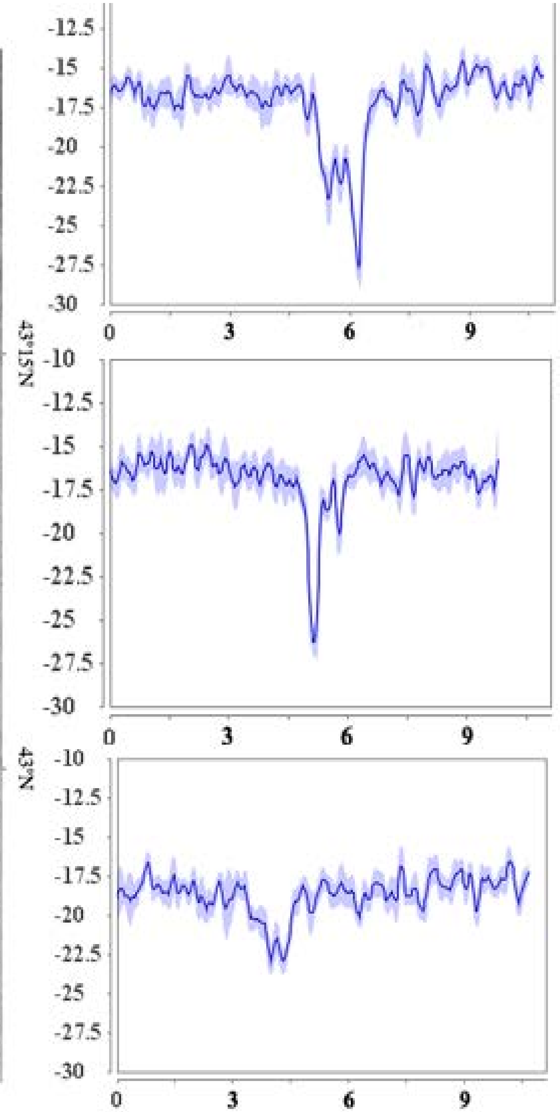

Зал. Петра Великого на изображении РСА PALSAR-2 на ГГ поляризации со спутника ALOS-2 30 декабря 2017 г. в 03:22 Гр. (а) и профили УЭПР вдоль сечений 1, 2 и 3 через полосы ледяного сала.

Взаимосвязь полей приводного ветра и облачности по данным спутникового зонди- рования в видимом, ИК- и СВЧ-диапазонах // Исследование Земли из космоса. 1987. № 4 Десятова Г.И., Ковбасюк В.В. Вольпян Г.П. Регистрация внутренних волн по данным радиофизического зондирования с ИСЗ и НИС «Акад. Александр Несмеянов» Исследование Земли из космоса. 1987. N. 3

Mitnik L.M. and V.B. Lobanov (1991) Reflection of the oceanic fronts on the satellite radar images. In: *Oceanography of Asian Marginal Seas*, K. Takano, editor, Elsevier Oceanography Series, vol. **54**, Elsevier, Amsterdam, pp. 85-101.

Mitnik L.M. and M.Yu. Shoom (1991) Microwave sensing of cloudy atmosphere over the ocean from space: Influence of antenna smoothing*. Radioengineering and Electronics*, vol. **36**, no. 5, pp. 891-901.

Mitnik L.M. and A.I. Kalmykov (1992) Structure and dynamics of the Sea of Okhotsk marginal ice zone from "Ocean" satellite radar sensing data. *J. Geophys. Res*., vol. **97**, no. C5, pp.7429-7445.

Mitnik L.M. (1992) Mesoscale coherent structures in the surface wind field during cold air outbreaks over the Far Eastern seas from the satellite side looking radar. *La mer*, vol. **30**, pp. 287-296.

Mitnik L.M. (1993) Surface wind variability from satellite side looking radar (SLR) data. In: *Satellite Remote Sensing of the Oceanic Environment*, edited by I.S.F. Jones, Y. Sugimory and R.W. Stewart, Seibutsu Kenkyusha Co., Ltd., pp. 200-208.

Mitnik L.M., M.-K. Hsu, C.-T. Liu and M.L. Mitnik (1994) Cloud influence on microwave sensing of the ocean. *Terrestrial, Atmospheric and Oceanic Sciences*. Vol. **5**, no. 4, pp. 537-555.

Liu C.-T., L.M. Mitnik, M.-K. Hsu and Y. Yang (1994) Oceanic phenomena northeast of Taiwan from Almaz SAR image. *ibid*, pp. 557-571.

Hsu M.-K., L.M. Mitnik and C.-T. Liu (1995) Upwelling area northeast off Taiwan on ERS-1 SAR images, *Acta Oceanografica Taiwanica*, vol. **34**, no. 3, pp. 27-38.

Mitnik L.M., M.-K. Hsu and M.L. Mitnik (1996) Sharp gradients and mesoscale organized structures in sea surface wind field in the regions of polar low formation. *The Global Atmosphere and Ocean System*. vol. **4**, no. 4, pp. 335-361.

Mitnik L.M., M.-K. Hsu and M.L. Mitnik (1996) Estimation of the spatial distribution of ocean surface and atmospheric parameters from coinciding satellite microwave radiometer and radar observations over the northwestern Pacific Ocean. In: COSPAR Colloquia Series - Volume **8***. Space Remote Sensing of Subtropical Oceans (SRSSO)*, pp. 143-153.

Mitnik L.M., M.-K. Hsu and C.-T. Liu (1996) ERS-1 SAR observations of dynamic features in the East-China Sea, *La mer*, vol. **34**, pp. 215-225.

M.L. Mitnik, L.M. Mitnik and M.-K. Hsu (1997). Radar and Microwave Radiometer Sensing of Typhoon Ryan. *Proc. IGARSS'97*, Singapore, 1997, vol. **1**, pp.70-72.

Mitnik M.L. and L.M. Mitnik (1998). Validation of total water vapor and liquid water algorithm for the ADEOS-II/AMSR: Using SSM/I observations. *Proc. IGARSS'98*, Seattle, pp. 722-724.

Mitnik L.M., M.L. Mitnik and M.-K. Hsu (1998). Satellite X-band real aperture radar signatures of nonprecipitating clouds, rain cells and rain bands. *ibid*, pp. 742-744.

Mitnik L.M. and M.-K. Hsu (1998). Atmospheric and oceanic vortex streets: observations by satellite radars. *J. Advanced Marine Science and Technology*, vol. **4**, no. 2, pp. 241-248.

Mitnik L.M., M.-K. Hsu and M.L. Mitnik (1998). Satellite active and passive microwave sensing of typhoon Angela. In: *Remote Sensing of the Pacific Ocean by Satellites*, R.A. Brown, editor, Earth Ocean & Space Publishing, pp. 78-89.

Mitnik L.M., G.I. Desyatova and M.L. Mitnik (1990) The sea surface wind and cloudiness fields of tropical storm Agnes from data of satellite radiophysical sensing. *Earth Observation and Remote Sensing (Soviet J. Remote Sensing),* no. 6, pp. 20-28 (in Russian).
Mitnik L.M. and V.B. Lobanov (1991) Reflection of the oceanic fronts on the satellite radar images. In: *Oceanography of Asian Marginal Seas*, K. Takano, editor, Elsevier Oceanography Series, vol. **54**, Elsevier, Amsterdam, pp. 85-101.
Mitnik L.M. and M.Yu. Shoom (1991) Microwave sensing of cloudy atmosphere over the ocean from space: Influence of antenna smoothing*. Radioengineering and Electronics*, vol. **36**, no. 5, pp. 891-901.
Mitnik L.M. and A.I. Kalmykov (1992) Structure and dynamics of the Sea of Okhotsk marginal ice zone from "Ocean" satellite radar sensing data. *J. Geophys. Res*., vol. **97**, no. C5, pp.7429-7445.
Mitnik L.M. (1992) Mesoscale coherent structures in the surface wind field during cold air outbreaks over the Far Eastern seas from the satellite side looking radar. *La mer*, vol. **30**, pp. 287-296.
Mitnik L.M. (1993) Surface wind variability from satellite side looking radar (SLR) data. In: *Satellite Remote Sensing of the Oceanic Environment*, edited by I.S.F. Jones, Y. Sugimory and R.W. Stewart, Seibutsu Kenkyusha Co., Ltd., pp. 200-208.
Mitnik L.M., M.-K. Hsu, C.-T. Liu and M.L. Mitnik (1994) Cloud influence on microwave sensing of the ocean. *Terrestrial, Atmospheric and Oceanic Sciences*. Vol. **5**, no. 4, pp. 537-555.
Liu C.-T., L.M. Mitnik, M.-K. Hsu and Y. Yang (1994) Oceanic phenomena northeast of Taiwan from Almaz SAR image. *ibid*, pp. 557-571.
Hsu M.-K., L.M. Mitnik and C.-T. Liu (1995) Upwelling area northeast off Taiwan on ERS-1 SAR images, *Acta Oceanografica Taiwanica*, vol. **34**, no. 3, pp. 27-38.
Mitnik L.M., M.-K. Hsu and M.L. Mitnik (1996) Sharp gradients and mesoscale organized structures in sea surface wind field in the regions of polar low formation. *The Global Atmosphere and Ocean System*. vol. **4**, no. 4, pp. 335-361.
Mitnik L.M., M.-K. Hsu and M.L. Mitnik (1996) Estimation of the spatial distribution of ocean surface and atmospheric parameters from coinciding satellite microwave radiometer and radar observations over the northwestern Pacific Ocean. In: COSPAR Colloquia Series - Volume **8**. *Space Remote Sensing of Subtropical Oceans (SRSSO)*, pp. 143-153.
Mitnik L.M., M.-K. Hsu and C.-T. Liu (1996) ERS-1 SAR observations of dynamic features in the East-China Sea, *La mer*, vol. **34**, pp. 215-225.
M.L. Mitnik, L.M. Mitnik and M.-K. Hsu (1997). Radar and Microwave Radiometer Sensing of Typhoon Ryan. *Proc. IGARSS'97*, Singapore, 1997, vol. **1**, pp.70-72.
Mitnik M.L. and L.M. Mitnik (1998). Validation of total water vapor and liquid water algorithm for the ADEOS-II/AMSR: Using SSM/I observations. *Proc. IGARSS'98*, Seattle, pp. 722-724.
Mitnik L.M., M.L. Mitnik and M.-K. Hsu (1998). Satellite X-band real aperture radar signatures of nonprecipitating clouds, rain cells and rain bands. *ibid*, pp. 742-744.
Mitnik L.M. and M.-K. Hsu (1998). Atmospheric and oceanic vortex streets: observations by satellite radars. *J. Advanced Marine Science and Technology*, vol. **4**, no. 2, pp. 241-248.
Mitnik L.M., M.-K. Hsu and M.L. Mitnik (1998). Satellite active and passive microwave sensing of typhoon Angela. In: *Remote Sensing of the Pacific Ocean by Satellites*, R.A. Brown, editor, Earth Ocean & Space Publishing, pp. 78-89.